NASA Contractor Report 182043

Space Station Definition, Design and Development — Task 5
Multiple Arm Telerobot Coordination and Control

Manipulator Design Methodology

R.M. Stoughton

MARTIN MARIETTA ASTRONAUTICS GROUP
Denver, Colorado

Contract NAS1-18230
July 1990

National Aeronautics and Space Administration

Langley Research Center
Hampton, Virginia 23665-5225

CONTENTS

FIGURES

Chapter 1
INTRODUCTION

The cooperative control of multiple robot arms by definition involves interaction with an environment force. This interaction is composed of two parts. The first contribution is the interaction force generated by the first robot on the second (possibly caused by small errors in the coordination of the two arms' movements), and vice versa. The second contribution to the interaction force is from the interaction of both robots with the passive environment. This environment may be primarily inertial, as in the case of a coordinated pick-and-place operation, or it may range to a complex, high order dynamic system with multiple structural resonances – such as the space station truss assemblies.

Understanding the dynamic relationship between the manipulator and the interaction forces operating on it, is a key issue in understanding the cooperative control of multiple robot arms.

The last ten years has seen a tremendous amount of research on the active control of the interface forces between a manipulator and its environment. Some of the resulting control strategies include Hybrid Position/Force control [MAS81,RAIB81,SER87], Active Stiffness Control [SAL80], Position and Torque Based Impedance Control [HOG85, LAW87,LAW88], as well as numerous variations on these strategies. The general technique for describing the virtues of any particular strategy is to perform a demonstrtion using that strategy for a specific task. Unfortunately this method does not provide any insight into the relative merits of the various strategies, nor any understanding on what are the fundamental limitations of the different strategies.

In order for manipulators to be reliably designed for such tasks as satellite servicing, Space-Station support or SDI support it is neccessary to find a way to compare the relative costs and merits of the various control strategies, for a desired application. A way must also be found to predict the difficulty of designing and building a robotic system for a particular task. This will be important for instance in determining if it is more cost effective to design the manipulator to do the task, to redesign the task to make it easier for a manipulator to accomplish, or to depend on a human to do the task (ie designing a manipulator to insert and remove single-slot screws would be, for many applications, much more difficult and expensive than modifying the task to use phillips or hex-head fasteners).

In short, manipulator technology has matured to the point where a rational design methodology is neccessary to ensure the success of large, important national programs depending on robotics as a key support technology (ie space-station, SDI). The maturity of the manipulator technology base is such that developing a design methodology is now an achievable undertaking.

This report discusses research jointly funded by NASA's Langley Research Center

and DARPA, to take the nucleus of this methodology and begin to explore ways of using it to gain greater insight into the use of manipulators for tasks requiring force interaction.

The organization of the report is described below. Chapter 2 describes our approach to a manipulator design methodology. Our design methodology centers on three key areas:

1) the translation of functional task requirements into static and dynamic system performance specifications,

2) a structure for evaluating the various design options and their overall cost in meeting the performance specification,

3) the ability to validate and verify the design, through testing, to ensure it meets the system performance specifications.

Chapter 3 describes the Dual Arm Testbed, which was used for the majority of our experiments. Chapter 4 discusses research results in defining dynamic performance requirements. Using a very simple task a comparison is made between analytical predictions for performance specifications and experimental results. A technique is also shown wherebye empirical methods may be used to define requirements for more complex tasks. Chapter 5 explores some of the constraints limiting the performance of manipulator systems. Techniques to verify the performance of the completed manipulator system are discussed in Chapter 6. Chapter 7 highlights some conclusions reached during the course of this research and concludes by suggesting the most fruitful directions for further research, to more fully define this emerging design methodology.

Chapter 2

DESIGN METHODOLOGY

The design approach we are proposing is based on the techniques common in other more mature technology disciplines. A prime example is the way in which aircraft and missile systems are specified, designed, and tested. From a large experience base, the user is able to precisely specify the properties that the end system must possess. This specification includes dynamic performance. Therefore, at the outset of the design process, unambiguous performance objectives can be established and used as a means of unifying the subsystem design efforts. Specifying, for example, pitch-axis response, in terms of step response, bandwidth, etc., allows early baselining of general system features since they can be rapidly checked in terms of general compliance with design objectives. More importantly, however, well-defined requirements lead to a concise method of validating end-item performance. Controlled laboratory tests can be used to verify compliance with performance specifications before committing to final flight hardware.

A similar set of processes must be established for robotic manipulator systems. To accomplish this, two goals must be achieved:

1. *Techniques must be developed that allow user functional requirements to be expressed in terms of manipulator performance requirements. The capability must exist for transforming* "remove a module",*or* , "insert a bolt" *into universal dynamic specifications.*

2. *Procedures must be developed that allow manipulator systems to be tested for compliance with performance specifications. This will require a testing procedure that is independent of the specific tasks to be performed since the objective is validation of general dynamic response properties.*

In section 2.1, a candidate approach to the solution of these problems is introduced. This focuses on the general design flow that is shown in Figure 2-1. This approach addresses the issue of relating functional and performance requirements, the role of these requirements in the simulation and hardware prototyping stages of the design, and final validation testing. The unifying concept that makes this approach possible is *dynamic end-effector impedance*, an analytical means of specifying "dexterity". In addition to introducing the basic concepts behind this approach, discussion in section 2.1 also addresses other ramifications and attributes of the proposed technique.

Section 2.2 is used to treat the technical issues associated with this design approach. Specific emphasis in this discussion is placed on the establishment of firm relationships between functional and performance requirements, the utility of end-effector impedance as a common basis for performance specification for both single and multiple arm systems,

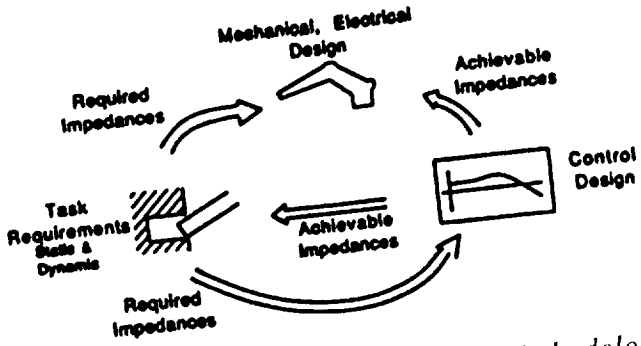

Figure 2-1: General Design Methodology

and autonomous and teleoperated systems, and existing techniques for manipulator system performance validation.

2.1 General Design Methodology

The overall structure for the design methodology is shown in Figure 2-1. From a structural standpoint, the heart of the methodology is the existence of design and analysis software tools that support each phase of the design process, allowing designers and analysts to easily examine parts of the manipulator system against established performance objectives. It is probable that all of the necessary software tools are in existence at this time, at least in a state where they could be easily modified to suit this purpose. The innovative aspects of the approach being described here do not lie in the actual mechanization of the tools, but rather in the philosophy that unites firm system performance requirements, the design process, and final validation of the system. The remainder of this section describes the basic elements of the design process; key technical issues are described further in section 2.2.

2.1.1 Design Flow

The key steps in the design process are listed below:

1. Derivation of a complete set of performance requirements for the manipulator system based on an analysis of functional requirements. Performance requirements include conventional measures such as peak force and torque, velocity and acceleration, accuracy and repeatability, work envelope, etc., *and* specification of dynamic performance in terms of *worst case* end-effector impedance.

2. Development of a preliminary design concept based on the established requirements. Design, at this point, reflects basic system attributes necessary to meet

design specifications with the subsystem elements defined with respect to performance criteria. Having a full set of performance requirements, both static and dynamic, will allow meaningful trade-offs among the various design options. The performance requirements may also be refined during this process. For instance the preliminary design may indicate it is more cost-effective to reduce the accuracy requirement and modify the dynamic impedance requirement to allow for greater inaccuracies.

3. Detailed system and subsystem design with the development of high fidelity digital computer simulation models and prototype hardware. Validation at the system and subsystem level of design elements *against performance criteria.*

4. System validation by testing the closed-loop hardware/software system in terms of the full set of performance requirements rather than isolated demonstrations on functional tasks.

The most important steps in the process above are the first and the last. Outwardly, the series of steps that have been outlined are those that everyone who has ever attempted to design a manipulator system has *tried* to follow. What has not been done, however, is to effectively relate dynamic performance to functional requirements as required in the first step. Instead, it is usually considered sufficient to specify that the system will have a "compliant" controller and hope that the final properties will be sufficient to accomplish the tasks for which the system is being designed. The problem, is that there is a tremendous amount of difference between "generally correct" behavior and a specific behavior required for task performance. In general, a compliant control structure can be implemented for any manipulator system. The difference lies in the degree to which arbitrary behavior can be commanded at the end-effector. The problem typically lies in the actuator design and time delays in the control system processor. Weight constraints generally lead to some type of torque multiplication, through gears, cables, etc. These introduce friction, often nonlinear, which limits the effectiveness of the final control system design. Without firm constraints on performance objectives, the ramifications of these decisions on manipulator performance are usually discovered too late.

The problem described above can be circumvented, to a large degree, if precise dynamic requirements are established at an early phase of the system design. These allow initial concepts to be realistically evaluated through simulation where the impact of friction, time delay, noise can be assessed *against final objectives.* This implies the need for a set of techniques for deriving dynamic performance objectives on the basis of task functional characteristics. This is a capability that does not currently exist, but the development of such a capability is certainly within the scope of current technology. Ideally, CAD/CAE techniques would come into play with sophisticated analytical techniques to automatically generate the dynamic requirements. In the interim, however, it appears that these requirements could be generated empirically.

A further advantage of demanding firm performance requirements lies in the ability to unambiguously assess system performance. Rather than relying on "proof-by-demo",

the validation process can be performed very objectively through simple measurements of observed closed-loop behavior. Assuming that impedance is the proper dynamic specification criteria, then validation can be performed in any laboratory setting where force can be applied to the manipulator end-effector and displacement measured. With measured impedance data available, validation becomes a simple process — either the manipulator achievable impedances match the impedance specification for dynamic performance or they don't !

2.1.2 Considerations

A general methodology for the specification, design, and validation of manipulator systems was outlined above. While technical issues remain to be resolved before such an approach could be fully implemented, it holds a great deal of promise with respect to overcoming many of the current shortcomings associated with the design of manipulator systems. With increasingly larger amounts of government resources going into the development of these systems, the adoption of a methodology such as that described is essential. Hopefully, this would lead to a unified set of design tools in common usage by the armed services and NASA to avoid conflicting standards, etc.

2.2 Technical Issues

In the previous section a design methodology was introduced. The methodology relies on a close inter-relationship between system performance requirements, the design process, and hardware validation. This section examines some aspects of this methodology in more detail. The derivation of dynamic performance requirements is considered from the standpoint of analytical, simulation, and empirical techniques. The actual design process is examined with respect to how the performance requirements are used. Finally, techniques for hardware system validation are considered.

2.2.1 Derivation of Dynamic Performance Requirements

The single most important and unique attribute of the design methodology that is being suggested is the adherence to the requirement that the design process must start with the translation of functional requirements into unambiguous static and dynamic performance requirements. This is critical for the design of manipulators for assembly tasks.

The static requirements include such specifications as peak force, accuracy, maximum reach and maximum tip speed. The importance of these specifications is well known and they are fairly easy to derive from the functional tasks.

Dynamic performance requirements are used to specify the transient behavior of the manipulator. If one commands a position change for the manipulator, the dynamic requirements specify how that change is to be accomplished — how long it takes to reach

the new position, the amount of overshoot in stopping at the new position, the number of oscillations after reaching the new position — all are determined by the manipulator dynamic response. The dynamic requirements also specify how a manipulator responds to force disturbances. Correctly specifying these characteristics are key to employing manipulators for assembly and other force interaction tasks.

The importance of static requirements has long been understood in the robotics community, and they have formed the basis for most of the current manipulator designs. The significance of dynamic performance requirements, as they relate to successful force interaction applications, has only recently been recognized. Without dynamic requirements it is difficult and in some cases impossible to meaningfully evaluate trade-offs between the available options during the preliminary design stage.

By having both static and dynamic requirements it is possible to approach the preliminary design in a rational and methodological manner — and most importantly — have a high degree of confidence that the resulting design will be one that meets the requirements for the minimum cost !

At a high level there are at least two conditions which must be met for an assembly task to be successful. First the interaction forces developed during assembly must be small enough so that nothing is damaged (assembly parts, manipulators or fixtures). Secondly the direction of the force must be such that the parts to be assembled do not stick or jam.

Translating this concepually simple requirement into quantitative, measurable performance specifications, for specific tasks, is a very complex problem. We have chosen end-effector impedance as our quantitative performance specification. The impedance of a mechanical system is defined as the relationship between the force applied to the system and the resulting position response of the system. If a system is described by the following equation of motion;

$$F = M\ddot{X} + B\dot{X} + KX, \qquad (2-1)$$

then the impedance, Z, of the system is defined as

$$Z \equiv \frac{F}{X} = Ms^2 + Bs + K. \qquad (2-2)$$

The end-effector impedance of a manipulator then relates the dynamic position response of the end-effector to force disturbances at the end-effector. We typically use a Cartesian-space representation of this impedance, allowing each of the translational and rotational axes to be independently specified. Using end-effector impedance allows one to specify the performance requirements in terms of easily understood physical quantities. That is the end-effector requirements may be specified in terms of inertial (J), damping (B), and stiffness (K), characteristics. For example it may be specified that for a given steady-state position misalignment, x, the maximum force allowable at the end-effector is f. Along this direction the maximum stiffness of the end-effector must then be limited to

$$K < \frac{f}{x}.$$

We have limited our investigation to impedance specifications of the form

$$Z = K + Bs + Js^2 \qquad (2-3)$$

along each Cartesian axis. Thus we are defining the end-effector to behave like a mass-spring-damper system.

Three directions are being followed in our investigation of dynamic performance requirements. Using a very simple planar insertion task we have attempted to analytically predict the required impedances to complete the task, allowing only translational misalignments, and taking into account such dynamic effects as the inertia of the workpiece. For more complex tasks we are developing simulation tools to enable the prediction of required impedance specifications. For very complex tasks, such as those which would be encountered in an actual work environment, we are exploring empirical methods to determing the optimum performance specifications.

The results from these investigations indicate that deriving impedance specifications to satisfy the first condition listed above (applied force low enough to prevent damage) can be developed easily and can be specified early in the design process. Simple analytic techniques can be employed to obtain these specifications. Meeting the second condition (force direction such to prevent jamming) is much more difficult to specify analytically. The results of the analytical efforts on simple tasks can provide considerable insight into the directions to be pursued for the simulation and empirical investigations. Empirical studies can relatively quickly characterize the required impedances for a specific task.

2.2.2 System Design

In the previous section, the need for firm manipulator performance specifications was stressed. Emphasis was placed on the means by which these specifications could be developed on the basis of functional task descriptions. In this section the impact of performance specification on the actual design process is explored. It is shown that one of the most significant benefits of having a complete set of both static and dynamic performance requirements early in the design phase is they enable *meaningful* interaction between mechanical, processing, and control system designers; something that is currently very difficult to achieve.

The system design process is that which takes the manipulator performance requirements and defines a complete manipulator system such that the performance requirements are achieved at some combination of minimum initial and life-cycle cost. The manipulator design process has traditionally been an evolutionary, empirical process. That is the various industrial manipulator manufacturers have modified their products over time, based on their performance in the workplace. The result is the development of manipulators which are good at traditional industrial applications, such as painting, spot welding, and pick and place operations.

The manipulator design process primarily involves three disciplines. These are:

- Mechanical Design and Analysis,

- Controller hardware Design and Analysis (both analog and discrete),
- Control algorithm Design and Analysis.

The manipulator design process has historically resulted in the above disciplines being independently pursued. Any interdisciplinary efforts were haphazard (as opposed to systematic) and based on heuristics and intuition.

While the above design process is certainly not attractive, up until recently there has been no real alternative. This is in large part the reason manipulator capabilities and applications have progressed so slowly.

The preliminary design phase has been and continues to be the weak link in the manipulator design process. The reason for this is obvious — Without meaningful performance requirements it is impossible to measure the effect of various design options on the manipulator's ability to meet its performance requirements. The result of this deficiency is that manipulator systems are designed and built with the hope that they will be able to accomplish their assigned tasks.

The concept of end-effector impedance allows us to obtain meaningful performance requirements. Once these requirements are available a systematic approach to using them in the design process is needed. It is at this stage that a strong interdisciplinary approach to the design process is most powerful.

Techniques for evaluating the relationship between the three disciplines discussed above (mechanical, hardware, software design) have been introduced in [LAW87] and [LAW88]. Specifically the effect of the computational delay, which is a function of controller hardware and software design; and the effect of the inner-loop controller structure, on the ability to achieve certain end-effector impedances was examined. Figure 2-2 is an example parametric plot from [LAW87], showing the impact of computational delay on achievable Cartesian end-effector impedance. This same approach has been applied to dual-arm systems.

A key concept in allowing one to relate the effects of joint properties and controllers on achievable Cartesian end-effector impedance is the 'Operational Space' approach described by Khatib [KHAT87] and by Depkovich [DEP88].

Prototype software has been developed which allows one to examine parametrically the relationship between inner-loop manipulator dyanamics, the computational delay, the achievable end-effector impedance, and the environment dynamics against which the manipulator is operating.

The key to a systematic, interdisciplinary design approach is the availabilty of meaningful, quantifiable performance requirements. Other approaches to making the design process more efficient will undoubtedly appear but they will all have in common a dependance on a full set of performance requirements!

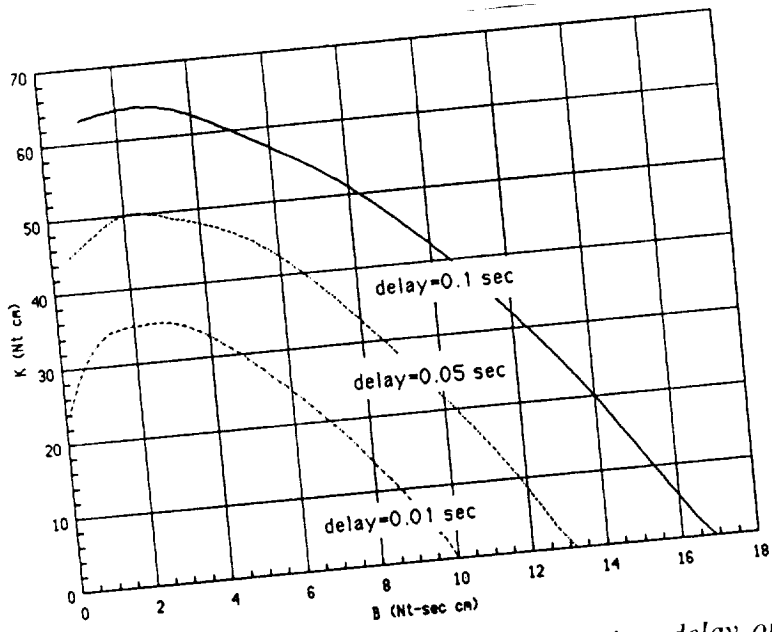

Figure 2-2: Example parametric plot showing effect of time delay on achievable end-effector impedance.

2.2.3 Performance Validation

A key component of the design methodology is the performance validation of the completed system. This can be most easily seen by examining a system which was built for a space application. There is no way to recreate the dynamic environment the manipulator will see in space, here on Earth. Therefore it is impossible to demonstrte the system will be able to perform all its tasks by duplicating them on earth. Thus the system must be sent into space with little more than a strong suspicion that it will perform as desired.

By having a measurable performance specification such as end-effector impedance it is possible to verify in the laboratory that the manipulator meets the performance specification, thus ensuring that the manipulator will be able to perform its appointed tasks.

For our initial investigations we have limited ourselves to dynamic specifications of the form:

$$F = M\ddot{X} + B\dot{X} + KX \qquad (2-4)$$

where
F is the vector of 6 Cartesian forces and torques,
X is the vector of 6 Cartesian positions and orientations,
M is the 6 x 6 diagonal matrix of inertia specifications,
B is the 6 x 6 diagonal matrix of damping specifications,
K is the 6 x 6 diagonal matrix of stiffness specifications.

It is certainly possible to come up with a higher order impedance specification, and/or to not restrict ourselves to diagonal specification matrices (which imply that the specifications for different axes are independent of each other), but at this early stage it is not at all clear that doing so is neccessary or even beneficial. Recall that dynamic

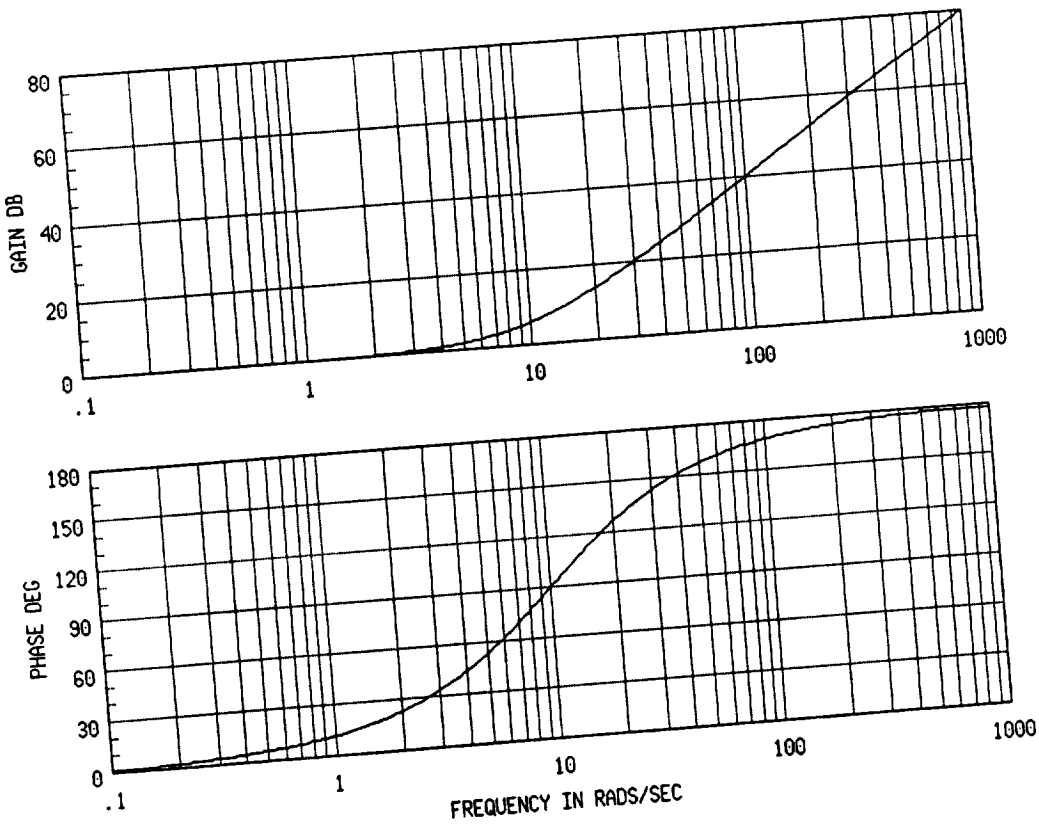

Figure 2-3: Example Impedance Specificatiion

specifications for aircraft, and many other systems are based on a second order model also.

Frequency response techniques appear to be the most viable method for validating system performance. If we examine the frequency response of (2-4), along a particular Cartesian axis, it will look similar to Figure 2-3. The DC value will correspond to the stiffness specification, and the higher frequency response will be that of the damping and inertial specifications.

The frequency response of the manipulator system, along a particular axis, can be obtained by connecting the end-effector to a force/torque source. The manipulator is then excited along a particular axis with this source, and the positions of all six axes are recorded. Through off-line processing the Fourier Transform of this data may be taken to yield the frequency response relating the position reponse of each of the axes to the force input along one axis.

For the axis along which the force/torque source was acting, the actual frequency response may be compared to the frequency response of the impedance specification, to ensure the dynamic performance is adequate. The cross-axis frequency responses will give some measure of the coupling in the system. In order for the various Cartesian axes to appear uncoupled, these responses must be very well attenuated. Figure 2-4 shows an actual measurement of the end-effector impedance from our Dual-Arm Testbed. The measurement was taken by connecting an HP 3562A Dynamic Signal Analyzer to the manipulator controller and recording the appropriate position and force signals, while exciting the end-effector.

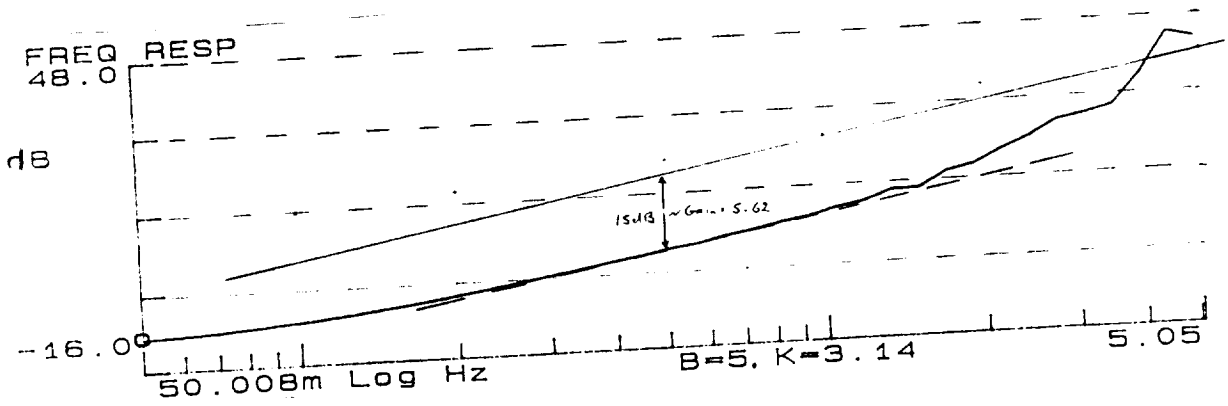

Figure 2-4: Example measurement of end-effector impedance on Dual Arm Testbed.

Chapter 3

DUAL ARM TESTBED

Martin Marietta began development of the Dual Arm Testbed in 1983. This development has matured to the point that this facility is one of the premier coordinated manipulator control laboratories in the world.

The Dual Arm Testbed uses two Cincinnati Milacron T3-726 manipulators. These were originally designed as industrial manipulators, with geared electric drives and six-degrees-of-freedom. Figure 3-1 is a picture showing the manipulator configuration.

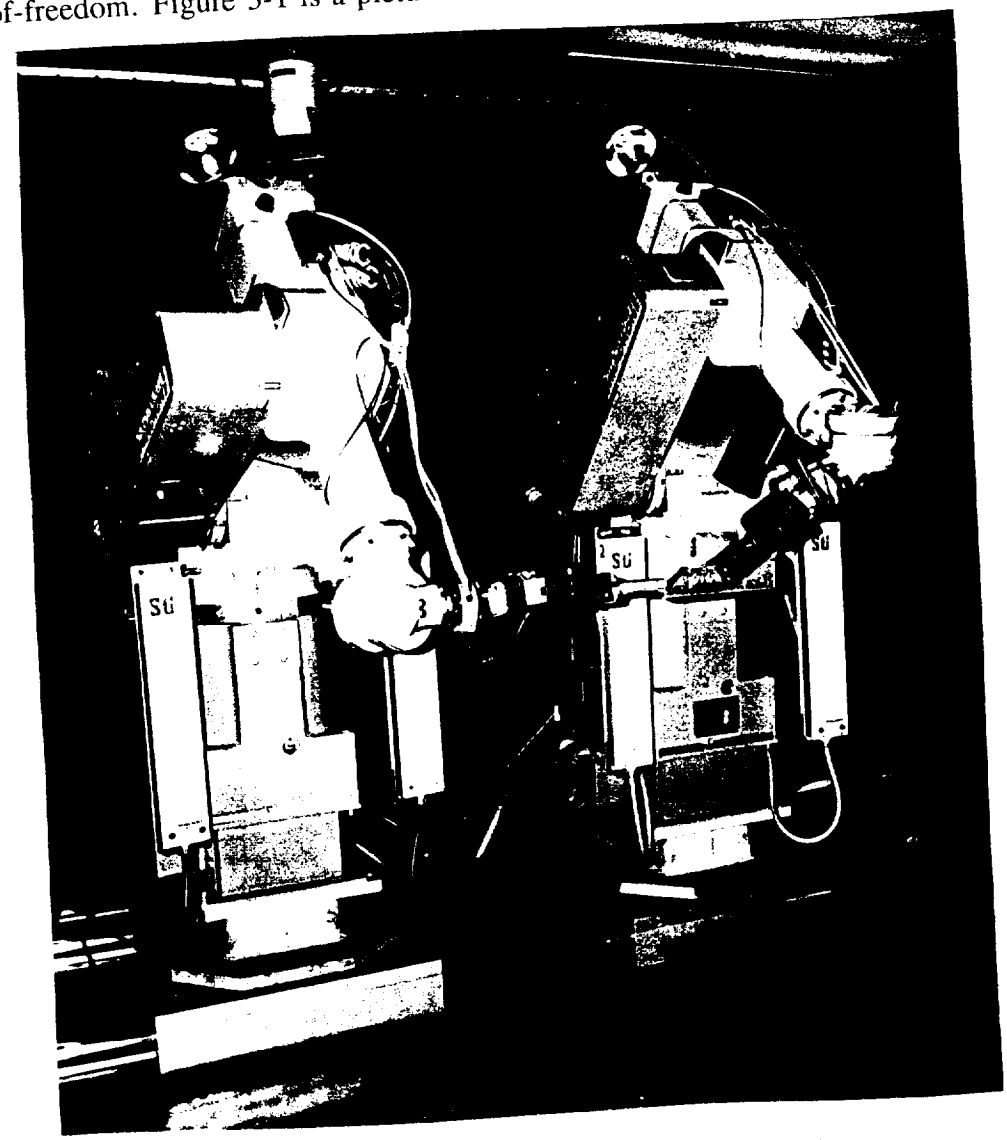

Figure 3-1: Martin Marietta Dual Arm Testbed

3.1 Controller Architecture

The original Cincinnati Milacron controllers for the manipulators have been stripped, retaining only the analog motor control cards and the Servo I/O cards. Martin Marietta has implemented a customer controller, based on a MULTIBUS chasis. The manipulators are controlled using a hierarchical control architecture, composed of 10 Intel 8086 single board computers and one Intel 80286 computer, housed in 4 MULTIBUS chassis and communicating across a Multichannel communications link (processors are currently being upgraded to Intel 80386 to decrease computational delay). Both autonomous path execution and teleoperation, using one of 3 hand controllers, is supported.

Figure 3-2 is a schematic of the control architecture, showing its hierarchical structure. All of the feedback control takes place in the robot controller chassis. Both position and force feedback are supported. The force information comes from Lord 6 DOF Force/Torque sensors mounted on the manipulator wrists.

The control station's two primary tasks are to serve as the user interface and to serve as the inter-arm controller. That is, all of the manipulator coordination is performed on the Control Station. For coordinated motion, the commands from the hand controller or the autonomous path generator are fed into the inter-arm controller. The inter-arm controller then develops the required commands for the two manipulators, to perform the coordinated movement.

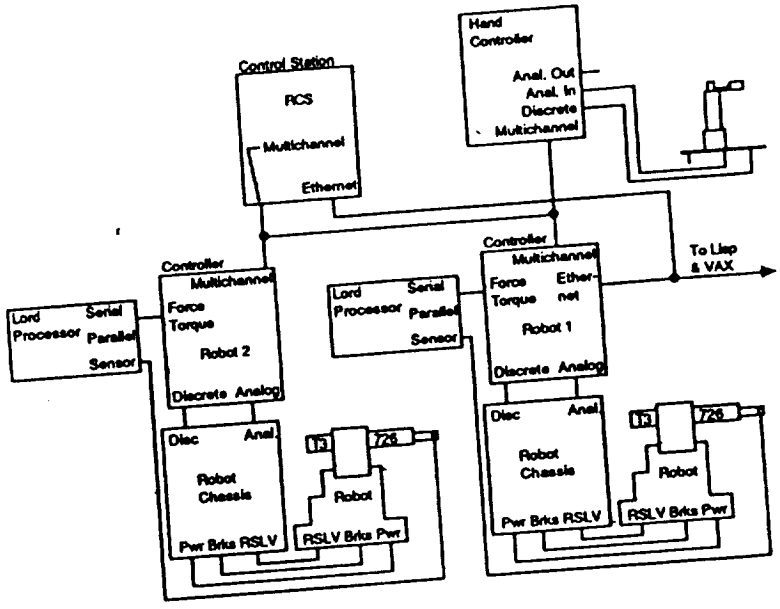

Figure 3-2: Controller Architecture of Dual Arm Testbed

3.2 Manipulator Feedback Controller

The feedback controller for each manipulator is also organized in a hierarchical structure. At the lowest level is an analog joint velocity controller. The next level incorporates a joint position controller. Above the joint controller is the Cartesian Controller.

3.2.1 Joint Control

Figure 3-3 is a block diagram of these two lowest level controllers, which together form the manipulator joint controller.

The compensator $H_v(s)$ was originally a PID compensator. This is a generic controller structure commonly used in applications requiring zero steady state velocity error. For robotic application we are not interested in achieving steady-state velocities. In light of this, better performance can be obtained with a PD compensator. Thus the integral part of $H_v(s)$ was disconnected.

The joint position controller is a digital controller, with a sample period of 30 msec. The compensator is a simple gain on the error between commanded and actual joint position. Figures 3-4 – 3-9 show the closed-loop frequency response of the manipulator joints, including both the velocity and position loops.

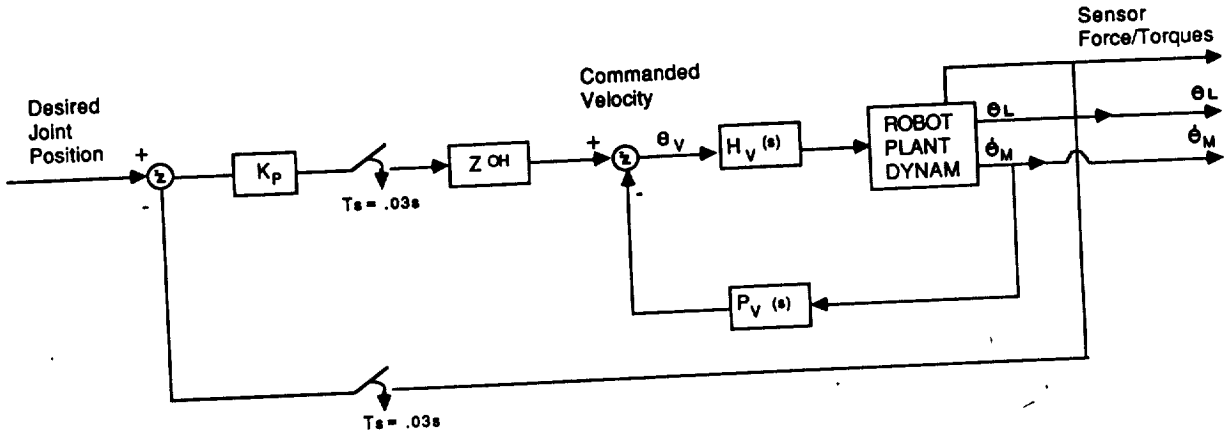

Figure 3-3: Joint control block diagram

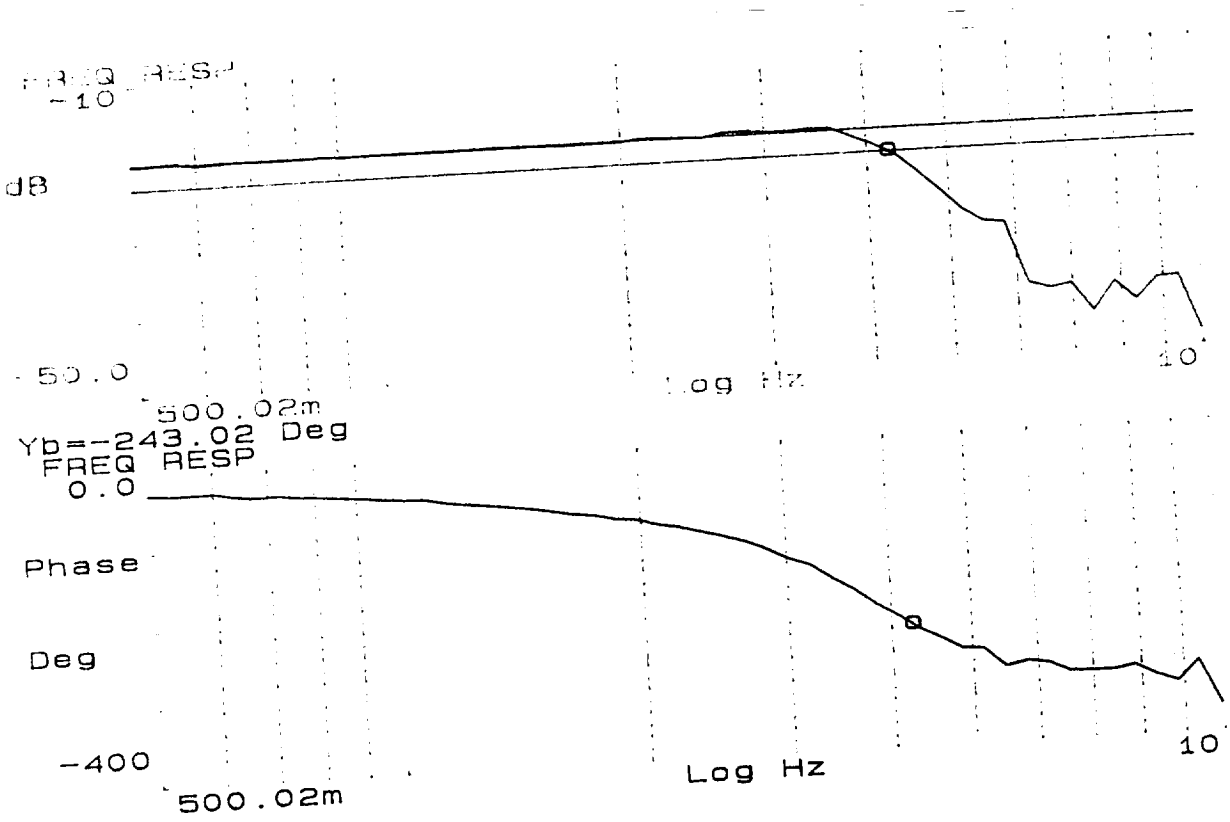

Figure 3-4: Frequency response of Base joint .

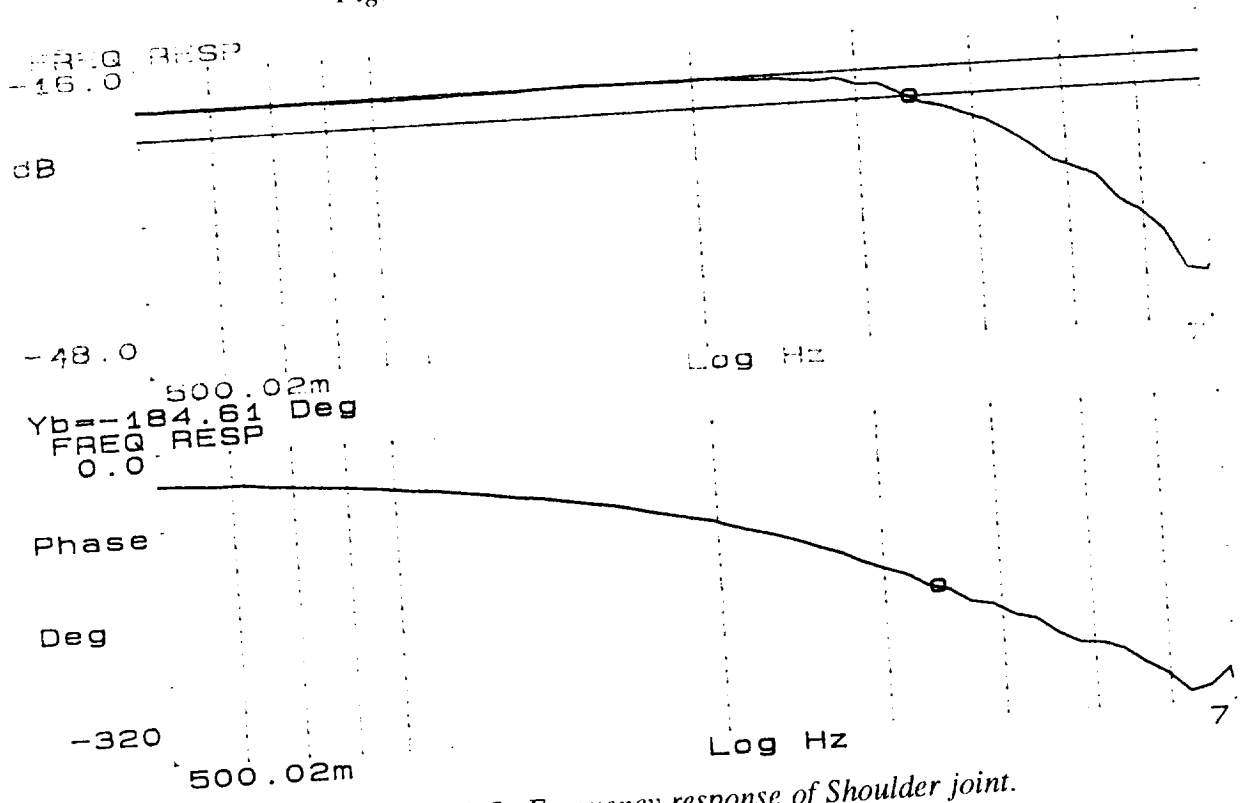

Figure 3-5: Frequency response of Shoulder joint.

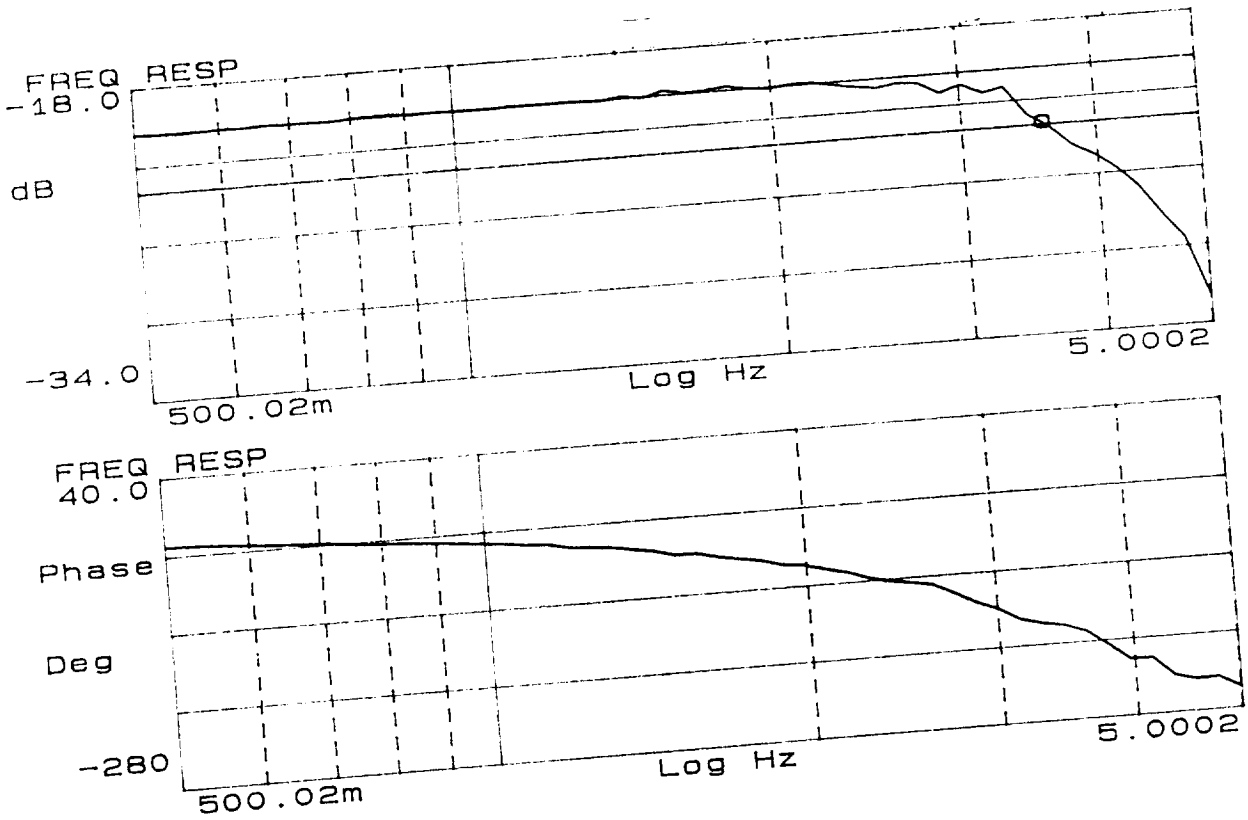

Figure 3-6: Frequency response of Elbow joint.

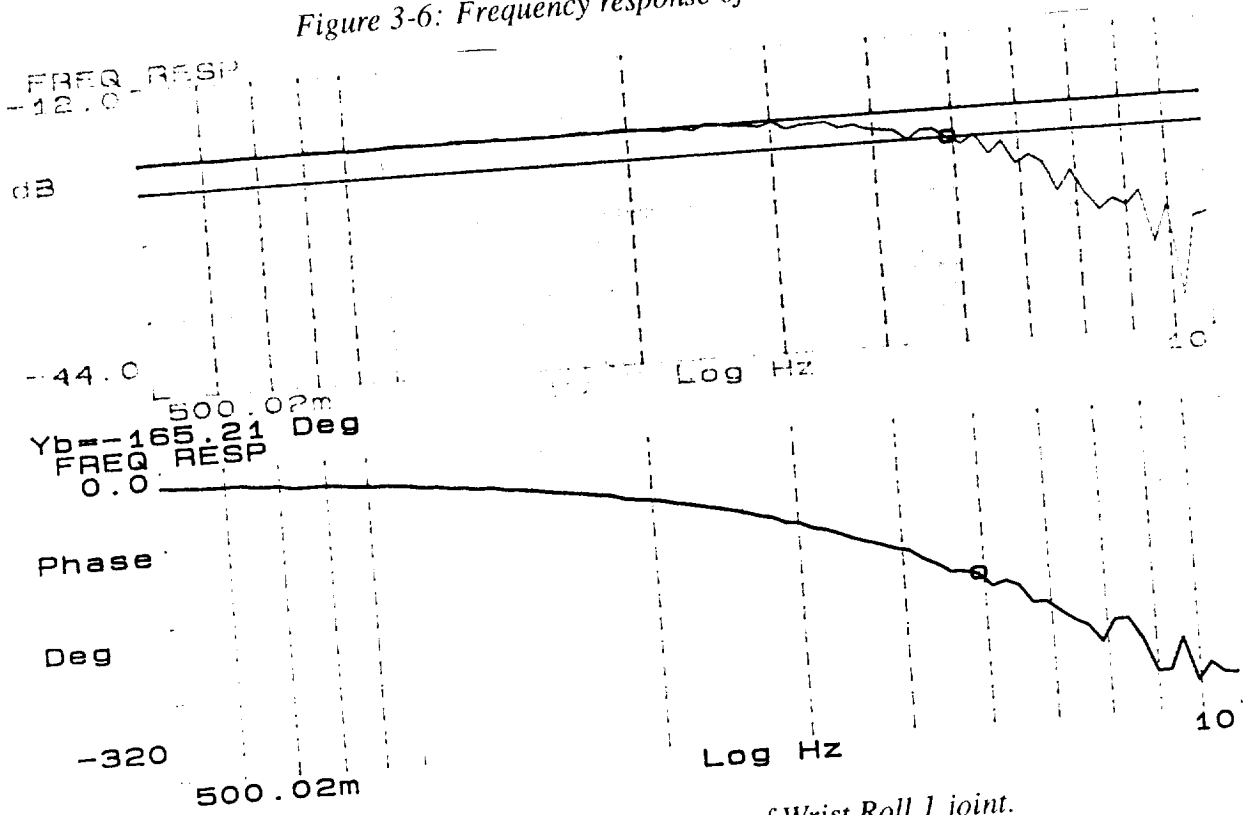

Figure 3-7: Frequency response of Wrist Roll 1 joint.

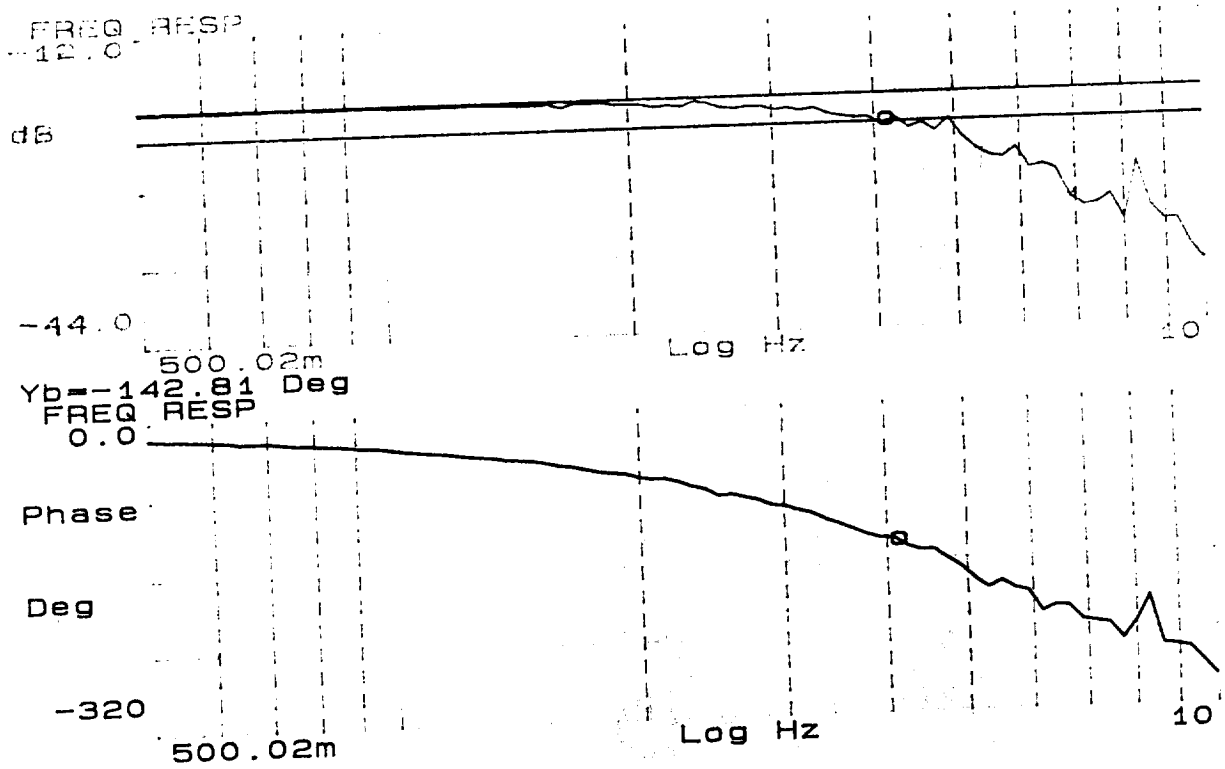

Figure 3-8: Frequency response of Wrist Roll 2 joint.

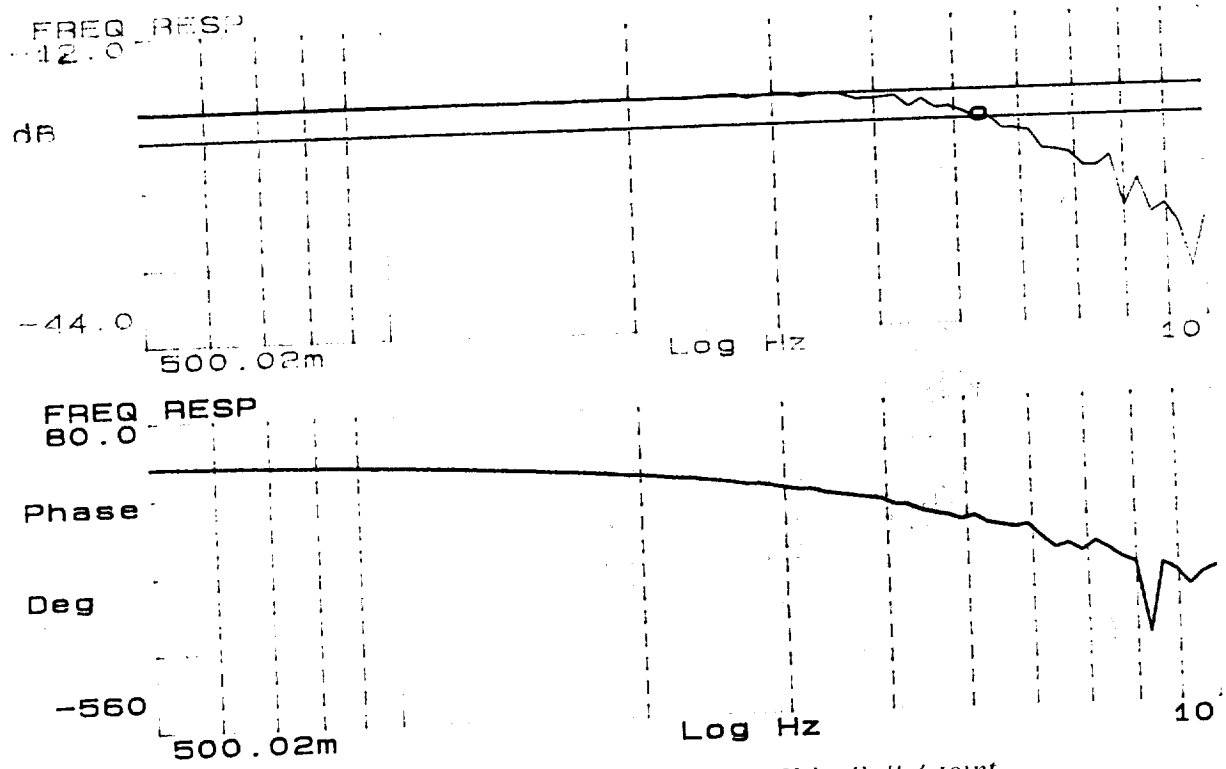

Figure 3-9: Frequency response of Wrist Roll 3 joint.

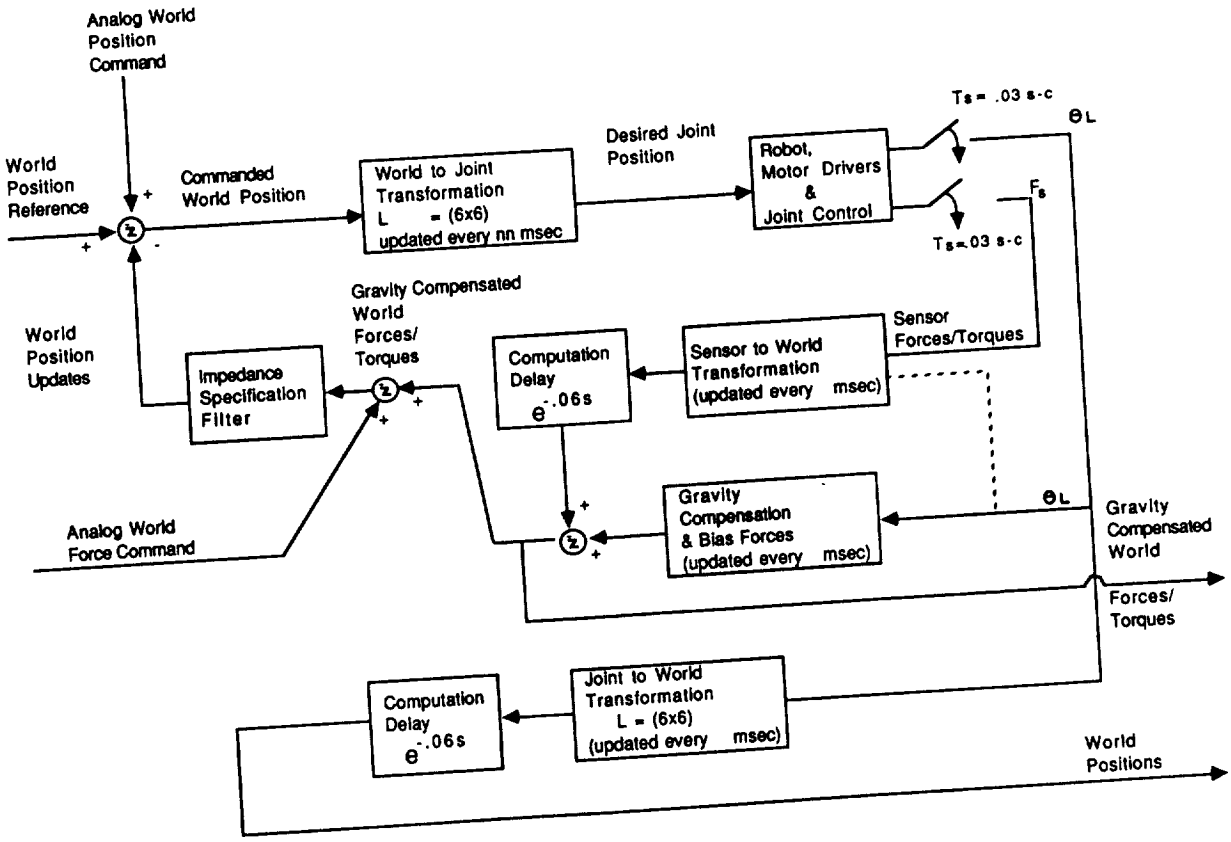

Figure 3-10: Cartesian control loop block diagram

3.2.2 Cartesian Control

Above the joint control is the Cartesian controller. This is a digital controller with a sample period of 30 msec. Figure 10 is a block diagram of the Cartesian controller. The Cartesian controller does not include a position feedback loop. The commanded Cartesian positions are transformed into commanded joint positions, and fed into the joint controller. Therefore the closed loop Cartesian position dynamics are only a combination of the 6 joint position dynamics. Figures 11–13 show the three translational Cartesian position frequency responses. Notice that their characteristics vary widely from axis to axis. For force interaction tasks this variation will not be significant, since the impedance filter acts like a low pass filter on the position dynamics, with the roll-off frequency consistantly below 1 Hz for our applications.

The Cartesian controller uses a 'Position Based' Impedance Control implementation to control the interaction forces at the end-effector. In this strategy the interaction forces are passed through an impedance specification filter (which is effectively a low-pass filter) and the output is summed with the reference Cartesian position command to form an offset commanded Cartesian position.

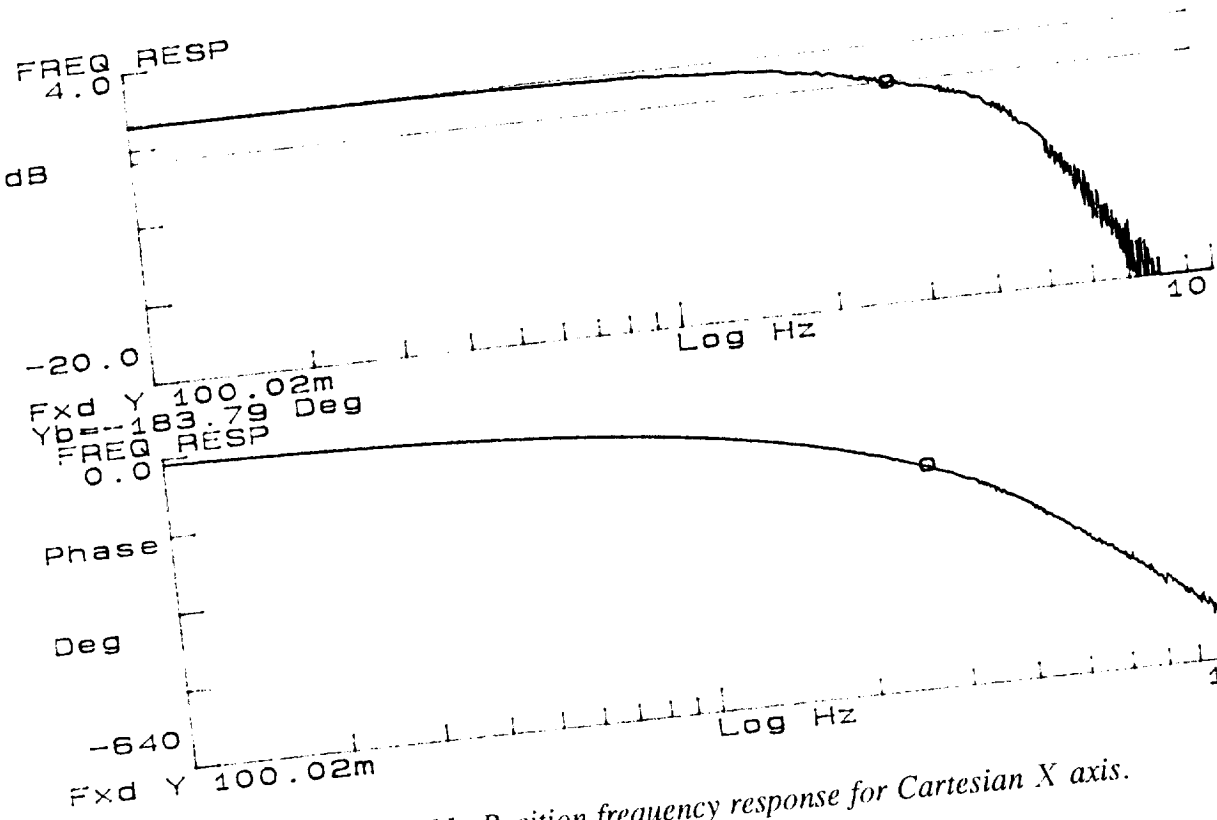

Figure 3-11: Position frequency response for Cartesian X axis.

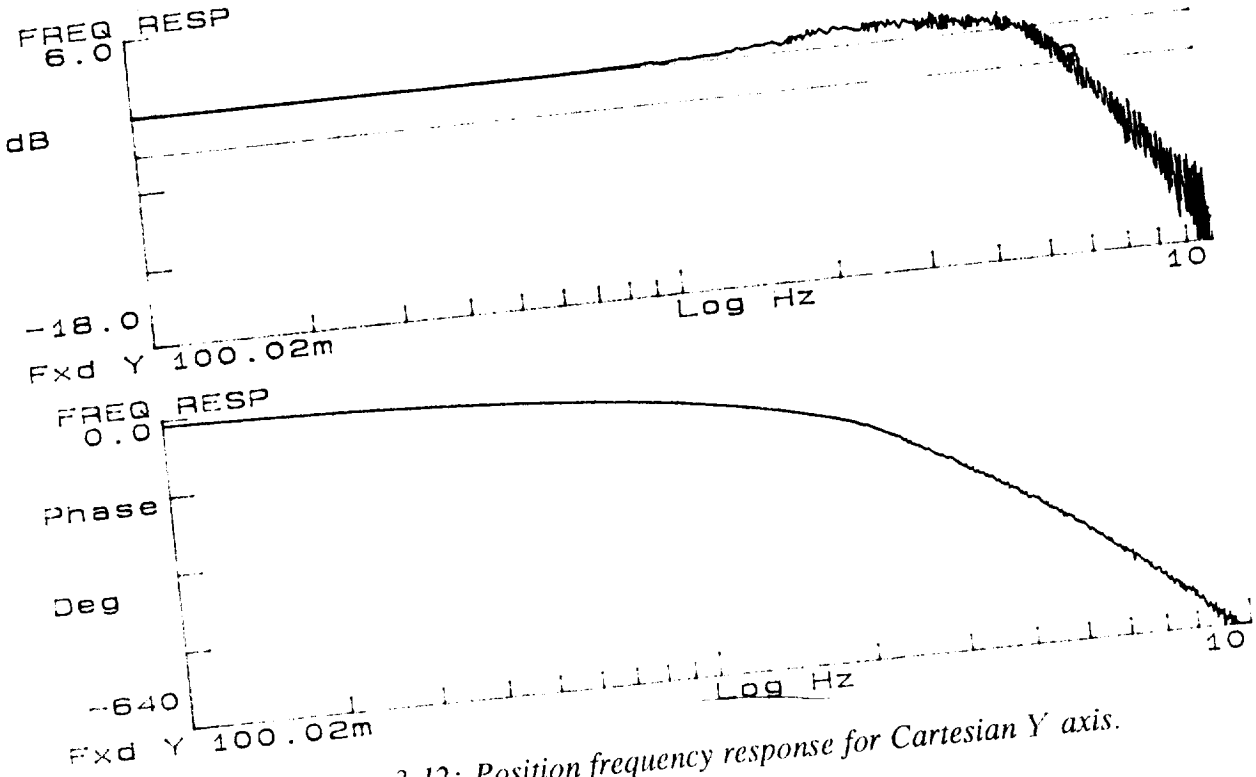

Figure 3-12: Position frequency response for Cartesian Y axis.

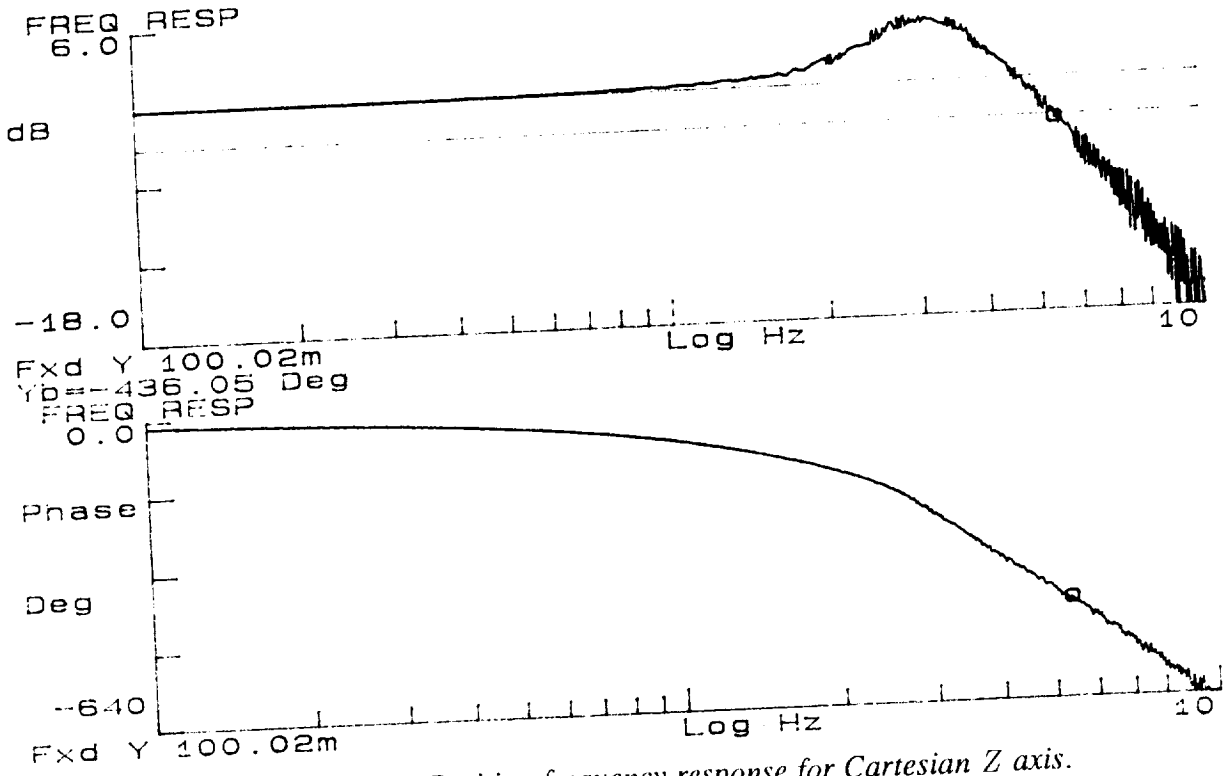

Figure 3-13: Position frequency response for Cartesian Z axis.

Impedance Filter:

A different impedance specification may be used along each Cartesian direction. For a specific Cartesian direction, the W-plane transfer function representation of the Impedance Specification Filter is

$$\frac{F_i(w)}{X_i(w)} = \frac{1}{Jw^2 + Bw + K} \qquad (3-1)$$

where:

F_i is the force sensed along the i'th Cartesian axis,
X_i is the displacement along the i'th Cartesian axis,
J, B, K are respectively the inertial, damping, and stiffness parameters associated with the desired impedance.

For example if K is set to 10 and J and B equal 0, then along that direction the end-effector behavior will resemble a spring of stiffness 10 lb/in.

Analog I/O

Analog input commands may be added to both the reference Cartesian position and the gravity compensated Cartesian forces and torques. Additionally any of the Cartesian positions/orientations or forces/torques may be directed to the 8 D/A channels. These are used, for among other things, to connect the system to a dynamic signal analyzer, which is used for system identification in general and specifically to measure the system end-effector impedance.

Chapter 4

PERFORMANCE REQUIREMENTS

In order for manipulators to be designed for assembly tasks it is neccessary to have both static and dynamic performance specifications, which if met will ensure successful task completion. The static requirements include such specifications as peak force, maximum reach and maximum tip speed. The importance of these specifications is well known and they are fairly easy to derive from the functional tasks.

Dynamic performance requirements are used to specify the transient behavior of the manipulator. If one commands a position change for the manipulator, the dynamic requirements specify how that change is to be accomplished — how long it takes to reach the new position, the amount of overshoot in stopping at the new position, the number of oscillations after reaching the new position — all are determined by the manipulator dynamic response. The dynamic requirements also specify how a manipulator responds to force disturbances. Correctly specifying these characteristics are key to employing manipulators for assembly and other force interaction tasks.

The importance of static requirements has long been understood in the robotics community, and they have formed the basis for most of the current manipulator designs. The significance of dynamic performance requirements, as they relate to successful force interaction applications, has only recently been recognized. Without dynamic requirements it is difficult and in some cases impossible to meaningfully evaluate trade-offs between the available options during the preliminary design stage.

By having both static and dynamic requirements it is possible to approach the preliminary design in a rational and methodological manner — and most importantly – have a high degree of confidance that the resulting design will be one that meets the requirements for the minimum cost !

At a high level there are at least two conditions which must be met for an assembly task to be successful. First the interaction forces developed during assembly must be small enough so that nothing is damaged (assembly parts, manipulators or fixtures). Secondly the direction of the force must be such that the parts to be assembled do not stick or jam.

Translating this conceptually simple requirement into quantitative, measurable performance specifications, for specific tasks, is a very complex problem. We have chosen end-effector impedance as our quantitative performance specification. Using end-effector impedance allows one to specify the performance requirements in terms of easily understood physical quantities. The end-effector requirements may be specified in terms of inertial (J), damping (B), and stiffness (K), characteristics. For example it may be specified that for a given steady-state position misalignment, x, the maximum force allowable at the end-effector is f. Along this direction the maximum stiffness of the

end-effector must then be limited to $K < \frac{f}{x}$.

We have limited our investigation to impedance specifications of the form

$$Z = K + Bs + Js^2 \qquad (4-1)$$

where:

Z is the impedance,

K, B, J are equivalent to stiffness, damping, inertial parameters,

s is the Laplace operator.

along each Cartesian axis. Thus we are defining the end-effector to behave like a mass-spring-damper system. For most of the experimentation accomplished to date we have set $J = 0$, so that we model the desired system behavior as a spring-damper combination.

Three directions have been followed in our investigation of dynamic performance requirements. Using a very simple task we have attempted to analytically predict the required impedances to accomplish the task. For more complex tasks we have begun to develop simulation tools to enable us to predict required impedance specifications. For complex tasks, such as those which would be encountered in an actual work environment, we are exploring empirical methods to finding the optimum performance specifications.

The results from these investigations indicate that deriving impedance specifications to satisfy the restriction on maximum applied force to prevent damage can be developed easily and can be specified early in the design process. Simple analytic techniques can be employed to obtain these specifications. Meeting the requirement on proper force direction to prevent jamming is much more difficult to specify analytically. The results of the analytical efforts on simple tasks can provide considerable insight into the directions to be pursued for the empirical investigations. Empirical studies can relatively quickly characterize the required impedances for a specific task.

4.1 Analytic Derivation of Performance Requirements

The ultimate goal of this approach is to develop techniques which may be incorporated into CAD/CAE systems so that when products are designed for robotic assembly the required impedance specifications for the assembly will be automatically output.

This specific investigation has focused on two goals; to develop techniques to derive bounds on impedance specifications, based on saftey requirements; and to derive impedance requirements for a very simple assembly task and experimentally verify the approach.

4.1.1 Analytic Bounds on Impedance Specifications

Recall that the general form of the impedance specification we are using is given by

$$Z = Js^2 + Bs + K. \qquad (4-2)$$

Assume that the maximum applied force before damage results is F_M. If the maximum possible misalignment during assembly is ΔX_M (possibly because of accuracy limitations of manipulator), then the maximum value for the stiffness specification, K, is given by

$$K = \frac{F_M}{\Delta X_M}. \qquad (4-3)$$

Similarly if the maximum velocity difference between the assembly parts is given by $\Delta \dot{X}_M$, then the maximum value for the damping specification, B, will be

$$B = \frac{F_M}{\Delta \dot{X}_M}. \qquad (4-4)$$

Likewise the maximum value for the inertia specification, J, assuming a maximum acceleration difference of $\Delta \ddot{X}_M$, is

$$J = \frac{F_M}{\Delta \ddot{X}_M}. \qquad (4-5)$$

These maximum values for K, B, and J assume the forces generated due to ΔX, $\Delta \dot{X}$, $\Delta \ddot{X}$, will never occur in combination with each other. To account for this possibility, the maximum value of K,B and J must be related so that

$$F_M \geq J\Delta \ddot{X}_M + B\Delta \dot{X}_M + K\Delta X_M. \qquad (4-6)$$

Figure 4-1 is a graphical representation of this relationship. The region enclosed by the tetrahedron is the region of allowable impedance specifications.

This analysis may be performed for each Cartesian axis, and from it a bound on the allowable impedances may be derived.

Assuming that we know the maximum allowable force levels, and the maximum errors in position, velocity and acceleration, it is possible to bound the range of allowable impedances for virtually any task! This then is the first step in deriving dynamic performance requirements. This step can be accomplished fairly early in the conceptual design stage, and will be iterated upon throughout the preliminary design.

4.1.2 Planar Insertion Task

To analytically derive impedance requirements for a successful task completion we took the very simple task of a planar insertion, with a fixed angle chamfer, and considered only translational misalignments. Figure 4-2 shows the task. For the task to be successfully completed the peg must contact the chamfer and exhibit enough compliance to slide along the chamfer and enter the slot.

To predict the success or failure of this task it is only neccessary to examine the contact point of the peg on the chamfer and the applied force at this contact point. If the direction of the applied force is correct the peg will slide along the chamfer and into the slot. If not the peg will stick along the chamfer.

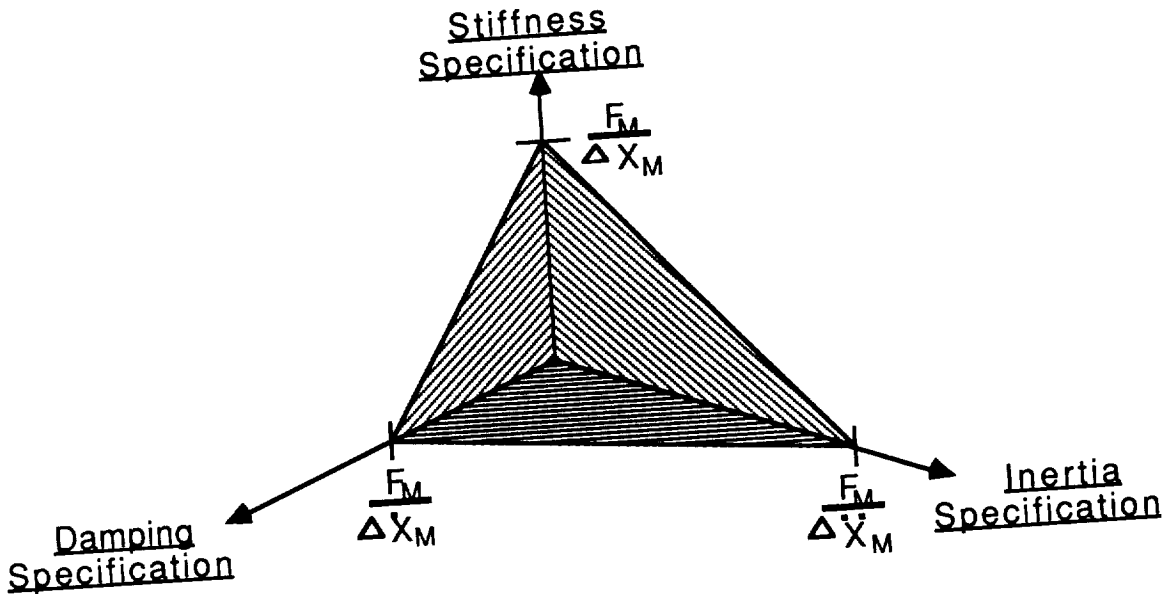

Figure 4-1: Region of allowable impedance specifications.

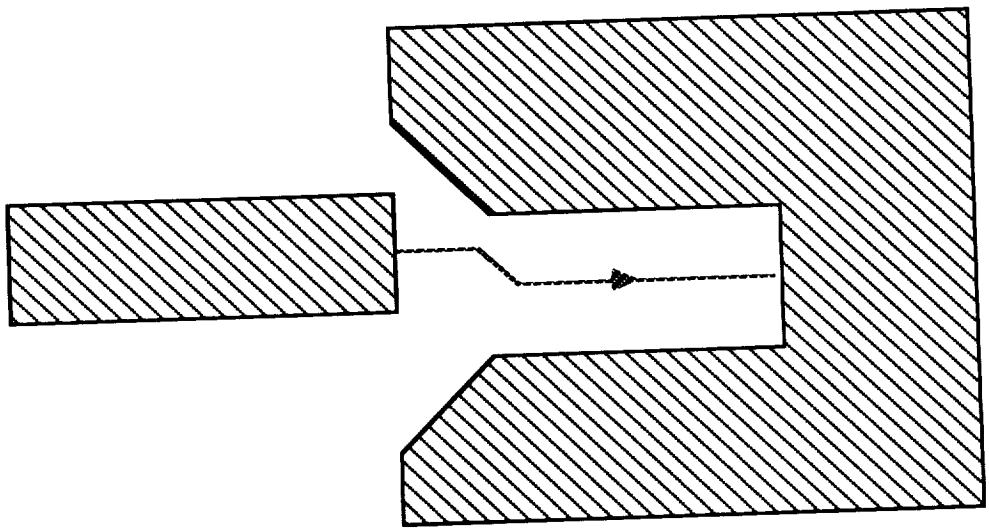

Figure 4-2: Planar insertion task

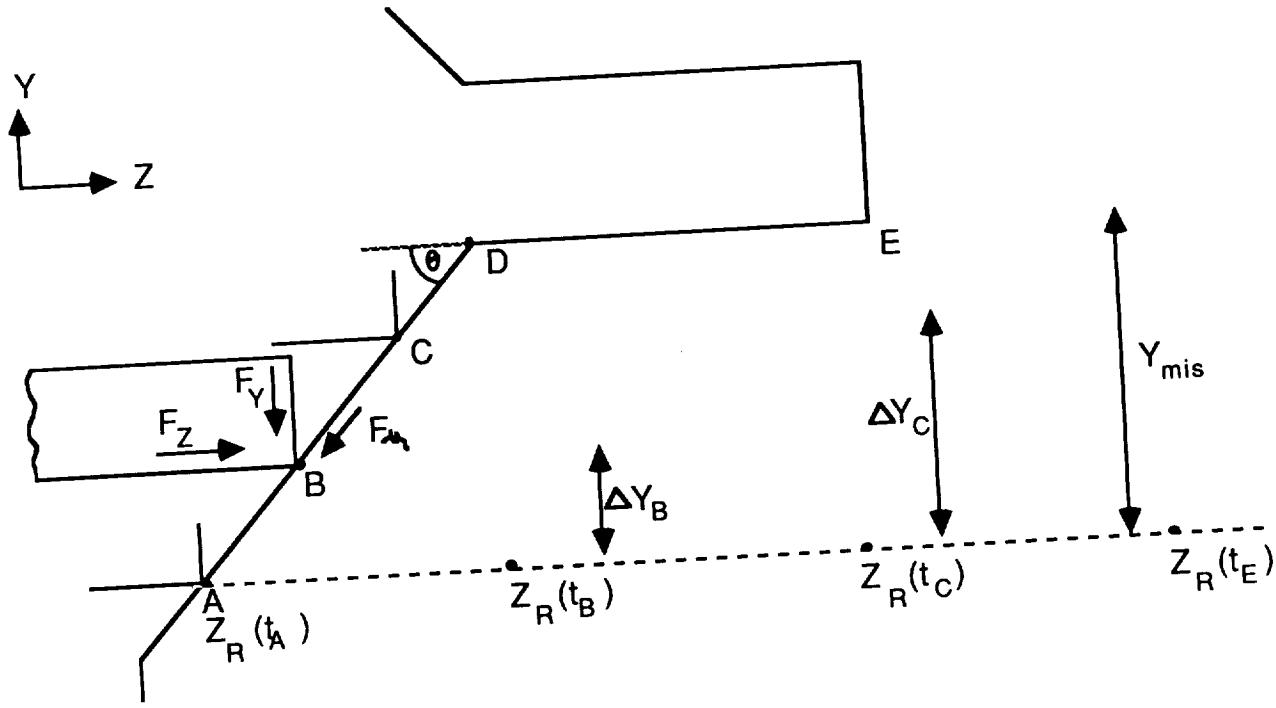

Figure 4-3: Forces acting at contact point

Figure 4-3 shows the contact point of the peg on the chamfer and the various forces acting at this contact point. The impedance of the peg, in the Cartesian Y and Z axes is specified as

$$Z_y = B_y s + K_y \tag{4-7}$$

$$Z_z = B_z s + K_z. \tag{4-8}$$

The chamfer and slot is assumed to be rigidly attached to ground.

The forces F_y and F_z are the result of errors between the peg's actual position and its reference position. The friction force, F_μ , is simply the normal components of F_y and F_z multiplied by the friction coefficient,μ.

The dotted line shows the reference trajectory. At time t_A the peg first contacts the chamfer, so that the actual and reference positions are identical. At time t_B the reference position is inside the assembly, because the assembly is misaligned by an amount Y_{mis}. The force F_y is given by

$$F_y = B_y \dot{Y} + K_y \Delta Y_B, \tag{4-9}$$

where:
$\dot{Y}$ is the peg velocity in Y direction,
ΔY_B is the Y component of distance peg has moved along chamfer.

The force F_z is likewise given by

$$F_z = B_z \Delta \dot{Z}_B + K_z \Delta Z_B, \tag{4-10}$$

where:

$$\Delta \dot{Z}_B = \dot{Z}_R(t_B) - \dot{Z}(t_B),$$

$$\Delta Z_B = Z_R(t_B) - Z(t_B).$$

Notice that F_y is not explicitly a function of the reference trajectory while F_z is a very strong function of the reference trajectory,Z_R. For the task to be successfully completed the reference trajectory and the peg impedance must be such that the peg complies along the chamfer to point D, and into the slot to point E.

The peg will continue to move along the slot as long as the component of F_z tangential to the chamfer is greater than the sum of F_μ plus the component of F_y tangential to the chamfer. Notice that as the peg moves further along the chamfer towards D the force F_y is increasing, because ΔY is increasing.

The resultant force of F_y and F_z may be described by a force component normal (F_N) to the chamfer, and a component tangential (F_T) to the chamfer. Refering back to figure 3, these forces are defined as

$$F_N = F_y \cos\theta + F_z \sin\theta \quad \text{(4-11)}$$

$$F_T = F_z \cos\theta - F_y \sin\theta \quad \text{(4-12)}$$

where:

θ is the chamfer angle.

As long as F_T is greater than F_μ the block will move along the chamfer in the correct direction.Recall that $F_\mu = F_N \mu$. The condition to prevent jamming is then

$$F_z(\cos\theta - \mu\sin\theta) > F_y(\sin\theta + \mu\cos\theta) \quad (4-13)$$

In examining conditions for jamming we will derive conditions for two cases, first for the peg jamming along the chamfer and second for the peg jamming along the slot, before reaching point E. The greatest possibility for jamming along the chamfer will occur just before point D, since this is the largest value for Y_{mis}. At the jamming condition $\Delta\dot{Y}$ and $\Delta\dot{Z}$ are both zero, therefore F_y and F_z are given by

$$F_y = K_y Y_{mis} \quad \text{(4-14)}$$

$$F_z = K_z(Z_R(t_f) - Z_D). \quad \text{(4-15)}$$

The jamming condition may now be written as

$$K_z(Z_R(t_f) - Z_D)(\cos\theta - \mu\sin\theta) = K_y Y_{mis}(\sin\theta + \mu\cos\theta). \quad (4-16)$$

The jamming condition for the peg jamming in the slot is much simpler. To prevent jamming, the direction of the force vector at point E must be such that the peg would continue moving into the slot if it could. Therefore to prevent jamming it is only necessary to look at the force balance at point E. At point E the friction force is given by $F_\mu = Y_{mis}\mu$. The tangential force, $F_N = F_z$. Therefore to prevent jamming along the slot it is only neccessary that

$$K_z(Z_R(t_f) - Z_E) > Y_{mis}\mu. \quad (4-17)$$

We will now derive the jamming conditions for a specific example. For this example

$$\begin{aligned} \theta &= 45^\circ \\ Y_{mis} &= 3.25cm \\ Z_D &= 3.25cm \\ Z_E &= 5.00cm \\ Z_R(t_f) &= 8.00cm \end{aligned}$$

Using the above values and referring to (4-16) the condition to prevent jamming is

$$K_z(1-\mu) > 0.684 K_y(1+\mu). \qquad (4-18)$$

Notice that there is a maximum allowable value for μ to prevent jamming. If $\mu \geq 1$ the peg will always stick on the chamfer, regardless of the values for K_z, K_y, or $\triangle z$. For a specific value of $\mu < 1$, there is also a minimum ratio of stiffness specifications to prevent jamming. The ratio of K_z to K_y is given as

$$\frac{K_z}{K_y} = 0.684(1+\mu)(1-\mu), \qquad \mu < 1. \qquad (4-19)$$

The slot and peg both are made of T6061 aluminum. The coefficient of friction is unknown since it is very dependent on the surface finish of the slot and peg, and these surfaces were not machined to a specific finish. Therefore it is not possible to predict the stiffness ratio at which jamming will occur. Four experiments were run using different stiffness ratios, to demonstrate the effect of stiffness ratio, and to see whether the μ value which fit these experimental results was reasonable.

A block of aluminum witha 45° angle cut, was held by the second robot, whose impedance was set very high ($K = 70 Nt/cm$, $B = 35 \frac{Nt-sec}{cm}$). The first robot held an aluminum peg, and its impedances in the Y and Z axes were adjusted over a small range The commanded path was set up as close as possible to that described in the above example. The level of damping specified for the first robot was neccessary to preserve stability - lowering the damping caused the system to approach instability. The axis system for the experiments was rotated, so that the reference trajectory is along the Y axis.

Figure 4 shows the results using the following impedances:

$$\begin{aligned} Z_y: \quad & B_y = 1.5 \frac{Nt-sec}{cm}, \; K_y = 0.62\, Nt/cm \\ Z_z: \quad & B_z = 1.5 \frac{Nt-sec}{cm}, \; K_z = 0.035\, Nt/cm. \end{aligned} \qquad (4\text{-}20)$$

The stiffness ratio for this experiment is $K_y/K_z = 17.5$. For this large stiffness ratio the maximum allowable friction coefficient to prevent jamming is $\mu = 0.92$. From Figure 4 the peg successfully travels past the edge of the chamfer and into the slot.

Figure 5 shows the results using the following impedances:

$$Z_y: \quad B_y = 1.5\,\frac{Nt-sec}{cm},\ K_y = 0.62\ Nt/cm$$
$$Z_z: \quad B_z = 1.5\,\frac{Nt-sec}{cm},\ K_z = 0.15\ Nt/cm. \tag{4-21}$$

These impedences result in a maximum allowable friction coefficient of $\mu = 0.72$ to prevent jamming along the chamfer.

Figure 6 shows the results using the following impedances:

$$Z_y: \quad B_y = 1.5\,\frac{Nt-sec}{cm},\ K_y = 0.62\ Nt/cm$$
$$Z_z: \quad B_z = 1.5\,\frac{Nt-sec}{cm},\ K_z = 0.35\ Nt/cm. \tag{4-22}$$

The stiffness ratio for this experiment is $K_y/K_z = 1.8$. The maximum allowable friction coefficient for successful insertion past the chamfer is $\mu = 0.44$.

All three of the above experiments show the peg successfully pasing over the chamfer and into the slot. As the stiffness ratio decreases the force levels show increased oscillation as the peg travels along the chamfer.

Figure 7 shows the results using the following impedances:

$$Z_y: \quad B_y = 3.5\,\frac{Nt-sec}{cm},\ K_y = .18\ Nt/cm$$
$$Z_z: \quad B_z = 3.5\,\frac{Nt-sec}{cm},\ K_z = .18\ Nt/cm. \tag{4-23}$$

The stiffness ratio for this fourth experiment is 1. From Figure 7 it can be seen that the peg stuck after travelling almost 1 inch along the chamfer. This indicates that the friction coefficient must be at least $\mu = 0.19$. Referring back to (4-16), and using Figure 7 to obtain approximate values for y_{mis} and $Z_R(t_f)$, a closer approximation to the friction coefficient can be estimated as $\mu \approx 0.44$.

The above experiments indicate that for successful task completion the stiffness ratio should be greater than 1.8. The apparent contradiction in the friction coefficient values predicted by experiments 3 and 4 is due to the crudeness of the experimental setup. The angle of the slot is only know to about $4°$, and the distance accuracy is only known to about 0.25 cm. Also the surface finish of the chamfer is not uniform, since as the peg contacts the chamfer it will slightly dent it. To reduce this effect the chamfered surface was resurfaced using a file every few experiments.

The above experiments show the effect of the friction coefficient on performance. Accurate knowledge of μ will be extremely important in analytically predicting performance, especially in situations where minimum forces are required to prevent breakage,

and it is not possible to generate large tangential forces to overcome a broad range of friction coefficients.

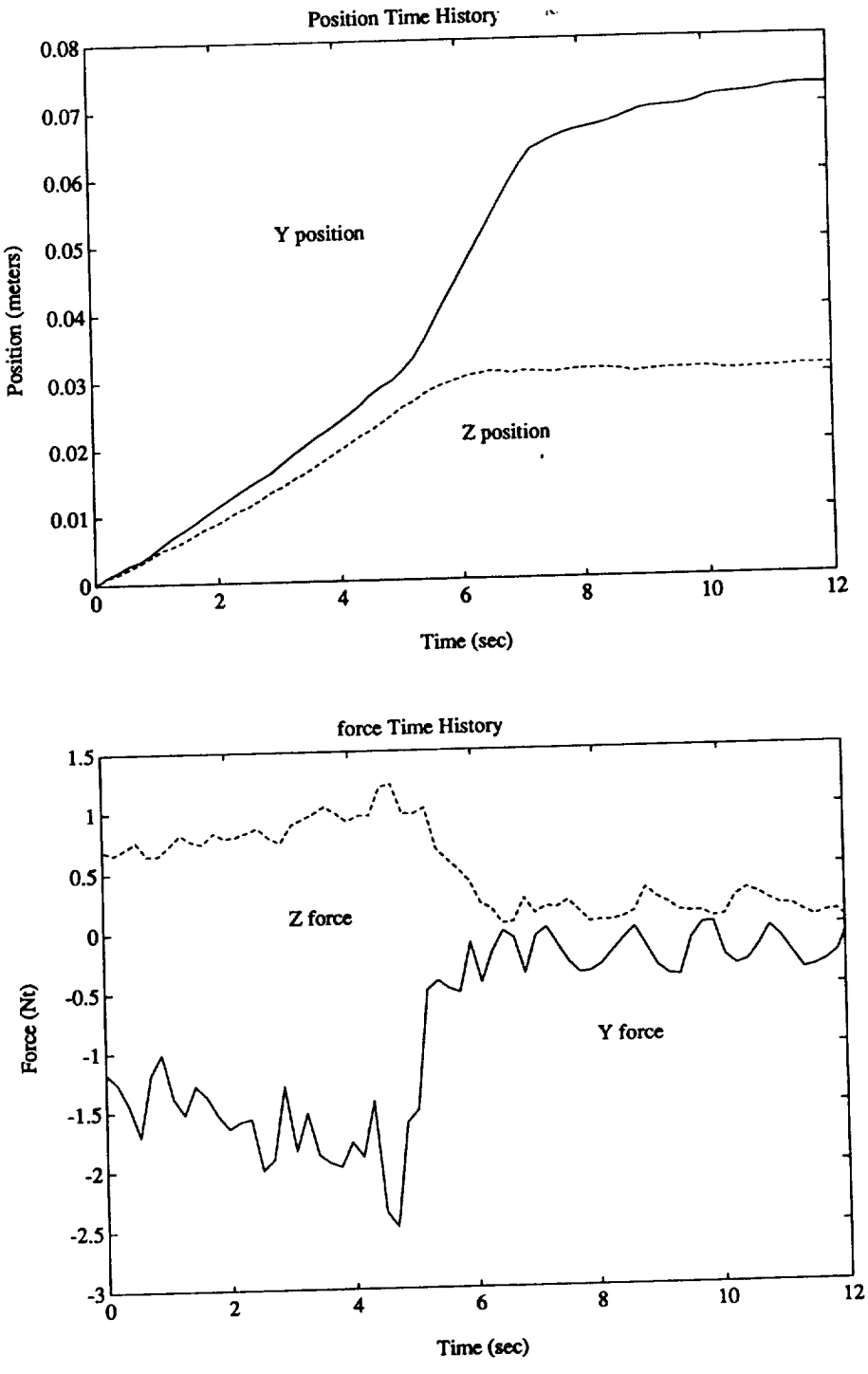

Figure 4-4: Position and force time histories for $K_y/K_z = 17.5$

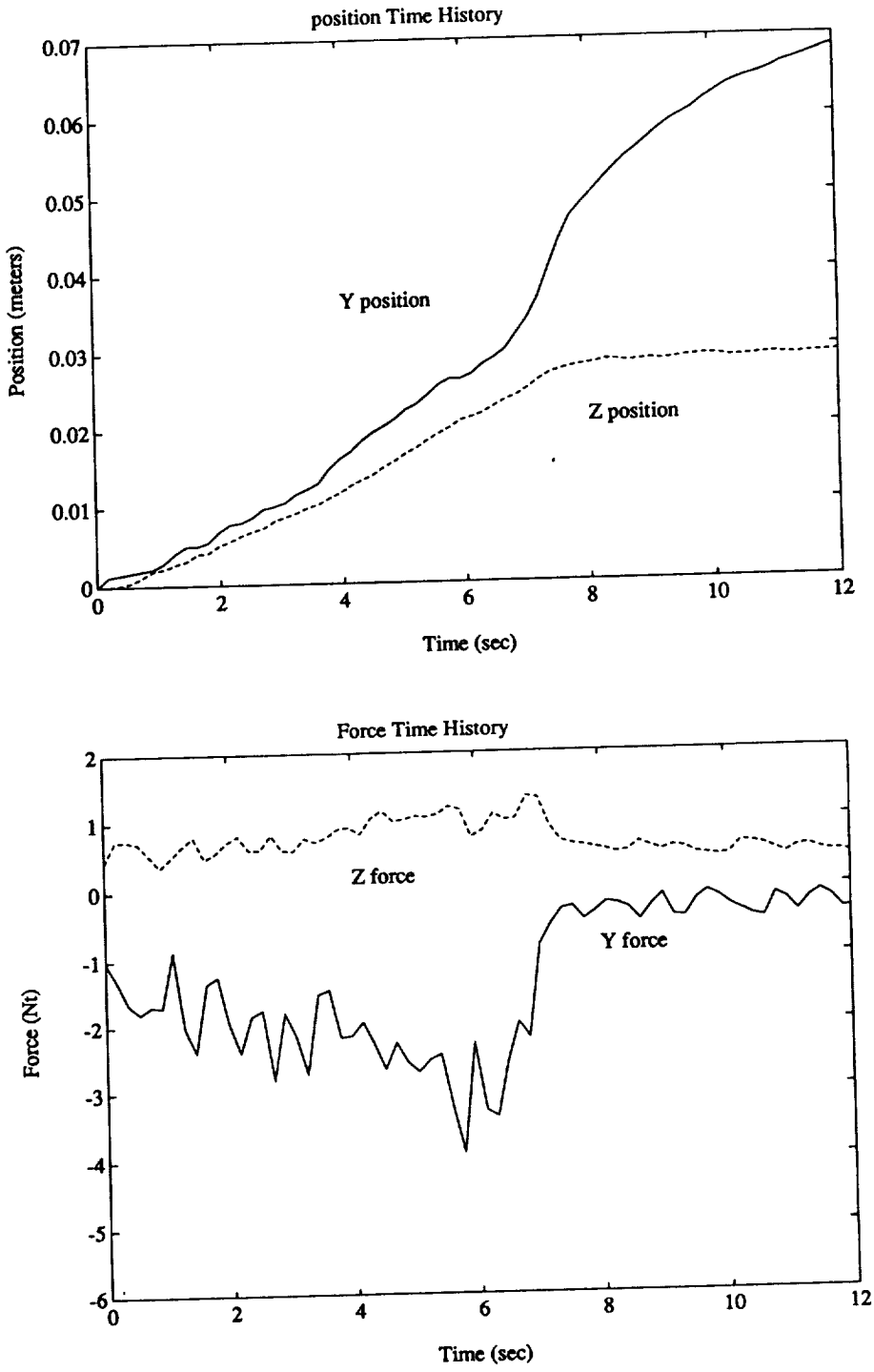

Figure 4-5: Position and force time histories for $K_y/K_z = 4.1$

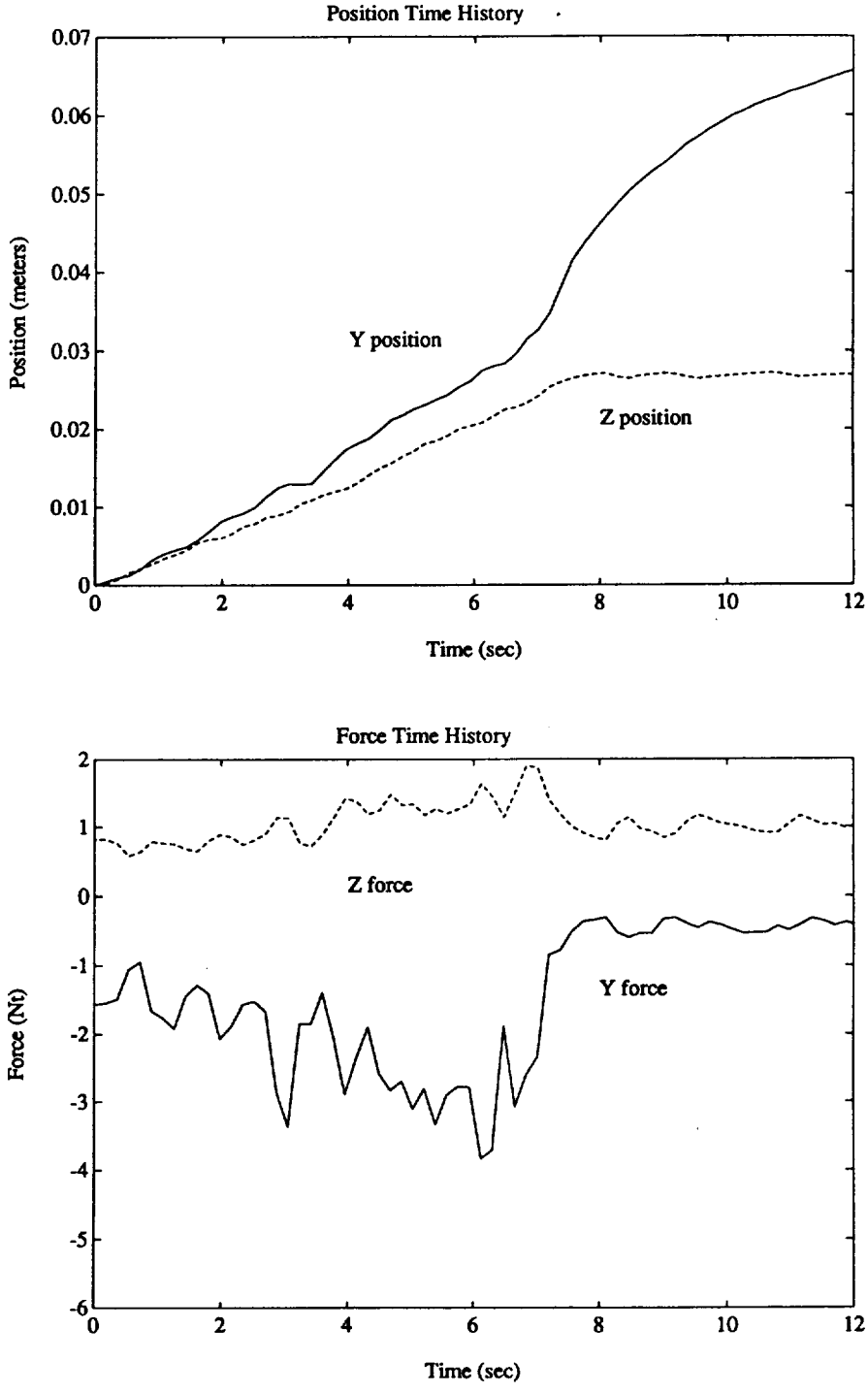

Figure 4-6: Position and force time histories for $K_y/K_z = 1.8$

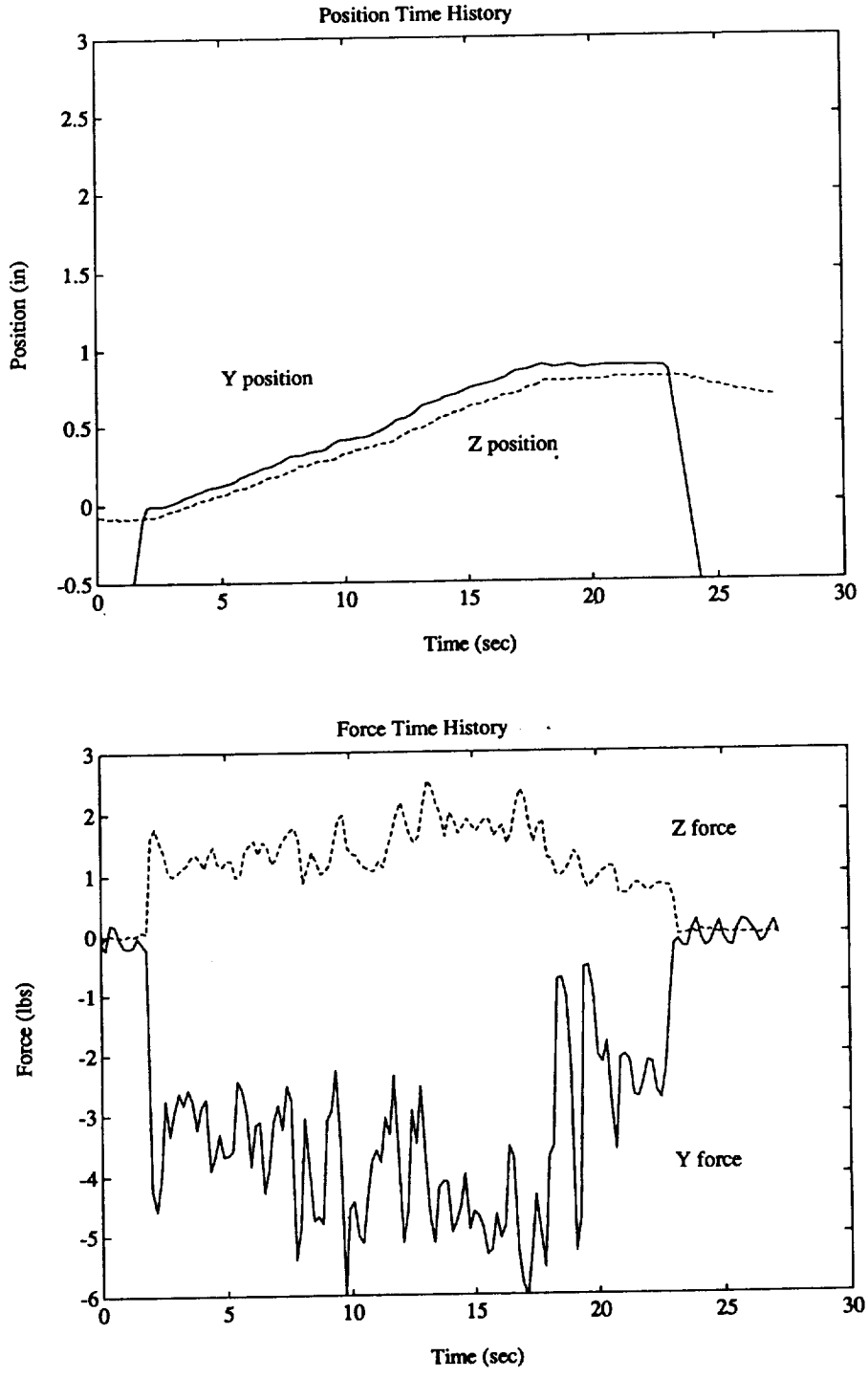

Figure 4-7: Position and force time histories for $K_y/K_z = 1$

4.2 Simulation Approach to Performance Requirements

A slightly more complex task was used to begin development of simulation techniques . The task chosen for this investigation was a planar insertion with both translational and rotational misalignments. Figure 5 is a diagram of this task, showing the force interaction between the peg and the slot. We have concentrated on developing a simulation of the peg and slot interaction. The simulation is being developed as a combination of user-defined blocks integrated into the $MATRIX_X$ simulation and control package.

4.2.1 Analytical model

A simplified, planar peg dynamics is described by the following uncoupled equations of motion:

$$M\ddot{y} = f_y - \mu(f_1 + f_2)\text{: translational motion in y direction} \qquad (4-24)$$

$$I\ddot{\alpha} = m_z - f_2 l - \mu r f_x\text{: rotational motion about } O_z \qquad (4-25)$$

where:

M = peg mass.
I = peg inertia about body O_z axis.
f_y, m_z = applied force and moment.
μ = coefficient of friction.
f_1, f_2 = normal forces at contact points = $(K_{stiff})(\triangle y_i)$, i = 1 , 2 .
K_{stiff} = spring stiffness at the contact point.
$\triangle y_i$ = spring deformation at contact point i.
l = peg inserted depth.
r = peg radius.

Note that the assumptions made here are:

- peg motion is in the X-Y plane.
- uncoupled motion.
- small misalignment angle between peg and hole.
- rigid peg and hole.

A very detailed analysis of the insertion process was given by Whitney in Ref [1].

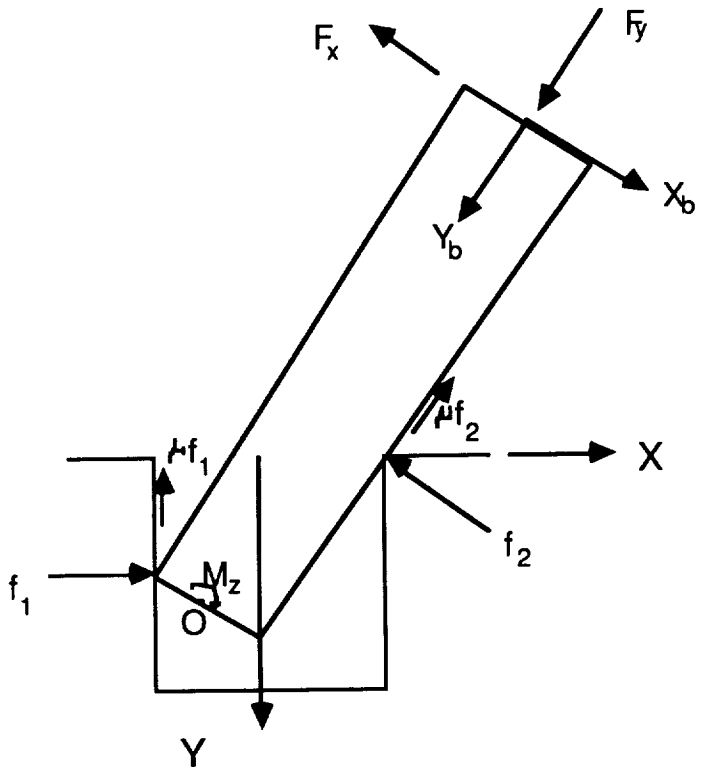

Figure 4-8: Force diagram at two point contact.

4.2.2 Simulation model

The insertion simulation is set up using the System Build function in $MATRIX_X$. The simulation program contains 4 different user - defined blocks:

- peg geometry description block.
- task geometry description block.
- contact force determination block.
- peg dynamics block.

This will allow the user to modify any one of the blocks to tailor the simulation to their own particular task. The inputs, outputs, and inter-connection of these blocks are shown in figure 2.

Following is a detailed description of the current implementation in each one of the blocks :

Peg geometry description block

This block computes the corner point coordinates and edge coefficients in the body frame, based on the following inputs:

- peg initial position relative to the fixed hole frame coordinate.
- peg length l and width w.

- peg angle α and travel distance y from initial position.

Currently, the peg geometry is modeled as a rectangular formed by 4 straight lines in the X-Y plane. Therefore, the corner point coordinates are calculated as follows:

$$\begin{aligned} P_1(\tfrac{W}{2}, 0) \quad & P_3(-\frac{W}{2}, L) \\ P_2(\tfrac{W}{2}, L) \quad & P_4(-\frac{W}{2}, 0) \end{aligned} \tag{4-26}$$

The edge coefficients A, B, C are calculated using the line equation that passes 2 corner points $P_1(x_1, y_1)$, $P_2(x_2, y_2)$, as followed:

$$Ax + By + C = 0$$

where:

$$A = \begin{cases} -\frac{y_2 - y_1}{x_2 - x_1} & \text{if } x_1 \neq x_2 \\ 1.0 & \text{if } x_1 = x_2 \end{cases}$$

$$B = \begin{cases} 1.0 & \text{if } x_1 \neq x_2 \\ 0.0 & \text{if } x_1 = x_2 \end{cases}$$

$$C = \begin{cases} -By_1 - Ax_1 & \text{if } x_1 \neq x_2 \\ -x_1 & \text{if } x_1 = x_2 \end{cases}$$

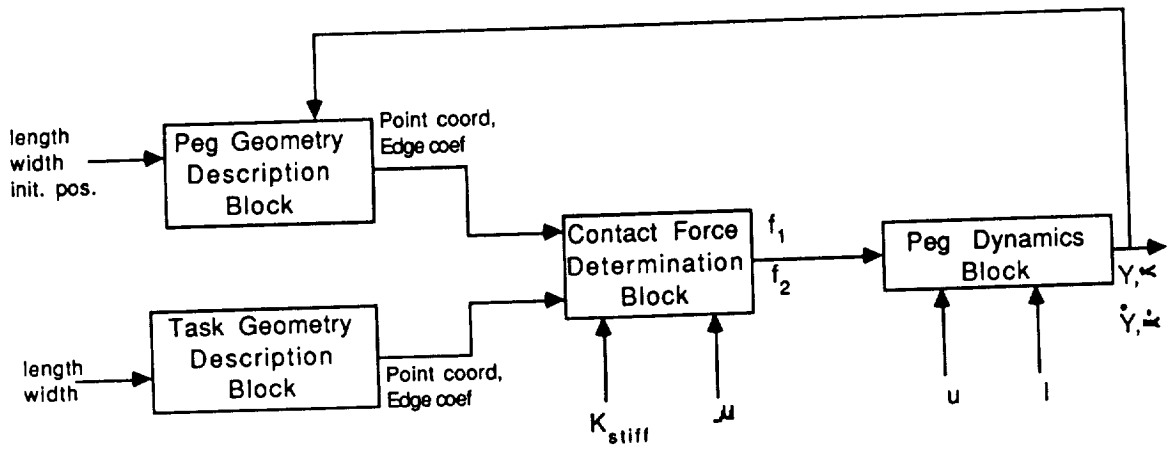

Figure 4-9: Flow diagram of the insertion simulation model.

Outputs from this block are:

- corner point coordinates
- edge coefficient

Task geometry description block

Similar to the procedure described for the peg geometry block, except that no coordinate transformation is needed.

Contact force determination block

This block determines the number of contact points and the appropriate forces f_1, f_2 as described in the analytical model section. The distance $\triangle y_i$ between a point $P_1(x_1, y_1)$ and a line $Ax + Bx + C = 0$ is calculated as followed:

$$\triangle y_1 = \frac{Ax_1 + By_1 + C}{\sigma\sqrt{A^2 + B^2}}$$

where:

$$\sigma = \begin{cases} +1 & \text{if } C > 0 \\ -1 & \text{if } C < 0 \end{cases}$$

If $\triangle y_i \leq$ a contact ϵ, which is defined to be 1.e-5, then the contact force f_i is calculated as followed:

$$f_i = K_{stiff} \star \triangle y_i$$

Inputs to this block are:

- peg point coordinates and edge coefficients.
- task point coordinates and edge coefficients.
- contact spring stiffness and friction coefficient.

Outputs from this block are:

- contact forces f_1, f_2.

Peg dynamics block

This block determines the translational and rotational motion of the peg. The current implementation is shown in figure 3. Inputs to this block are:

- contact forces f_1, f_2.
- applied force f_y and moment m_z.
- compliant force f_x.
- peg mass M and inertia I.

Outputs from this block are:

- peg translational and rotational distance.

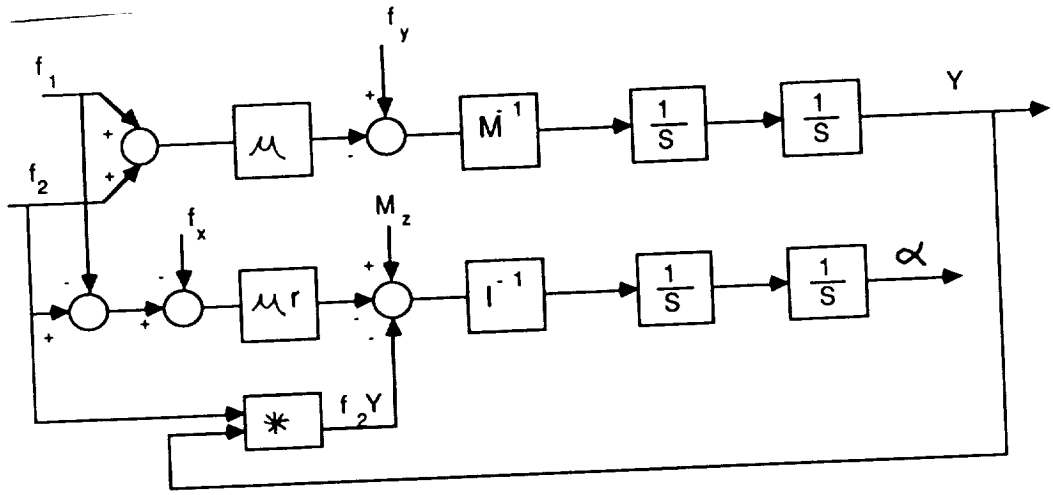

Figure 4-10: Peg dynamics block.

This task was pursued to the point where the individual user-blocks were developed. At that point it was decided that pursuing empirical techniques for deriving impedance specifications would be more valuable.

4.3 Empirical Approach to Performance Requirements

Virtually all of the assembly and other force interaction tasks envisioned for near-term applications are too complex to use either analytic or simulation methods to derive performance requirements. Instead near-term applications must depend on empirical methods for determining impedance specifications.

For this investigation we chose the task of connecting a candidate truss connector for the Space Station. Figure 11 shows this connector. Each half of the connector was mounted in one of the robot's end-effectors. The second robot was again programmed to have a very high impedance in all axes (to approximate a rigid attachment); however, there was an undetermined amount of compliance in the end-effector. The first robot had very high impedances in the rotational axes, while the impedances of the translational axes was varied to find the best set of impedance to accomplish the task.

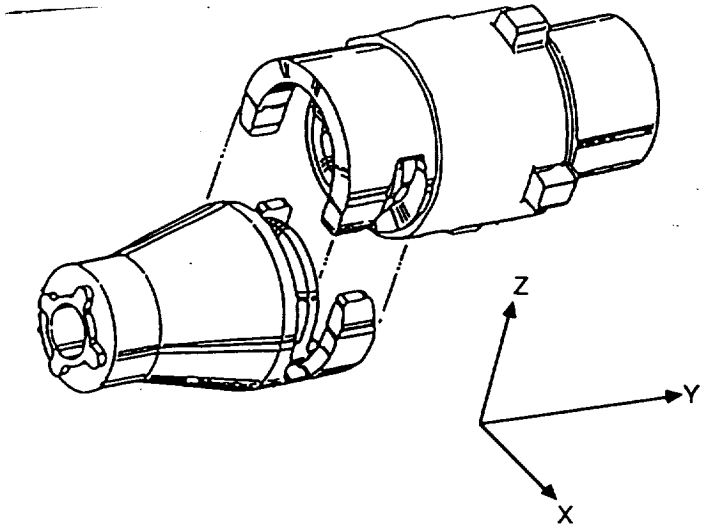

Figure 4-11: NASA truss connector used for performance requirements experiments.

The damping specification of robot 1 was kept at $1.26\frac{Nt-sec}{cm}$. With this relatively high damping specification it was necessary to use low velocities during the insertion/connection tests. Using a high velocity would have resulted in large end-effector forces, due to the damping specification, and it would be difficult to identify the effect of changing stiffnesses.

To choose the best set of impedances for the task three criteria were considered. First the task must be successfully completed. Second we tried to minimize the interface forces, and third we looked for a smooth insertion profile, with minimal sticking or bouncing

4.3.1 Test Setup

Figure 11 shows the connector used for this experiment. The connector may either be assembled in a manually locking mode or a self-locking mode. All the experiments to date have used the manually locking mode. This eases the assembly task since it is not necessary to overcome the spring force of the self-locking mechanism. The connector is designed so that fairly large misalignments in the X direction will still allow a smooth assembly (approx. 2cm max misalignment). In the Y direction the allowable misalignments are much smaller. Misalignments of more than approx 0.5 cm will result in a unsuccessful assembly. The connector is also very limited in the allowable rotational misalignments about the X and Y axes.

Two sets of experiments were performed, one with misalignments in the X axis and one with misalignments along the Y axis. From these experiments it is possible to choose a set of impedance specifications, along each of these axes, which ensures successful task completion.

4.3.2 X Axis Impedance Specification

To find the best impedance specification for X axis misalignments an autonomous assembly path was generated, with the X coordinate offset 1 cm. Various combinations of impedance specifications were tried and the position and force time histories of the assembly recorded.

Autonomous Path Description

Figure 12 shows the autonomous path used for this series of experiments. The connector halves begin 3.8 cm apart in Z direction and offset 1 cm in the X direction. The Y misalignment was made as small as possible. The upper half of the connector was then commanded to move at a velocity of 0.2 cm/sec, in the Z direction, to a position 0.5 cm below the fully engaged position. The X misalignment was maintained during this entire movement. The commanded position was maintained for 10 seconds, to allow transiants to decay, and then the connectors were commanded to separate.

Experimental Results for X Misalignments

For the first experiment the stiffness in the X direction was specified as 2.7 $\frac{Nt}{cm}$ and in the Z direction as 0.18 $\frac{Nt}{cm}$. Recall from the analytical derivation of impedance requirements, that the ratio of stiffness specifications is important in ensuring the parts don't jam. The stiffness ratio, K_x/K_z is very small (= 0.0667), for the assembly to be successful either ΔZ must be >> ΔX or the contact angle between the pieces must be very small. Figures 13 and 14 show the position and force time histories for the X and Z axes respectively. Notice in the Z position time history that the connector is jammed and makes almost no progress towards mating with the other half. The force in the Z direction is very

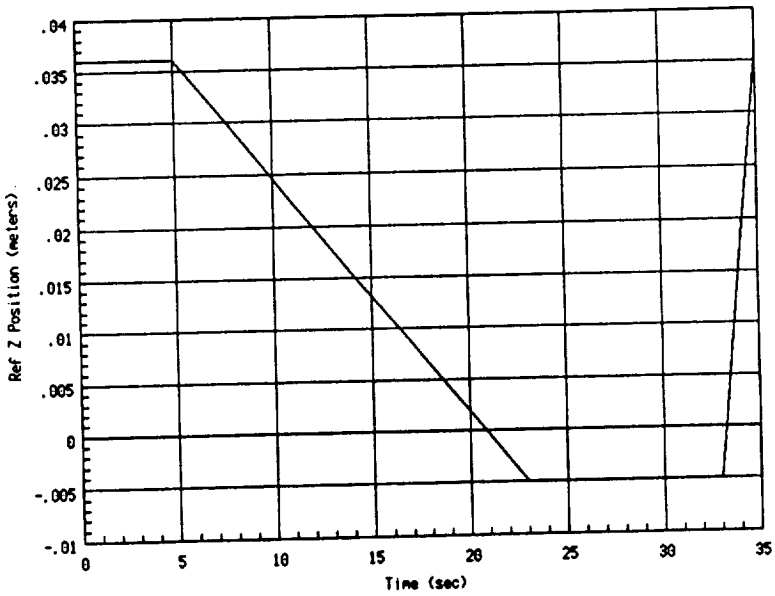

Figure 4-12: Reference path used for X misalignment experiments.

oscillatory and is increasing over the range 3 – 20 seconds (while ΔZ is increasing). While the forces, in X axis, are not very large (since stiffness very low) they do show a large, high frequency oscillation.

For the second experiment the stiffness in the Z axis was reduced to $1.8\frac{Nt}{cm}$. Figures 15 and 16 again show the position and force time histories for the X and Z axes, respectively. The X axis shows slightly more compliance (approx 2 mm), with about the same force levels as the first experiment. The Z axis position moves about 8 mm before jamming. The force again increases as the commanded Z position continues to move towards the mated position.

For the third experiment, the stiffness in the Z axis was reduced to 1.8 $\frac{Nt}{cm}$. Figures 17 and 18 show the X and Z axis time histories for this case. Notice that the X axis finally shows significant compliance, deflecting about 8 mm. The forces in the X axis are still small and don't show any appreciable change. The connector moves about 1 cm in the Z direction. The Z force shows a very slight decrease in peak amplitudes, to about 0.9 Nt.

For the fourth experiment the stiffness in the X axis was reduced to 0.54 Nt/cm. This corresponds to a stiffness ratio of 0.33. With this set of impedances it was possible to successfully complete the task. Figures 19 and 20 show the X and Z axis time histories. The X axis position complies 1 cm and then remains fairly stable, with only small oscillations. The force level remains small until the connectors are fully mated. At this point forces increase significantly. This increased force is caused by the increased stiffness of the connector halves in the fully mated position, and the affect of this stiffness on the stability of the first robot. The Z position time history shows a much smoother response. The force increases at first and then begins decreasing as the connector complies

down and seats itself.

For the fifth experiment we kept the same ratio of stiffness gains, $K_x/K_z = 0.33$. However, the values of both K_x and K_z were doubled to 1.08 and 0.36 respectively. Figures 21 and 22 again show the time histories in the X and Z axes. From the position time histories it is clear that the connector is tracking the commanded trajectory much closer. This is primarily the result of the increased stiffness in the Z axis. The forces in both axes show as approximate doubling in values — which is just as expected.

From this series of experiments it appears that, for a maximum possible X axis misalignment of 1 cm, the minimum stiffness ratio, K_x/K_z for successful task completion is 0.33. The actual stiffness values will be dependent on the maximum allowable force levels. The fifth experiment indicates that to get the best performance we should use the highest stiffness values possible without exceeding the maximum force limitations.

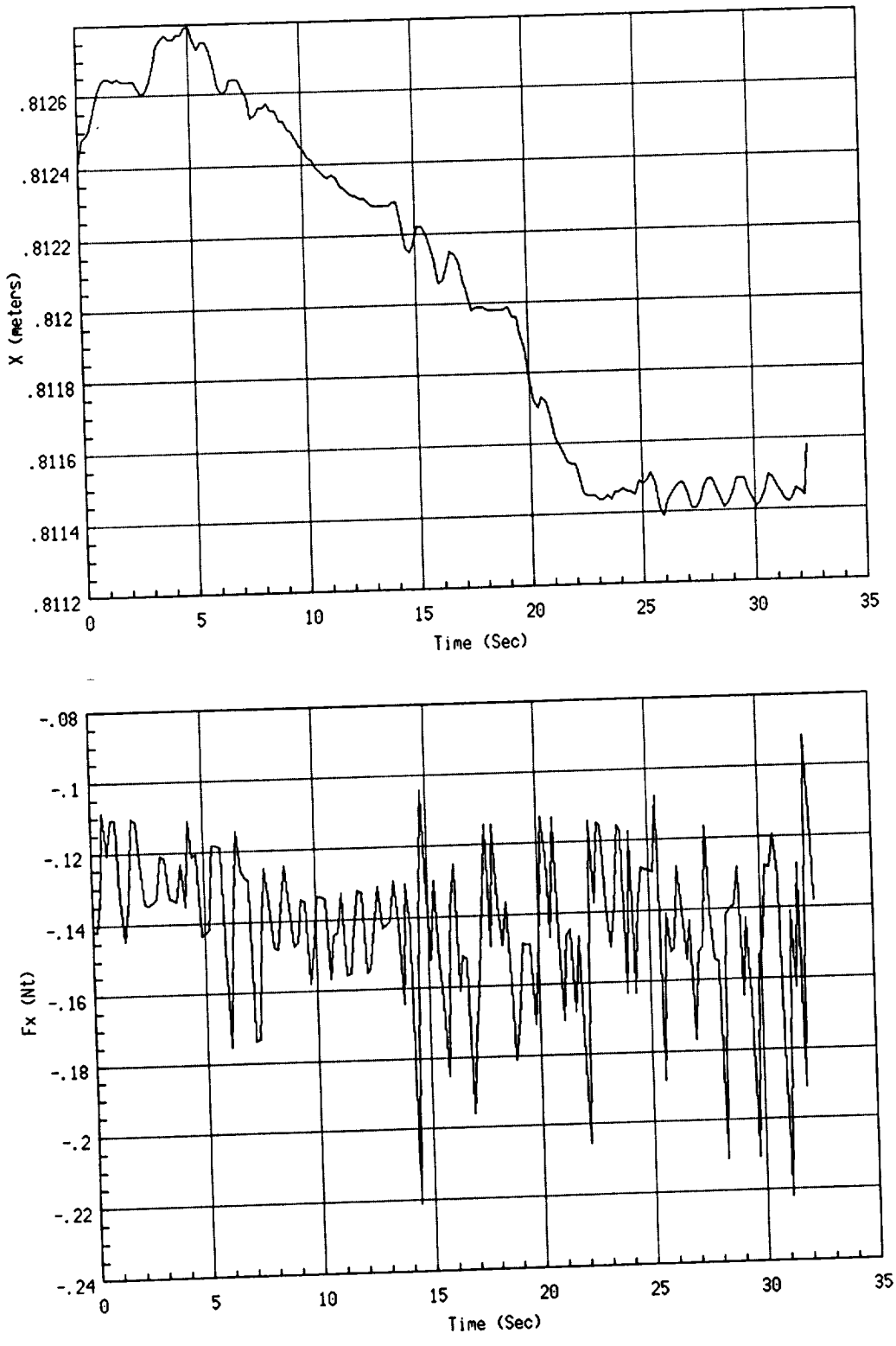

Figure 4-13: X Axis position and force time histories for experiment 1

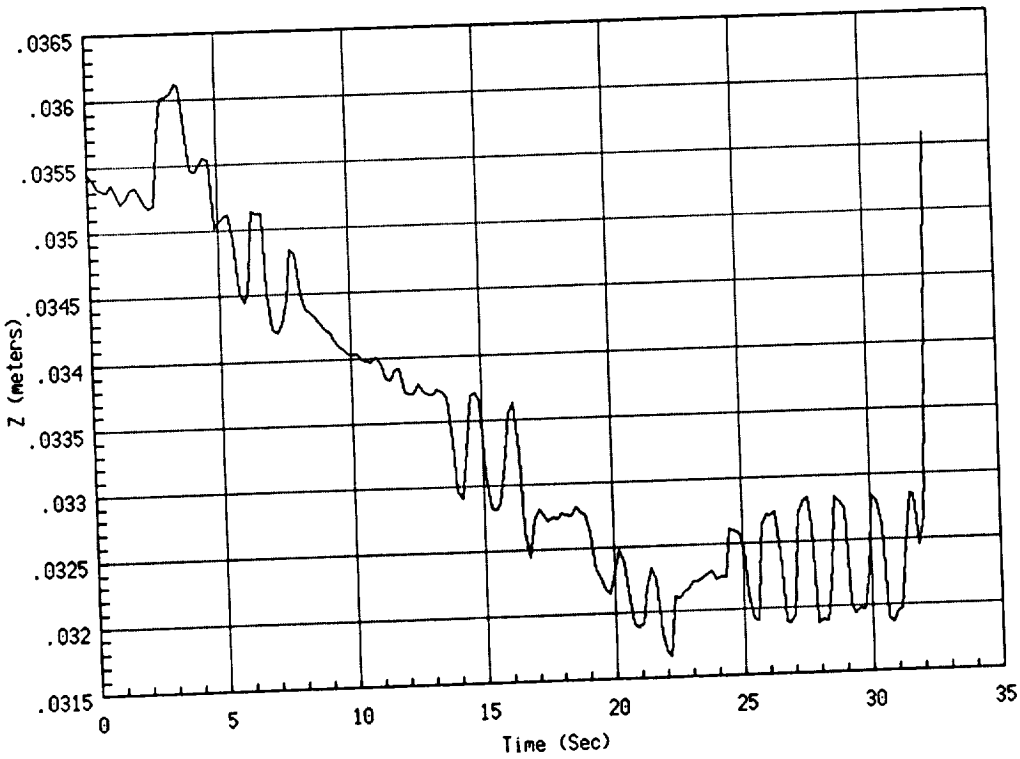

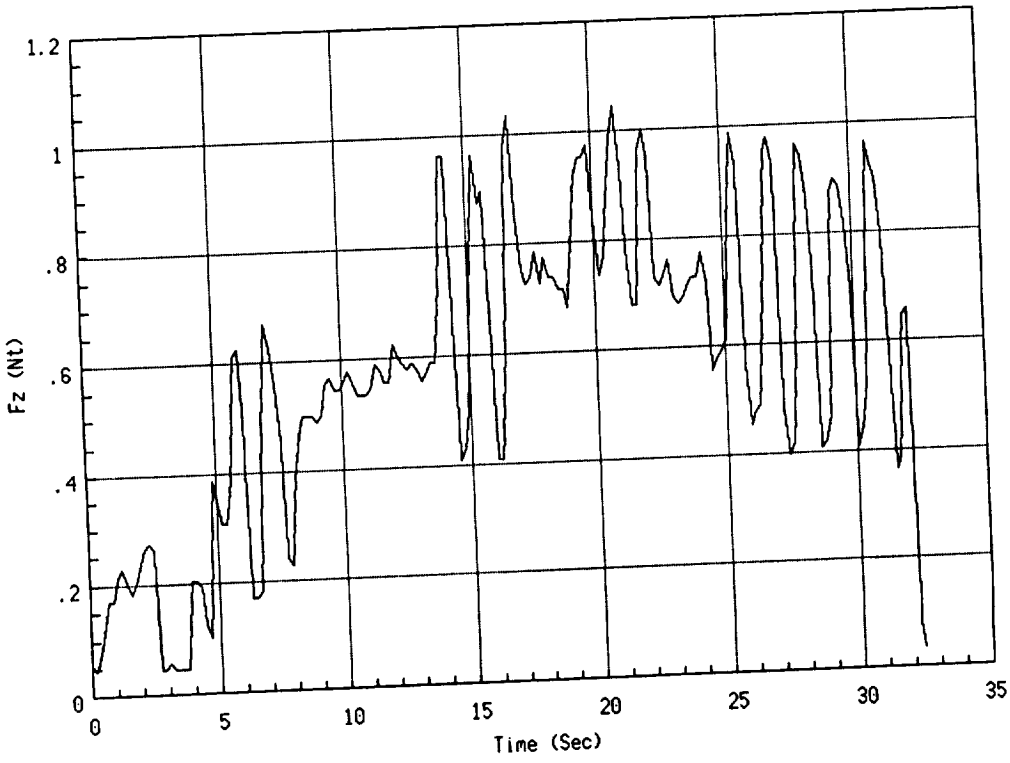

Figure 4-14: Z Axis position and force time histories for experiment 1

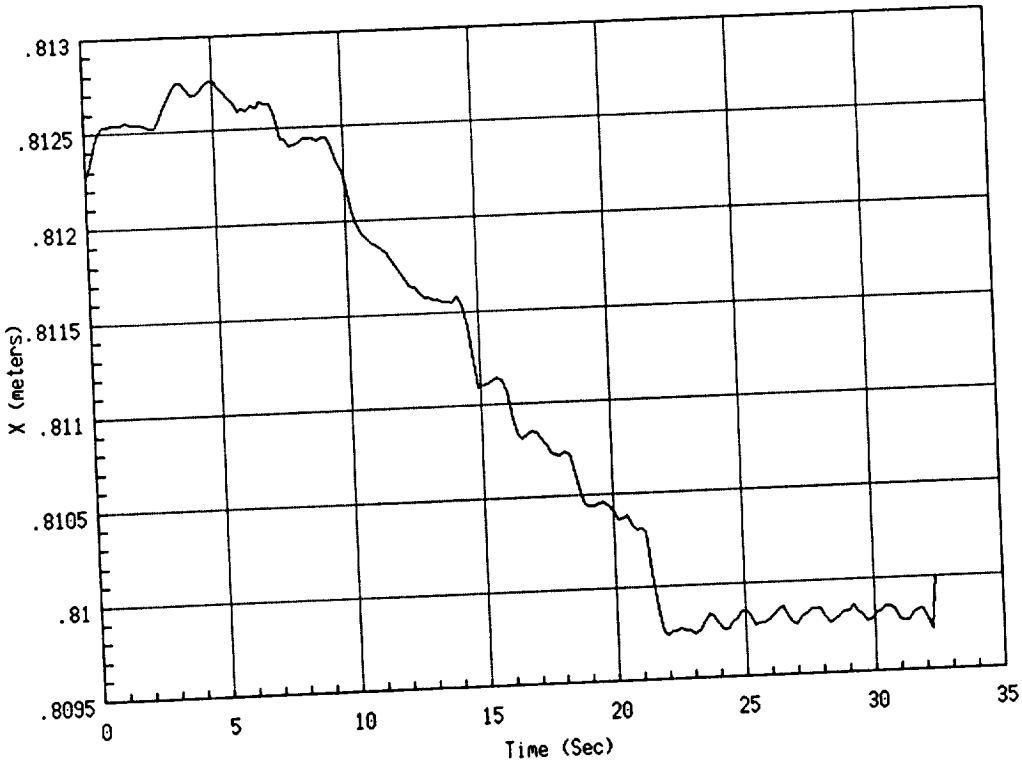

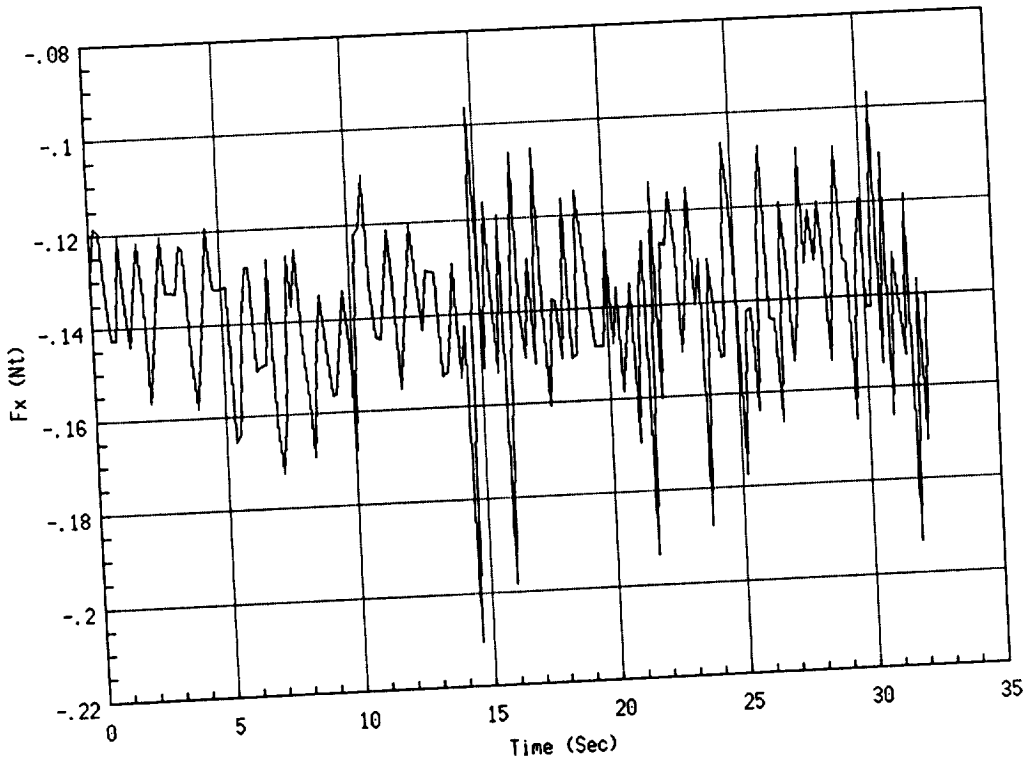

Figure 4-15: X Axis position and force time histories for experiment 2

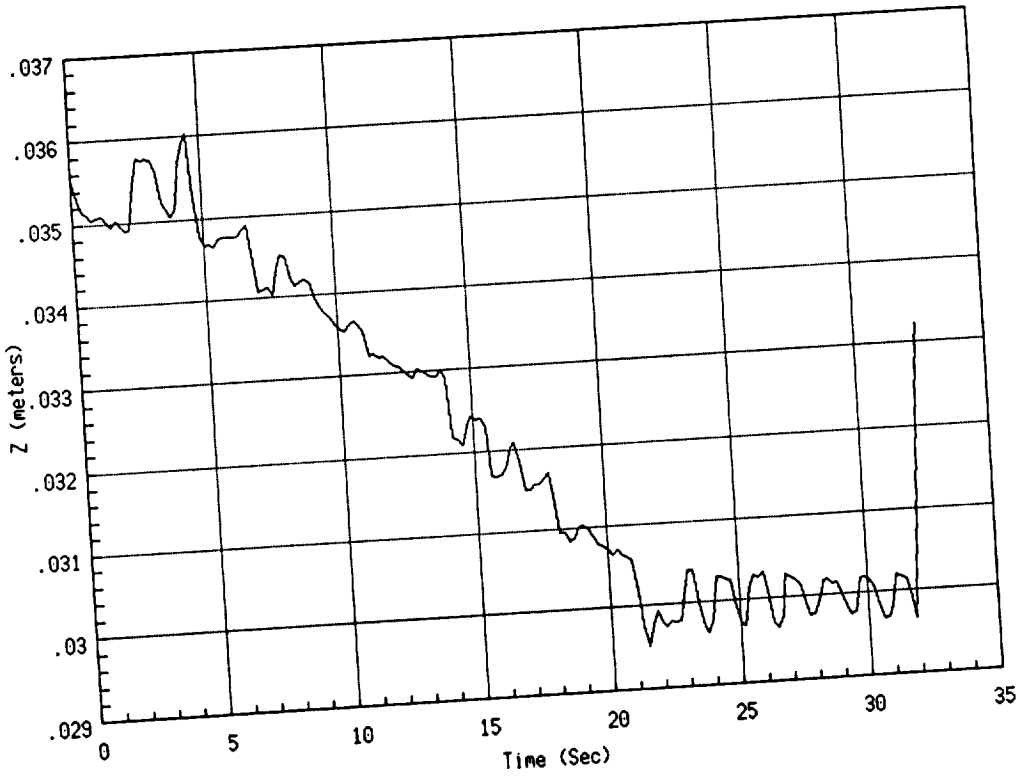

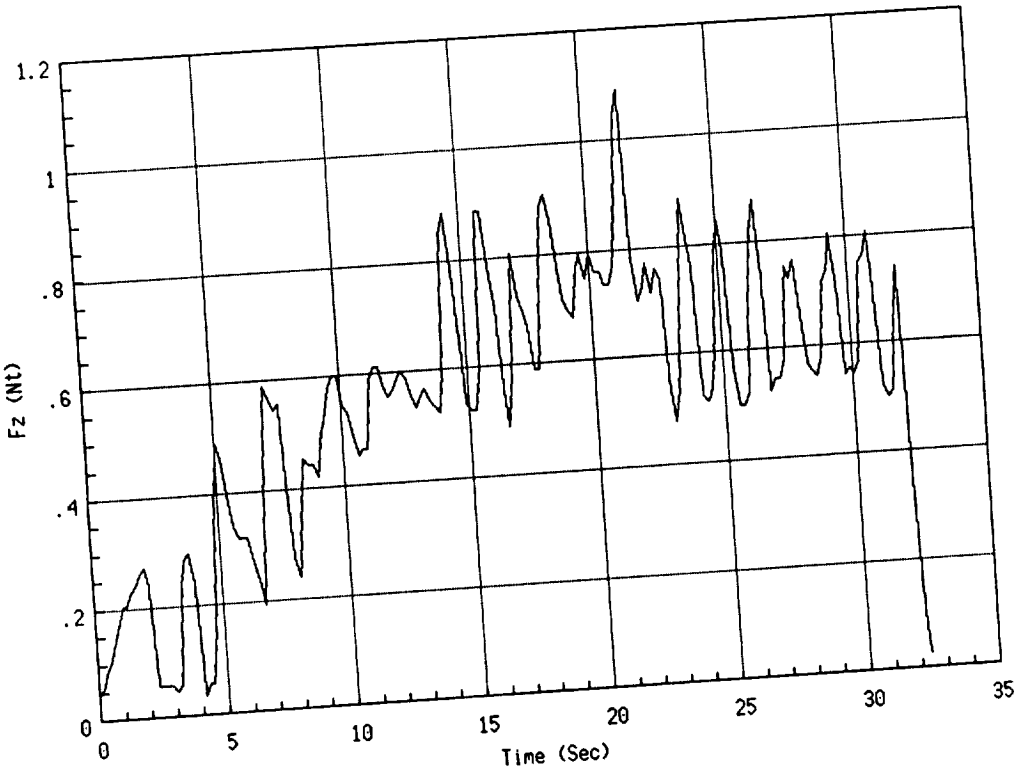

Figure 4-16: Z Axis position and force time histories for experiment 2

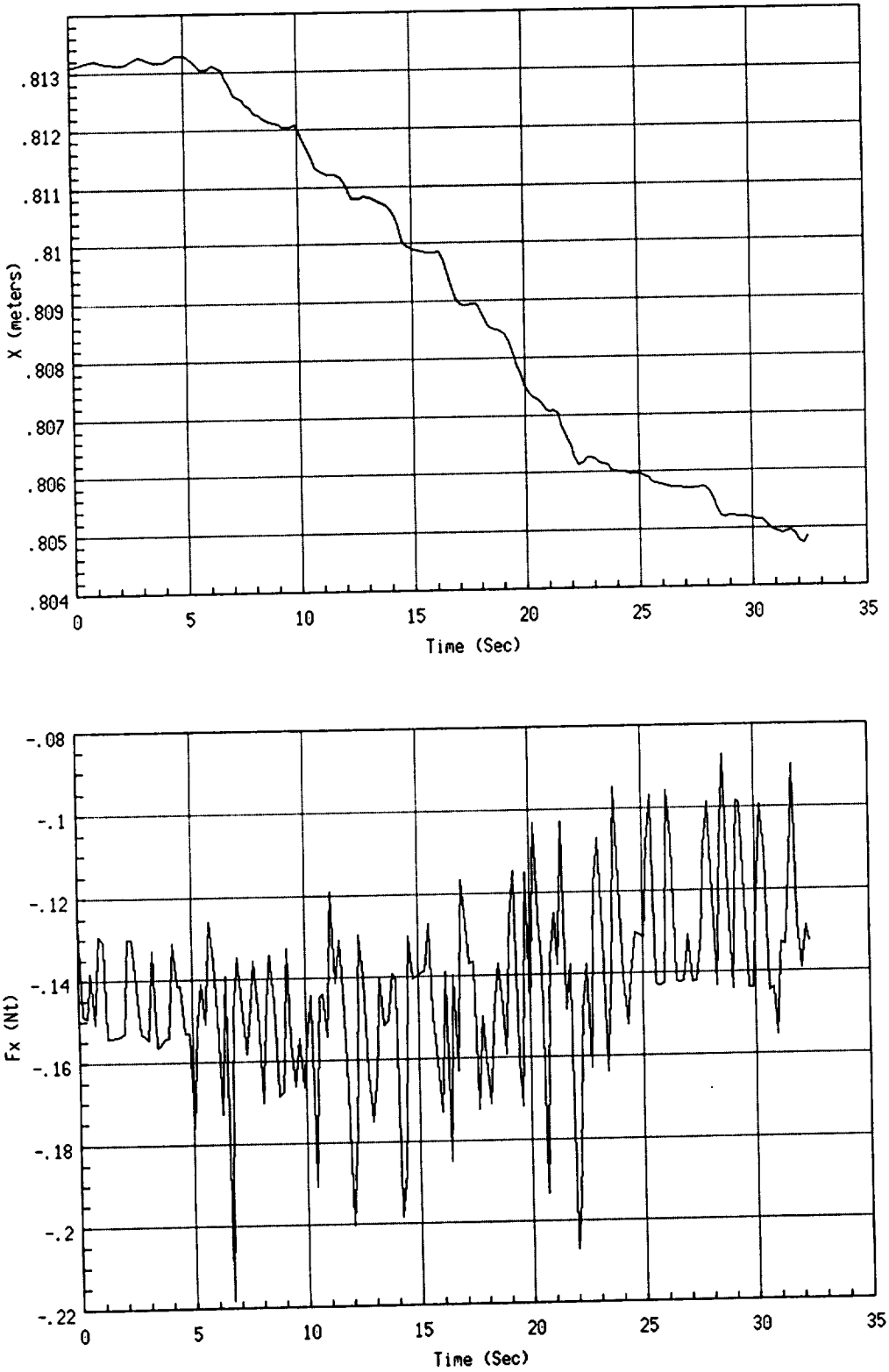

Figure 4-17: X Axis position and force time histories for experiment 3

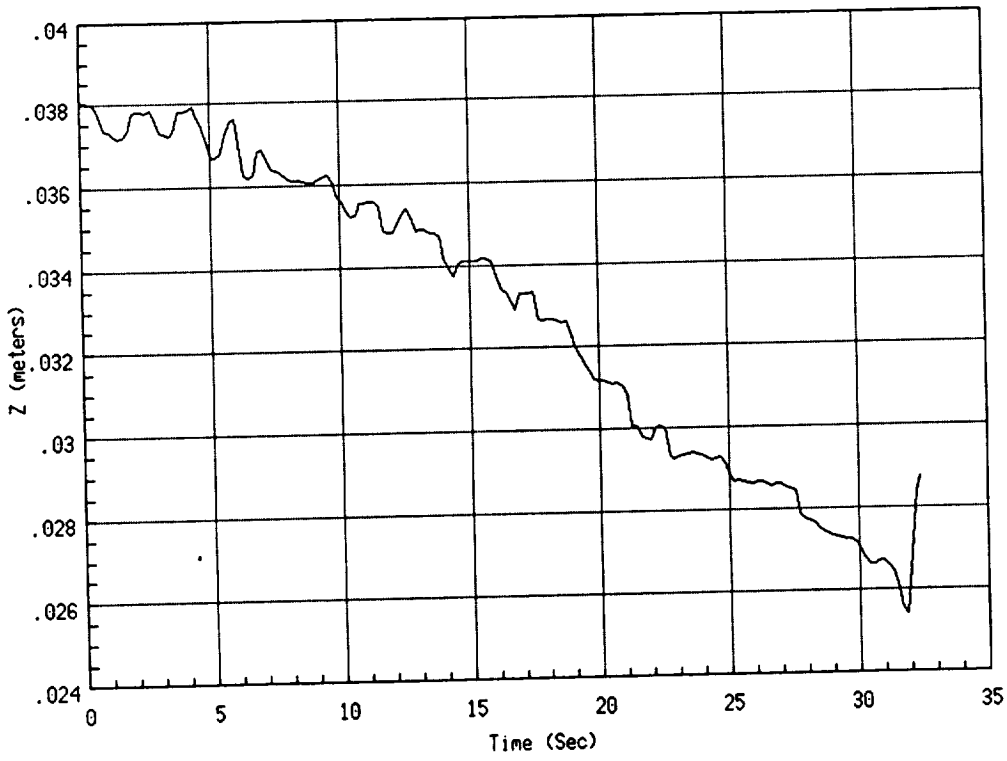

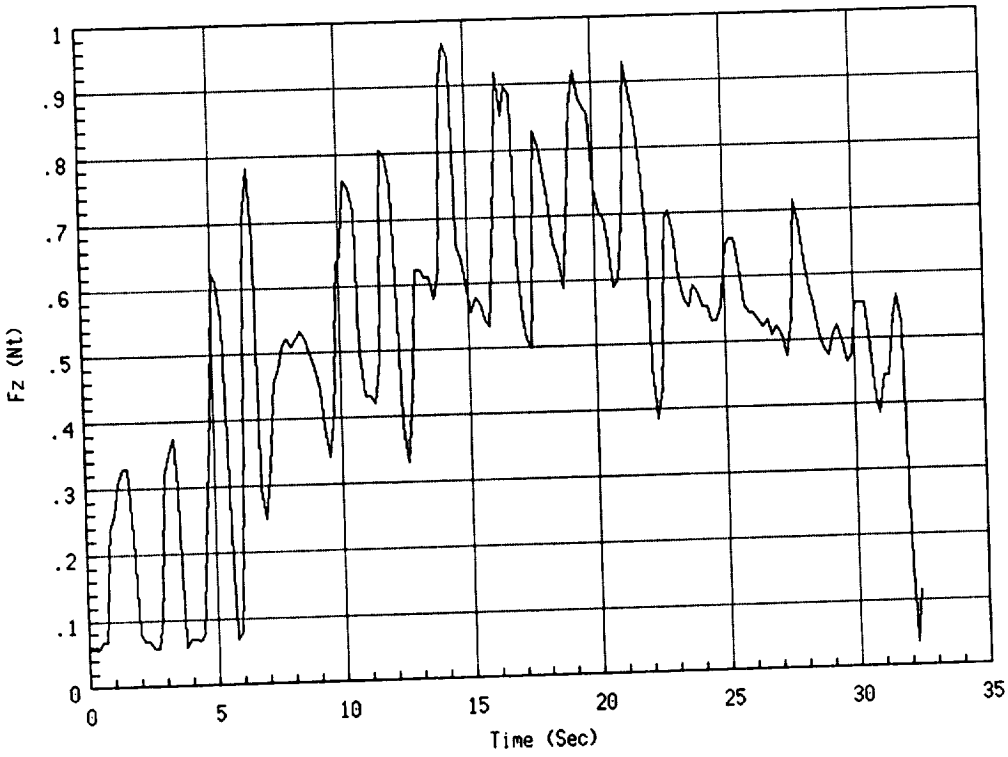

Figure 4-18: Z Axis position and force time histories for experiment 3

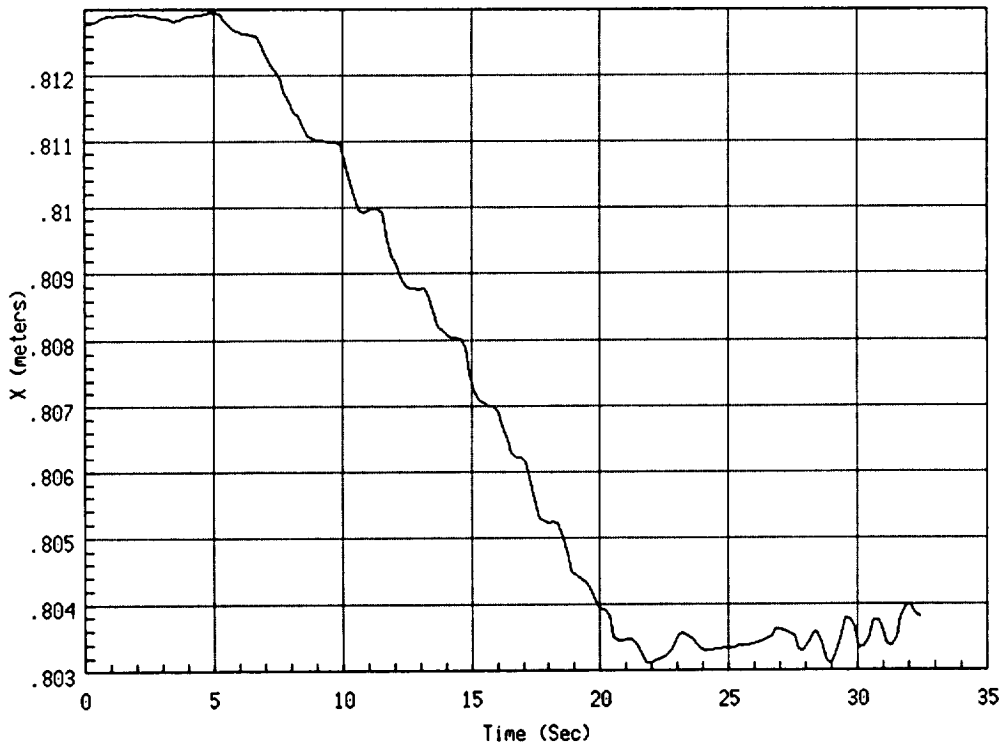

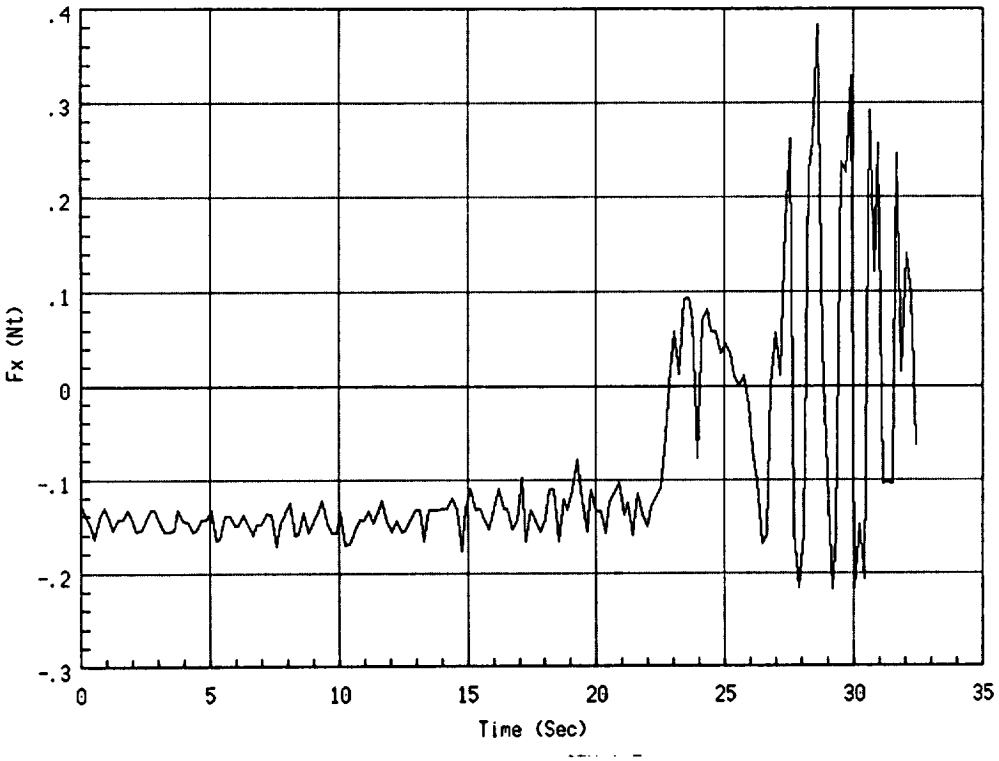

Figure 4-19: X Axis position and force time histories for experiment 4

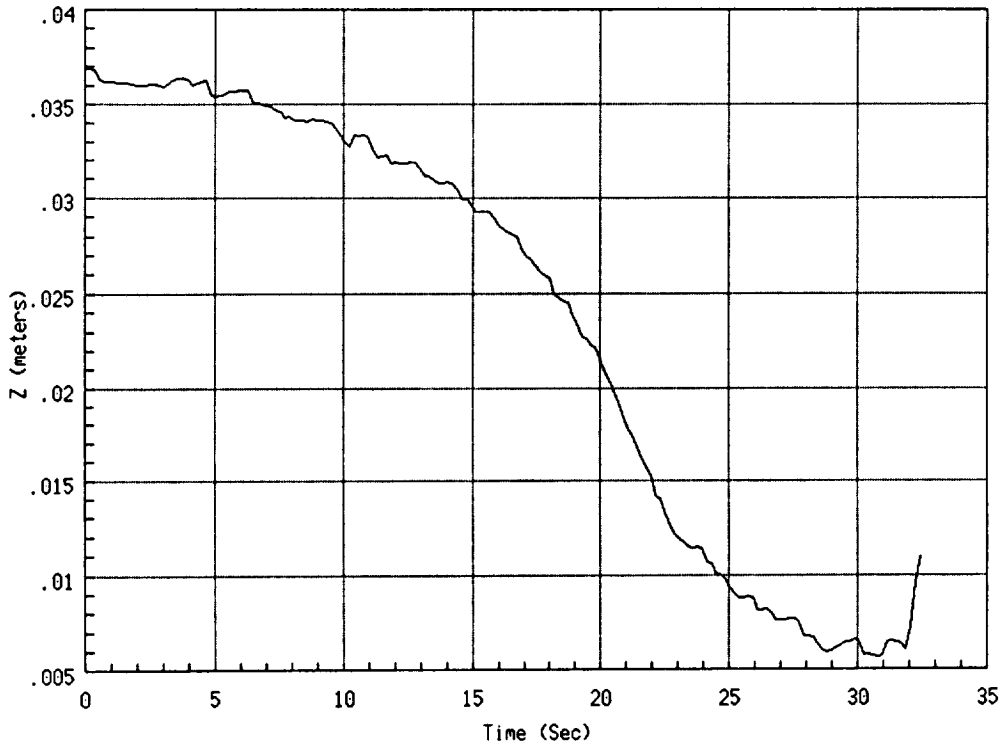

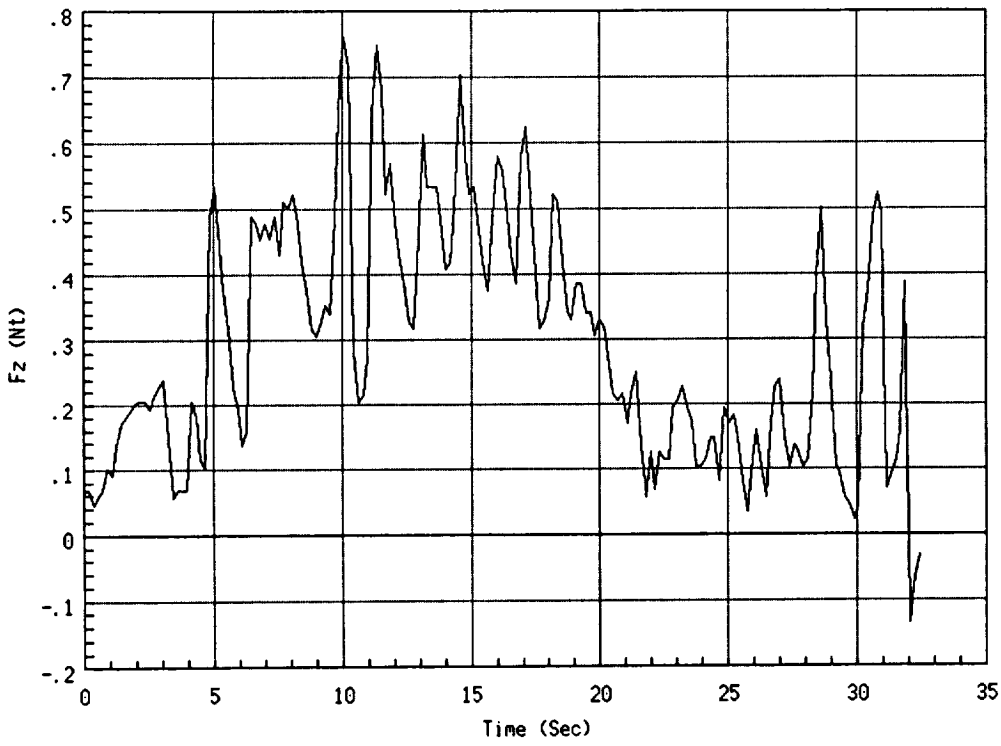

Figure 4-20: Z Axis position and force time histories for experiment 4

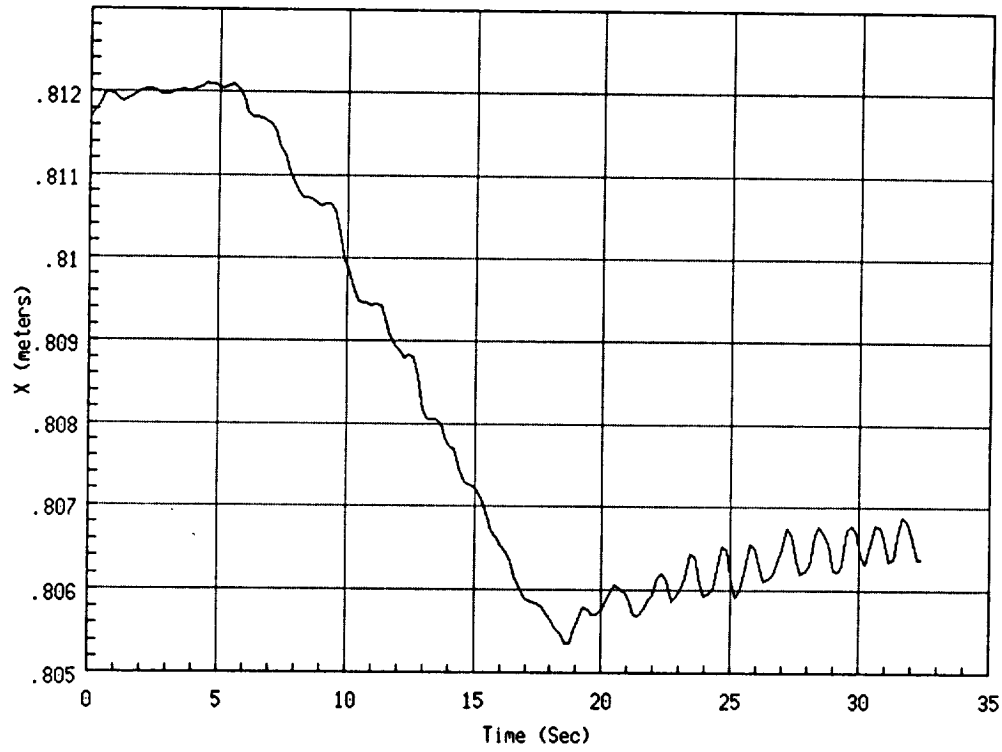

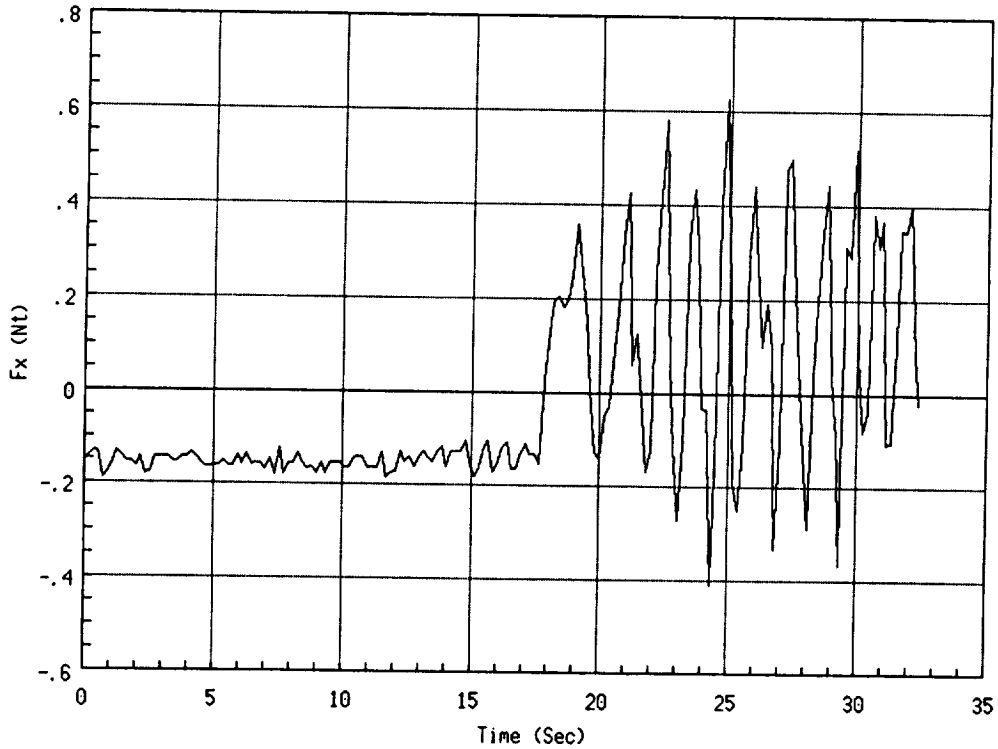

Figure 4-21: X Axis position and force time histories for experiment 5

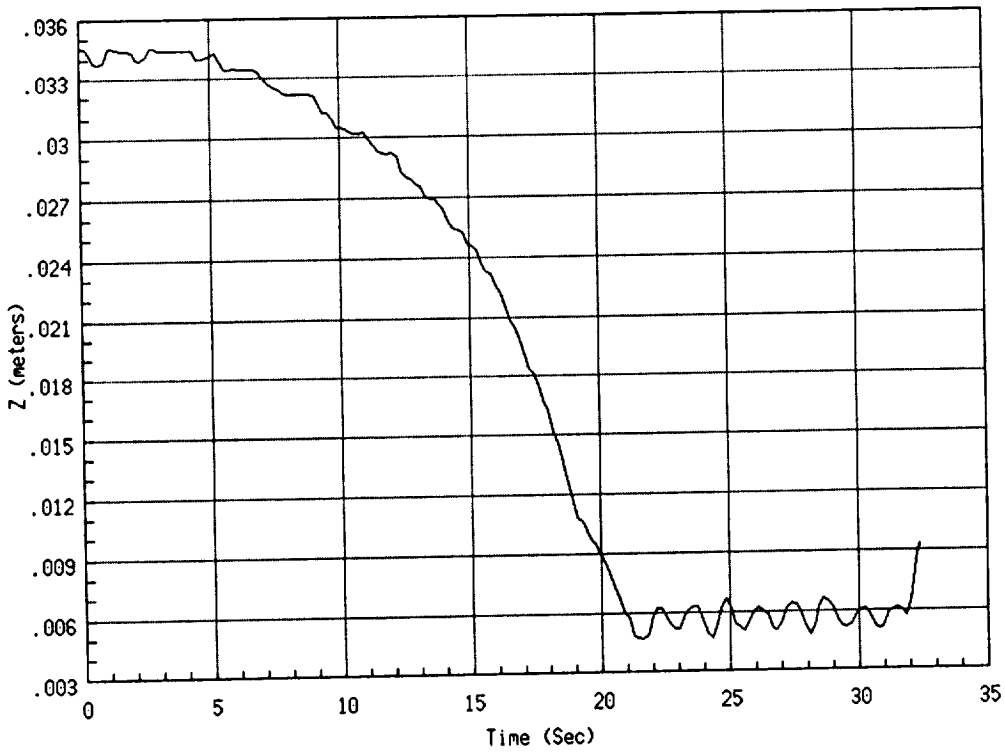

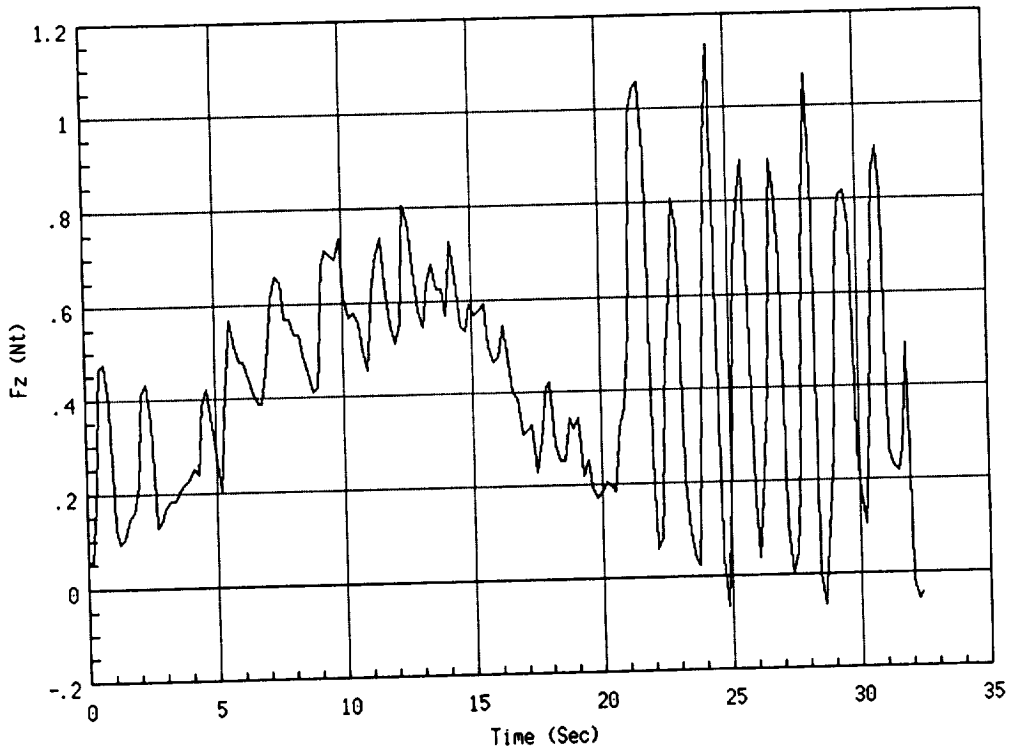

Figure 4-22: Z Axis position and force time histories for experiment 5

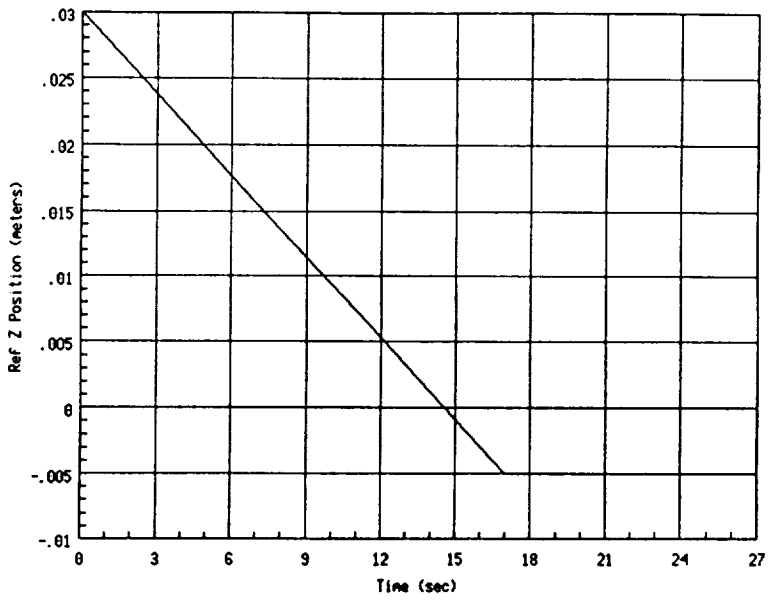

Figure 4-23: Reference path used for Y axis misalignment experiments.

4.3.3 Impedance Specification for Y Misalignments

To investigate impedance specifications for Y axis misalignments, an autonomous assembly path was generated, with the Y coordinate offset 3 mm. A number of experiments were then run, using this path with varying impedance specifications for the first robot. The second robot was programmed to have a very large impedance and thus emulate a rigid environment, to which one half of the truss connector was mounted.

Autonomous Path Description

The autonomous path for Y misalignments is shown in Figure 23. The path begins with the upper connector half offset 3 cm above the lower half. The connector is also offset 3 mm in the Y direction (See Figure 11). The X misalignment was made as small as possible. From the starting point the commanded trajectory moves with a velocity of 2 mm/sec to a point 5 mm below the fully mated position, maintaining the 3 mm Y offset. This commanded position was maintained for 10 seconds to allow transients to die out. The connector halves were then commanded to separate.

Experimental Results for Y Misalignments

The second robot, holding the lower half of the connector, was programmed to have very a large impedance in all 6 Cartesian axes. The first robot, holding the upper half of the connector was programmed to have a very large impedance about each of the rotational Cartesian directions. Therefore, torques in these directions will not cause compliance of the end-effector. The damping specification for Robot 1 translational axes was held at

1.26 $\frac{Nt-sec}{cm}$. This was necessary to ensure adequate stability margin during the assembly task. As will be shown in the next section, lower damping levels lead to a severe decrease in system stability.

For the first experiment, the stiffness specifications in the Y and Z axes were set at 1.8 and 2.7 $\frac{Nt}{cm}$, respectively. This corresponds to a stiffness ratio, K_z/K_y, of 1.5. Figures 24 and 25 show the position and force time histories for the Y and Z axes respectively. From the Z axis response one can observe that the connectors mated fairly smoothly, with the actual position tracking the commanded position, until they were fully mated. Once the connectors were fully mated there was a low frequency limit sycle of approximately 2 mm amplitude. The Z axis force response shows low levels of force until the two connector halves are fully assembled. Then, as the reference Z position continues to move, to Z = -0.5 cm, the force builds. Also the low frequency position limit cycle causes a corresponding oscillation in the force response. The Y axis response shows also that the connector complied to the fully mated position of Y = 39.5 cm. The Y forces are very small and oscillatory. This data is very consistent with the design of the connector. The contact angle, due to Y misalignments, is very small; therefore, the connector should easily mate with the stiffness specification given here and generate very low forces in the Y direction.

For the second experiment the stiffness in the Z axis was reduced to $1.8\frac{Nt}{cm}$, resulting in $K_z/K_y = 1.0$. Figures 26 and 27 show the Y and Z axis time histories, respectively. The Y axis response is very similar to that of the first experiment. The Z axis response is also similar, although the limit cycles damp out to a much lower amplitude. The decrease in Z axis stiffness, and the damped limit cycles are reflected in the force response as significantly lower force levels.

For the third experiment the Z stiffness was further reduced to 0.9 Nt/cm, resulting in $K_z/K_y = 0.5$. Figures 28 and 29 show the Y and Z axis time histories. The Y position response does not show quite as smooth compliance as the earlier experiments, and the peak forces are about double those of the first experiment. The Z position response still looks smooth and the peak forc levels have again been reduced.

For the fourth experiment a Y stiffness of $2.7\frac{Nt}{cm}$, and a Z stiffness of $0.54\frac{Nt}{cm}$ was used. This results in $K_z/K_y = 0.2$. Figures 30 and 31 show the Y and Z time histories. The Y position move is showing an increased irregularity. The limit cycle after fully mating is getting stronger, and as expected the forces are increasing. The Z position response is showing a marked lag behind the reference position. Once the connector begins moving its trajectory is smooth. The force response shows an initial rise in force level until the connector begins moving. The force level then drops until the connector is fully mated, when there is another rise. This rise is caused by the difference between the fully mated Z position and the reference Z position. The Z position limit cycles also cause a corresponding limit cycle in the force response.

For the fifth experiment the Y stiffness was raised to $4.3\frac{Nt}{cm}$. The resulting stiffness ratio is 0.125. Figures 32 and 33 show the time histories for the Y and Z axes, respectively. Both position time histories show a lag of about 7 seconds. The assembly

then proceeds smoothly to the fully mated position. With the increased lag, the Z force buildup before movement is larger than in the fourth experiment.

For the sixth experiment K_y was increased to $3.6\frac{Nt}{cm}$. The stiffness ratio is therefore now $K_z/Ky = 0.1$. Figures 34 and 35 show the Y and Z axis time histories. The lag has been increased to 14 seconds, before the connector begins to seat itself. Once it is in the fully mated position both the Y and Z position time histories show small amplitude, erratic movements. With the longer time lag the Z force rises considerably higher before movement begins — to about 1.7 Nt.

From this series of experiments it is obvious that the ability to successfully mate the connector halves is fairly insensitive to the stiffness ratio. In looking back at the diagram of the truss connector (Figure 11) the reason for this is clear — the contact angle between the connector halves is very small for Y misalignments. This would indicate that very small stiffness ratios would still result in successful task completion.

As the Y stiffness is increased, the normal force acting at the contact point is increased. This translates directly into an increase in friction force. This is the cause for the lag in the connector movement. The ΔZ must get larger before the tangential force component of $K_z\Delta Z$ will overcome the friction force. Once the connector begins moving the sliding friction is lower than the stiction; also, the contact angle is reduced as the connectors halves are mated. Therefore, once the connector begins moving it quickly mates itself to the other half.

From the above series of experiments, the impedance specifications for experiment 2 clearly stand out as providing the best task completion. The connector closely and smoothly follows the reference position and the limit cycles after assembly are well damped. The Z forces also damp out after assembly. This experiment used a Y and Z stiffness of $1.8\frac{Nt}{cm}$. Thus, the stiffness ratio, K_z and K_y, is 1.0. If the force levels from these experiments are judged too high it would only be necessary to keep the same stiffness ratio and decrease both K_z and K_y so that the interface forces are acceptable.

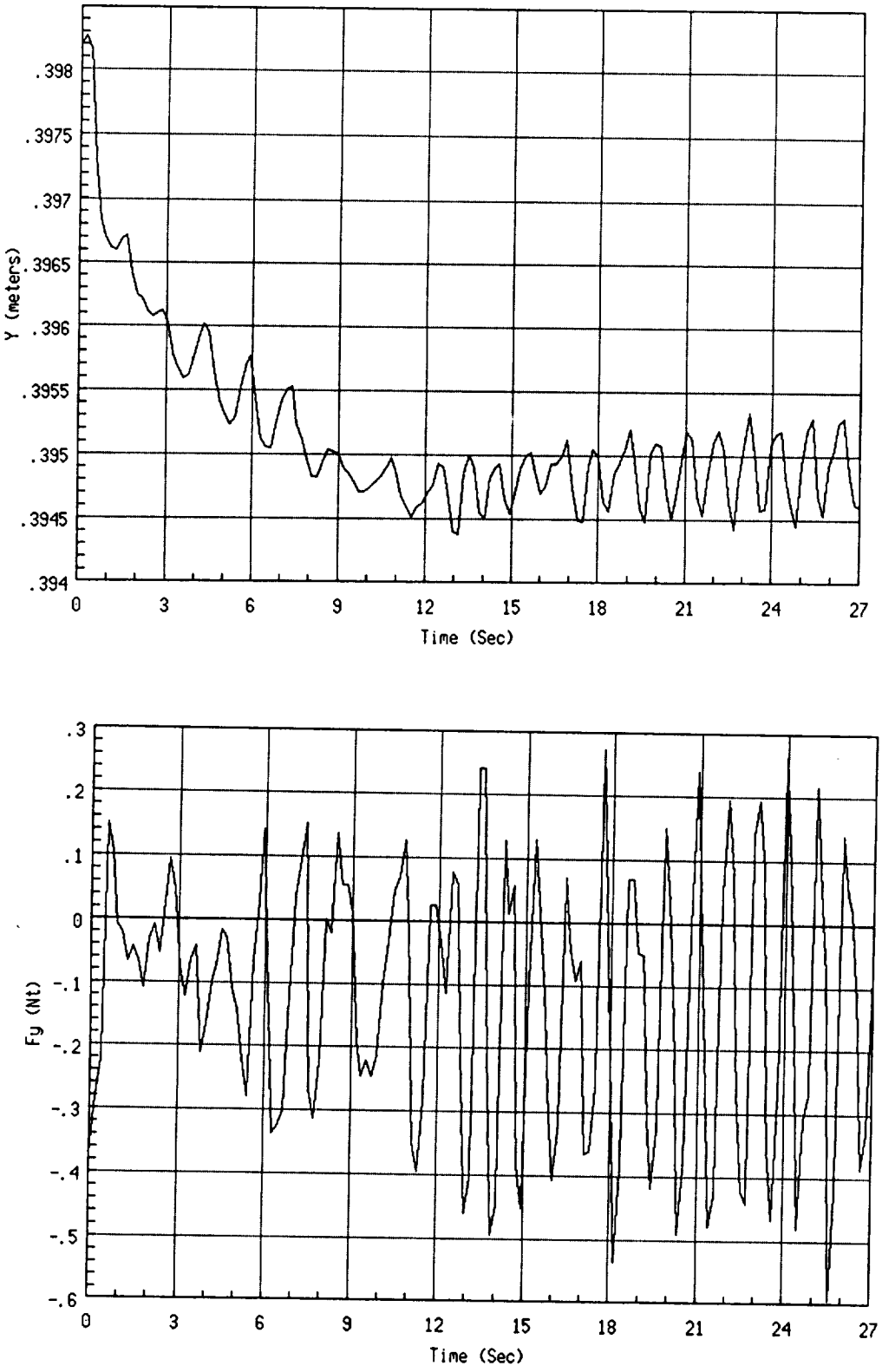

Figure 4-24: Y Axis position and force time histories for experiment 1

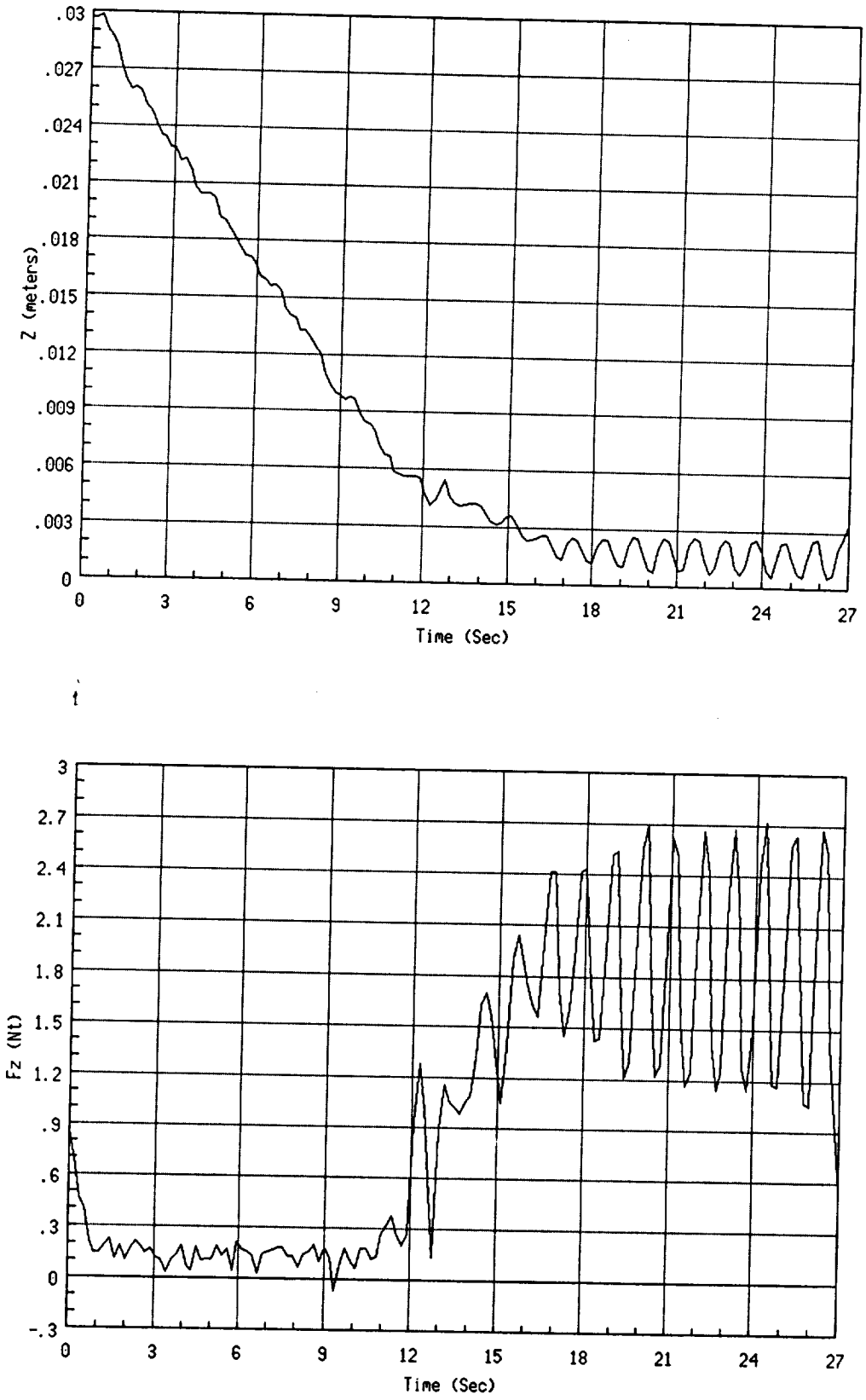

Figure 4-25: Z Axis position and force time histories for experiment 1

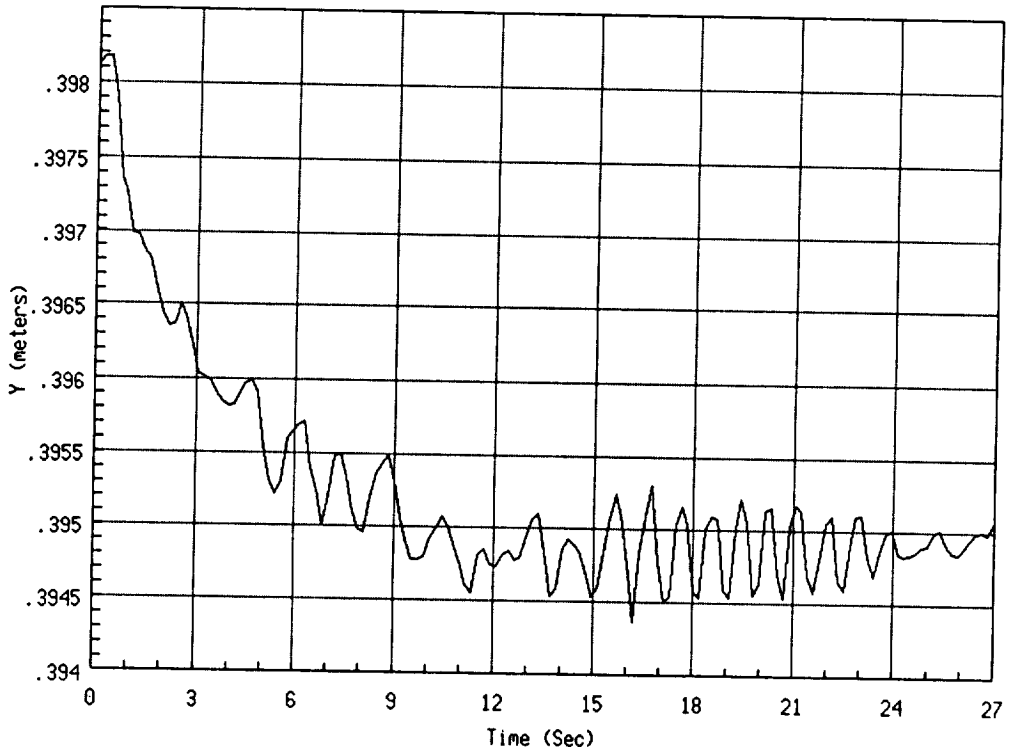

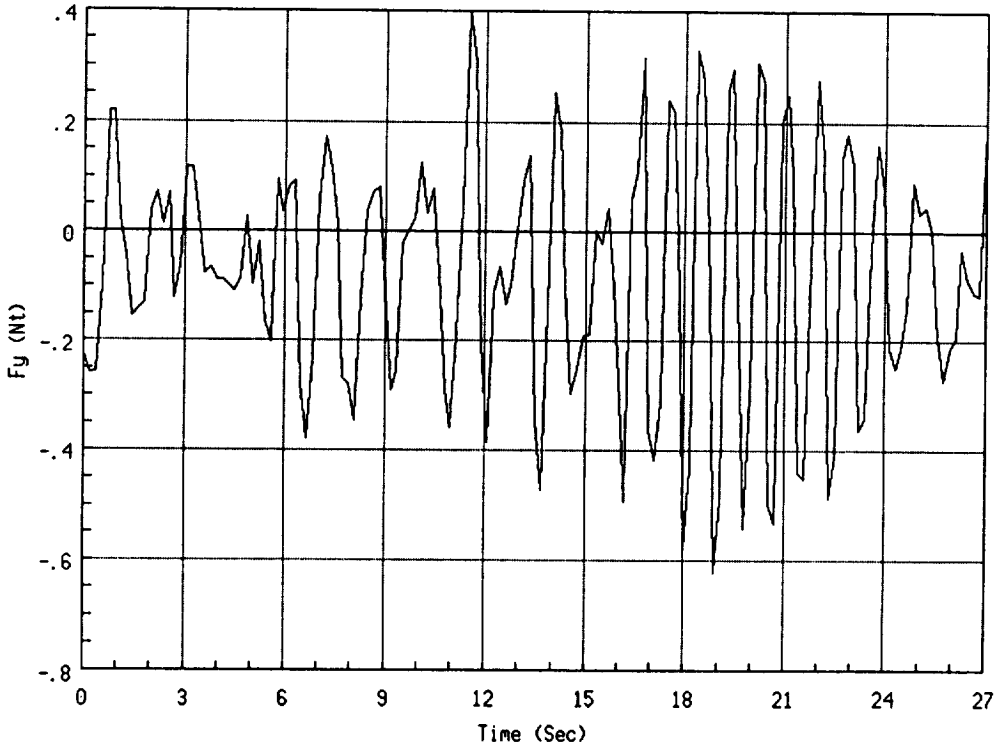

Figure 4-26: Y Axis position and force time histories for experiment 2

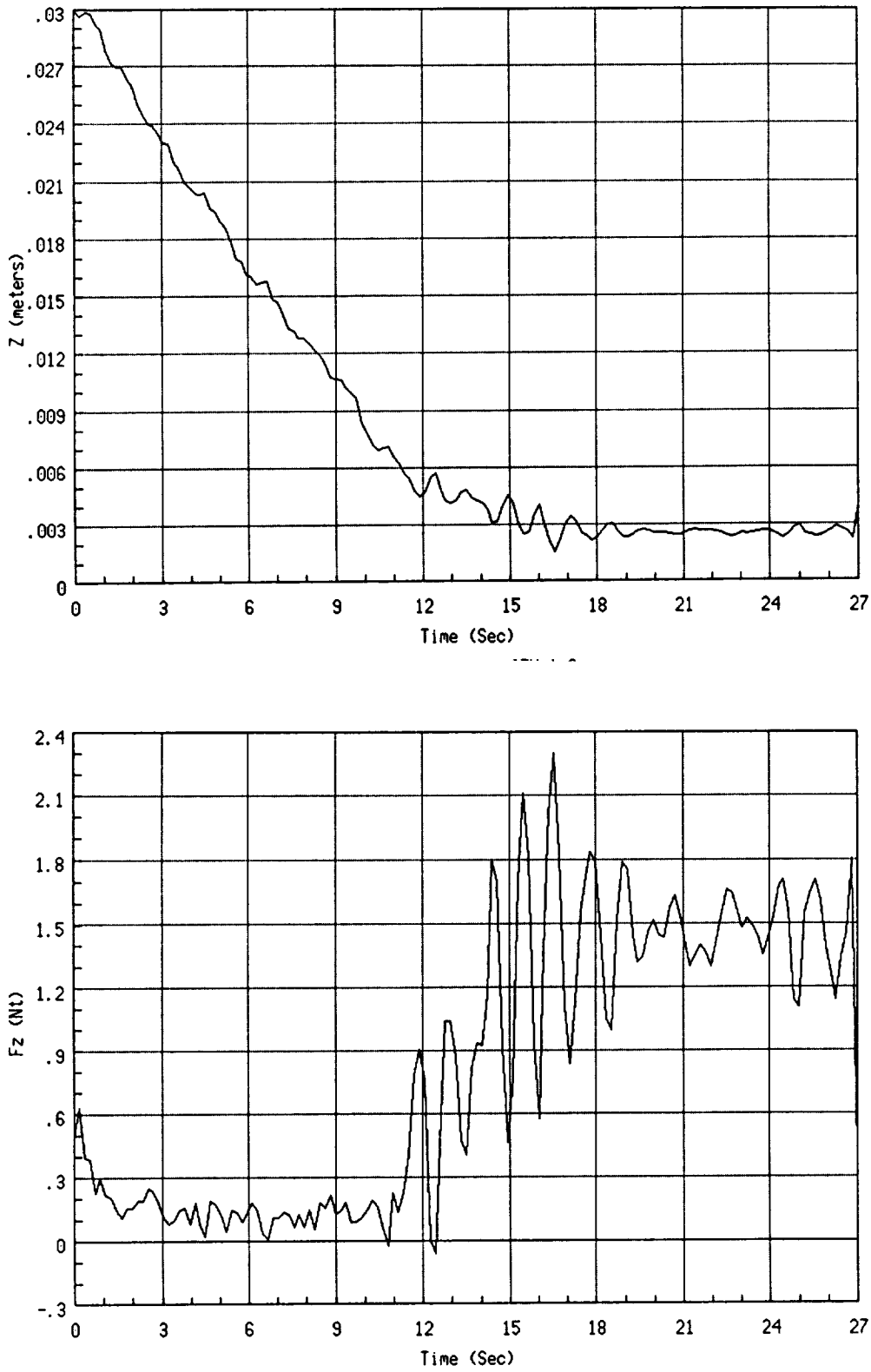

Figure 4-27: Z Axis position and force time histories for experiment 2

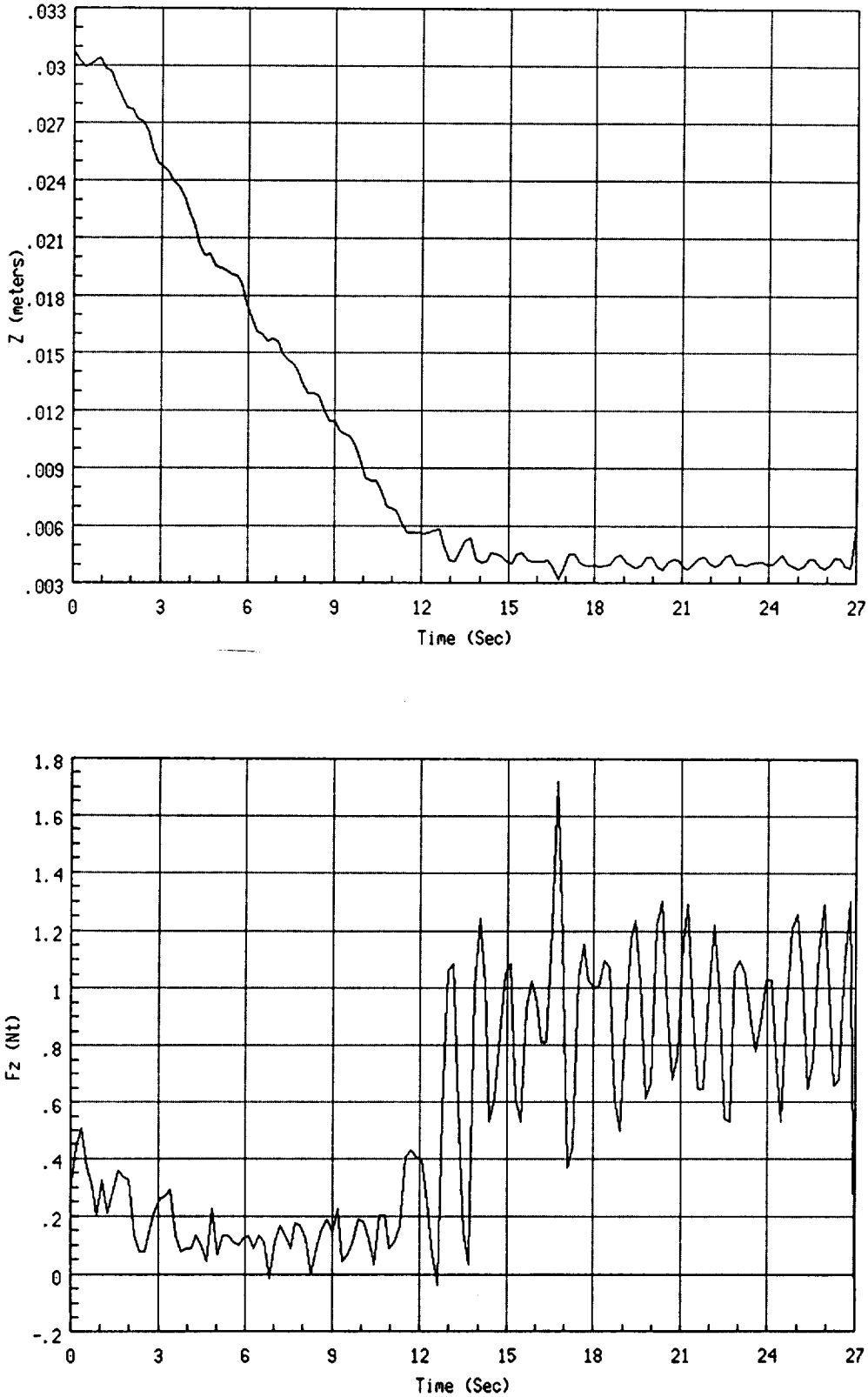

Figure 4-28: Y Axis position and force time histories for experiment 3

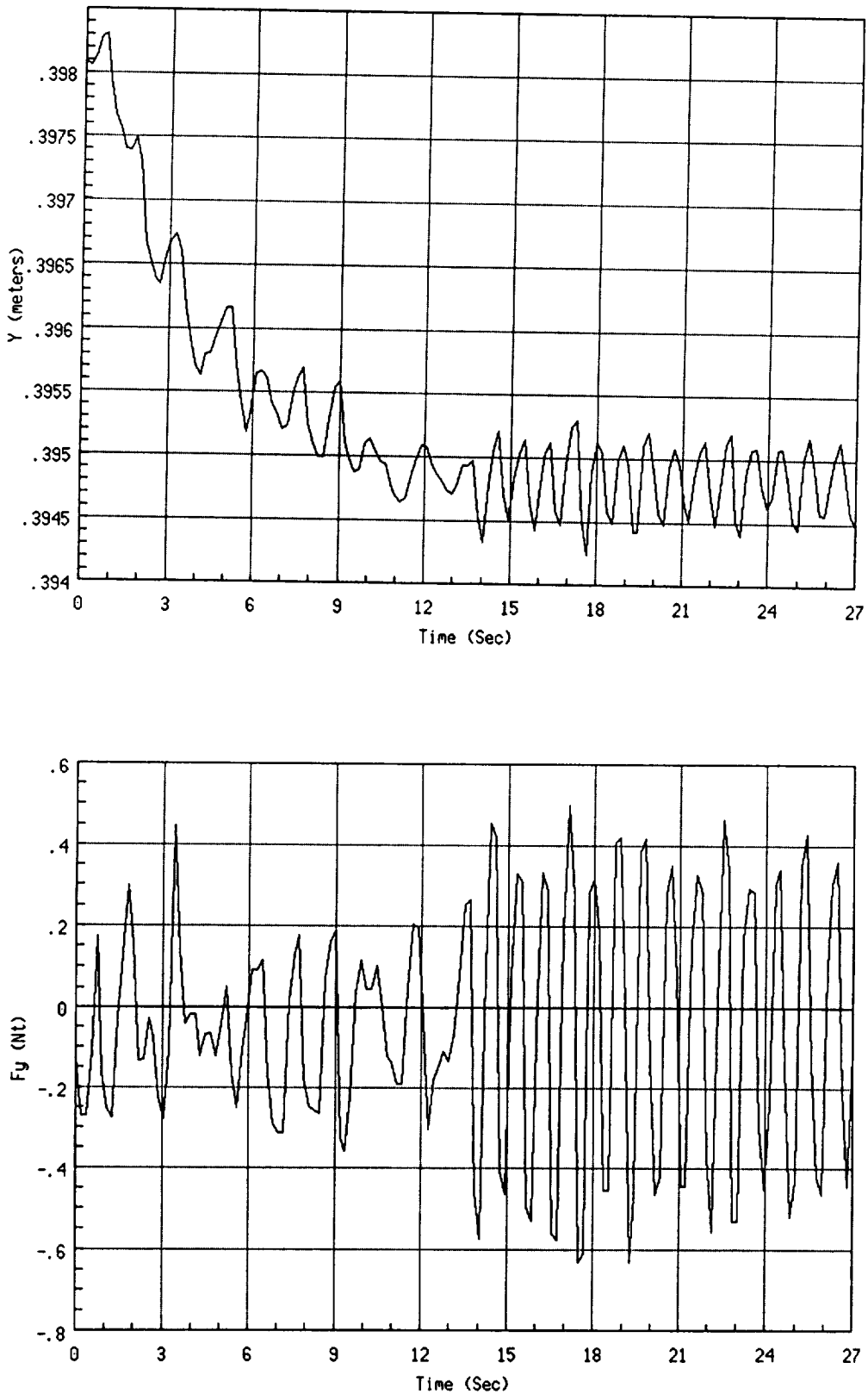

Figure 4-29: Z Axis position and force time histories for experiment 3

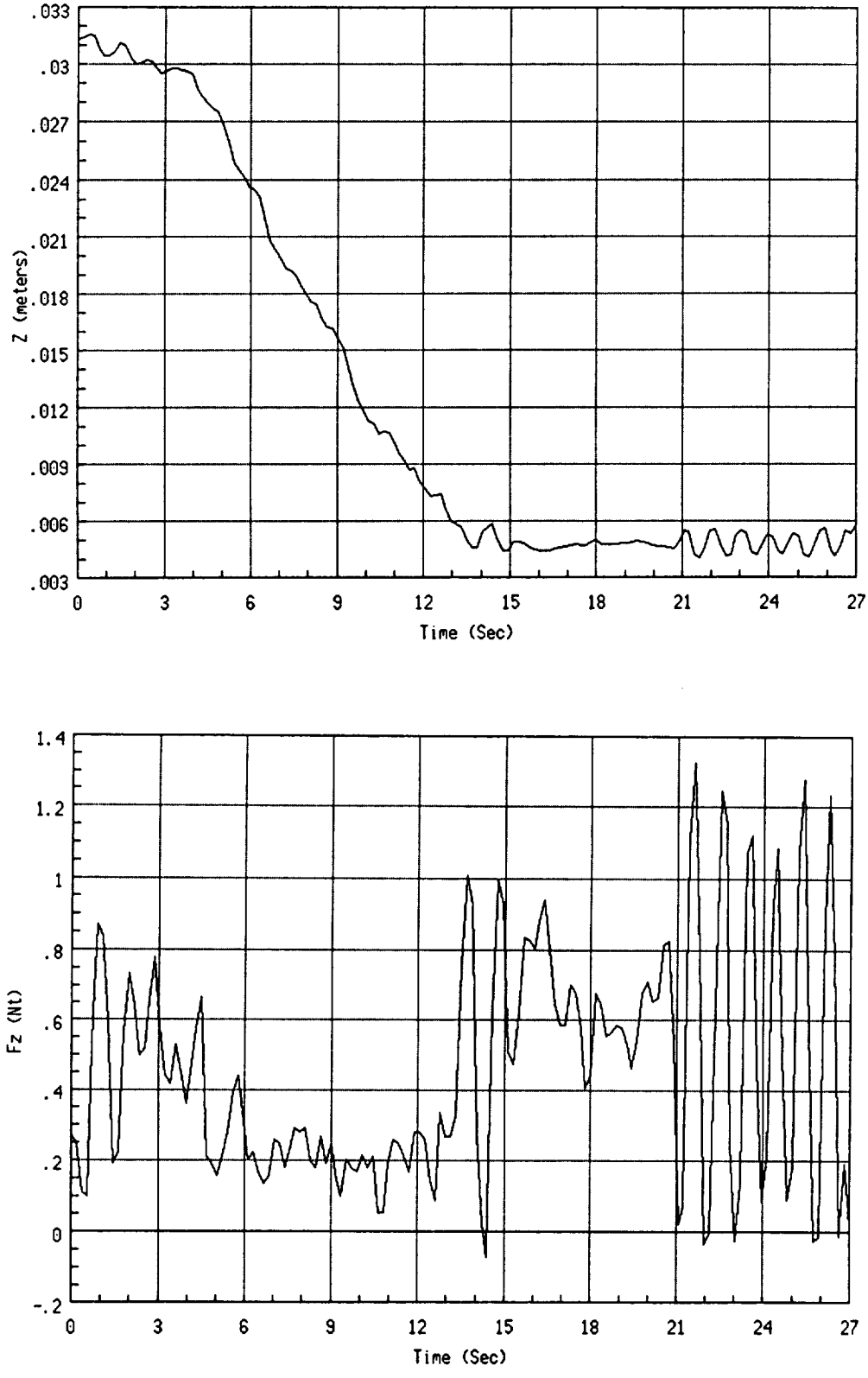

Figure 4-30: Y Axis position and force time histories for experiment 4

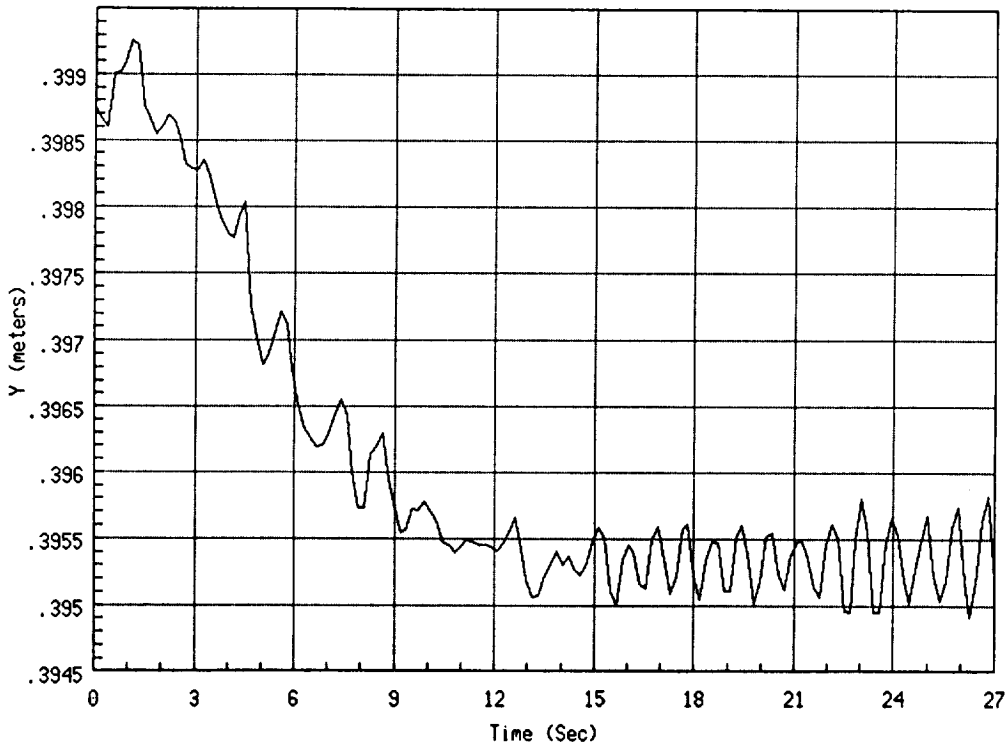

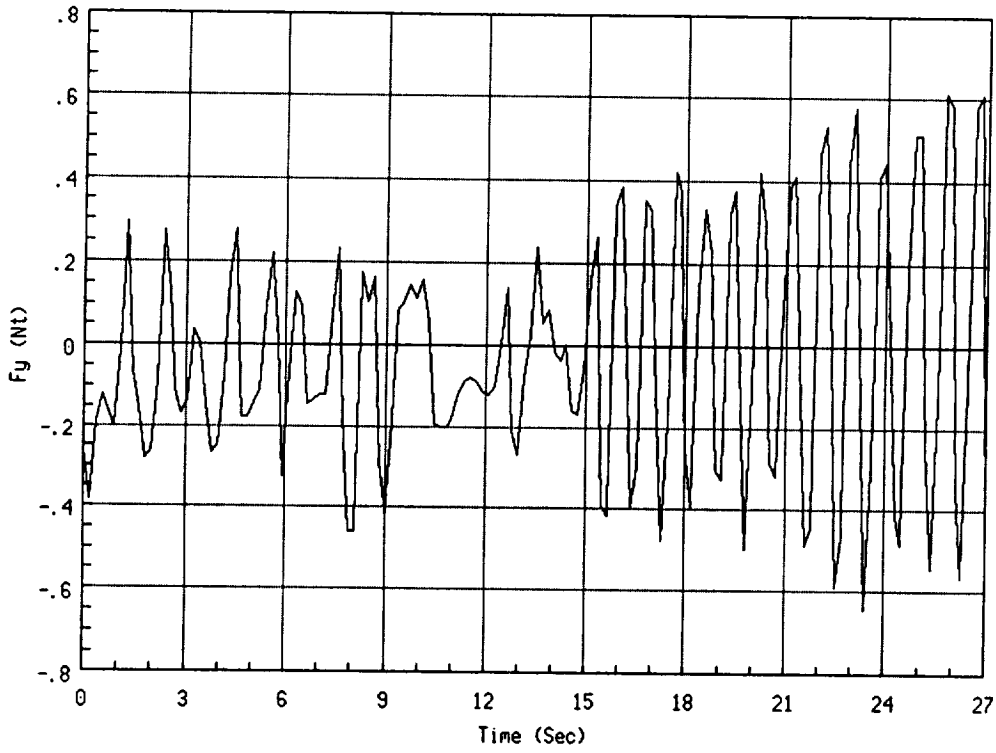

Figure 4-31: Z Axis position and force time histories for experiment 4

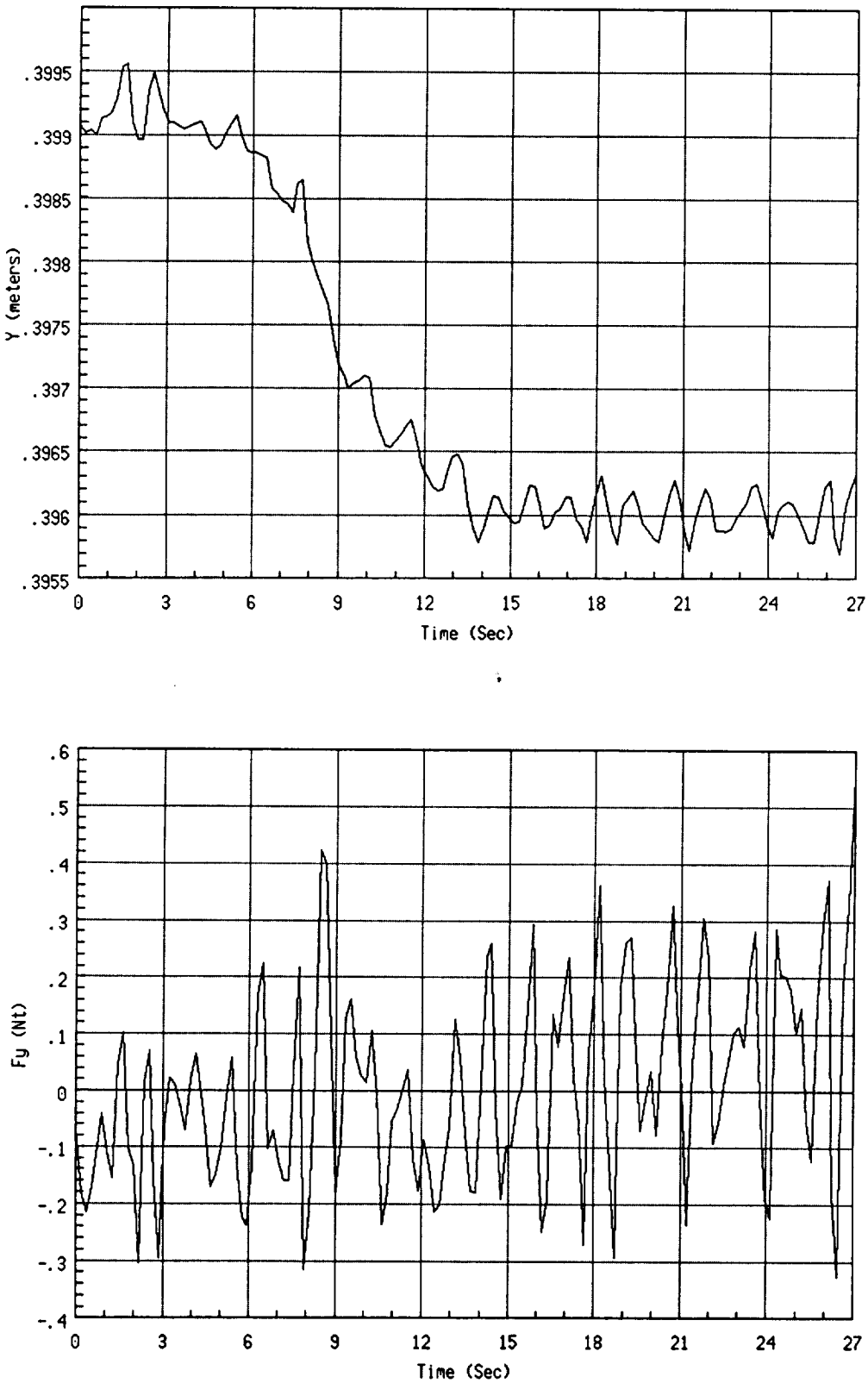

Figure 4-32: Y Axis position and force time histories for experiment 5

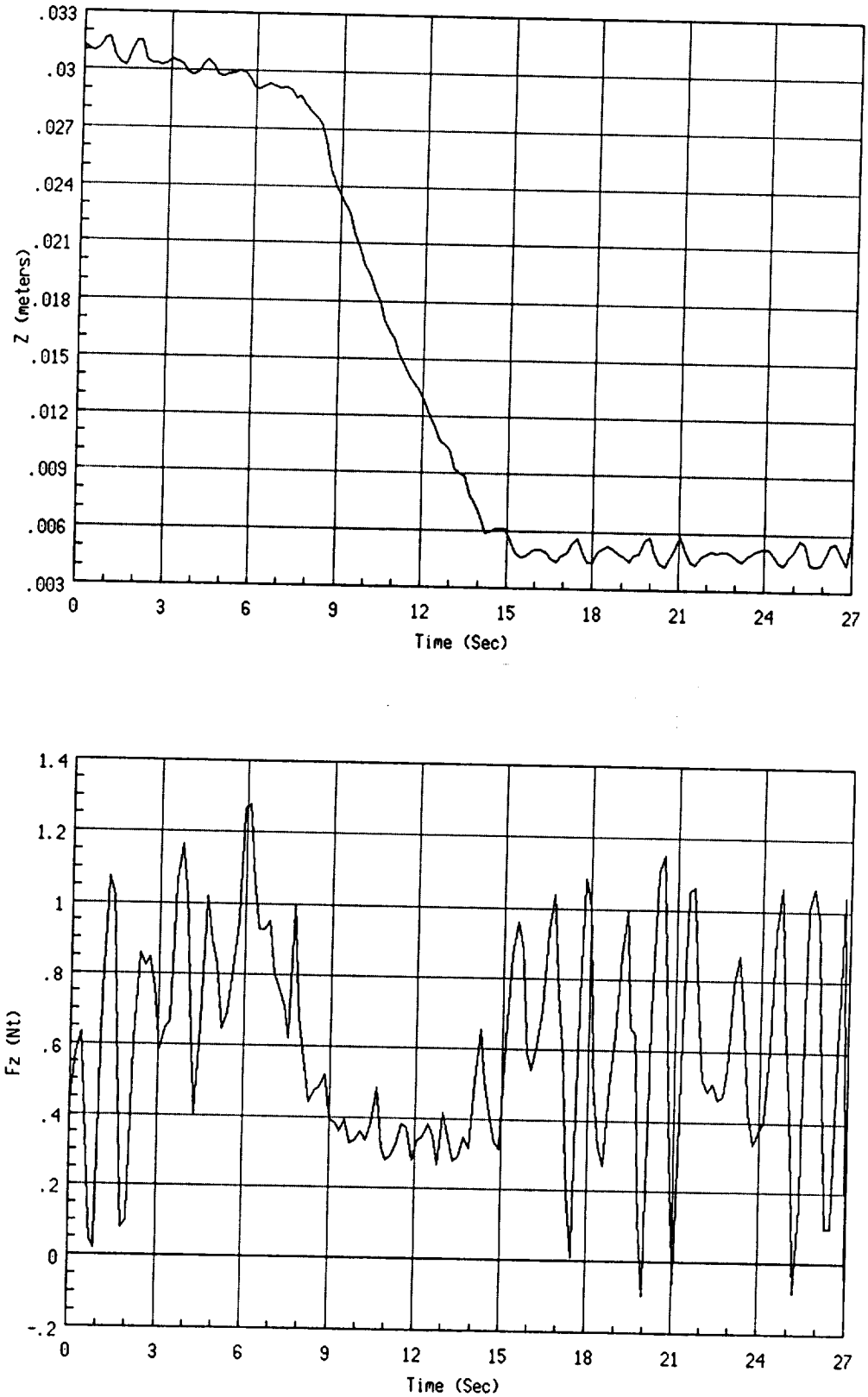

Figure 4-33: Z Axis position and force time histories for experiment 5

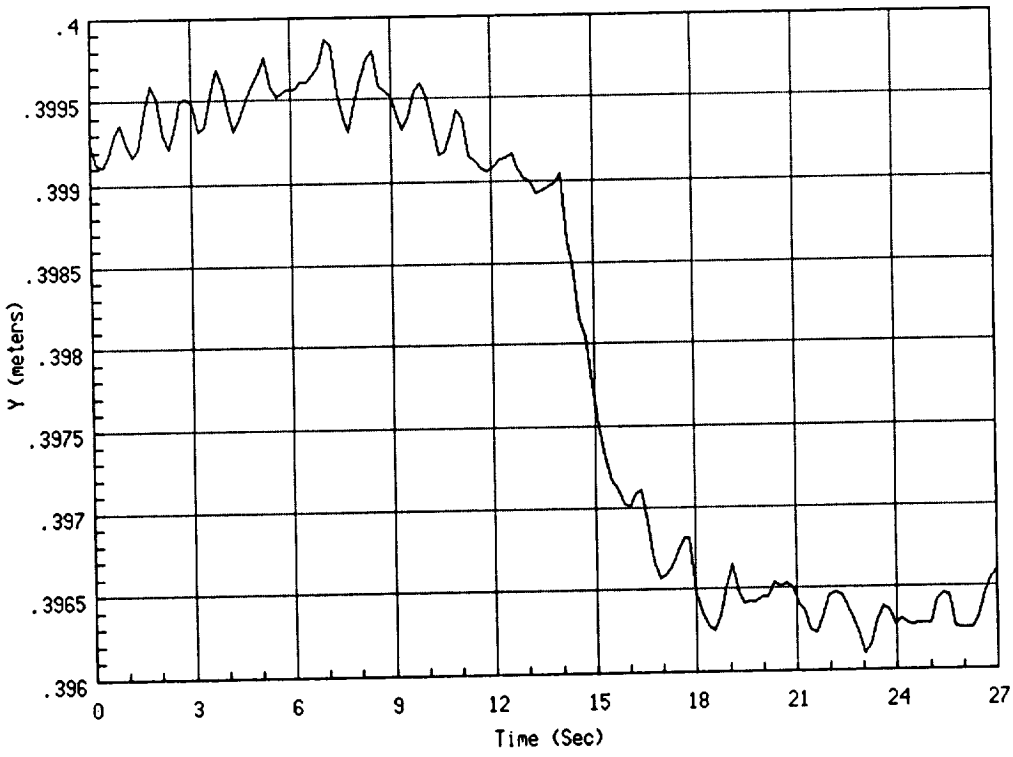

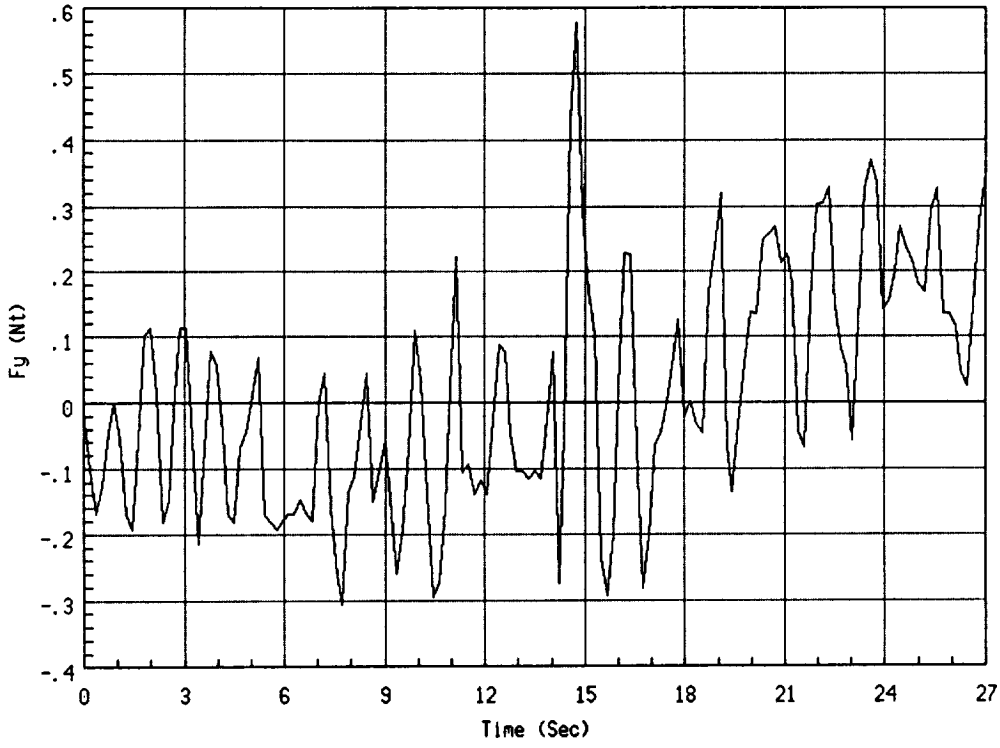

Figure 4-34: Y Axis position and force time histories for experiment 6

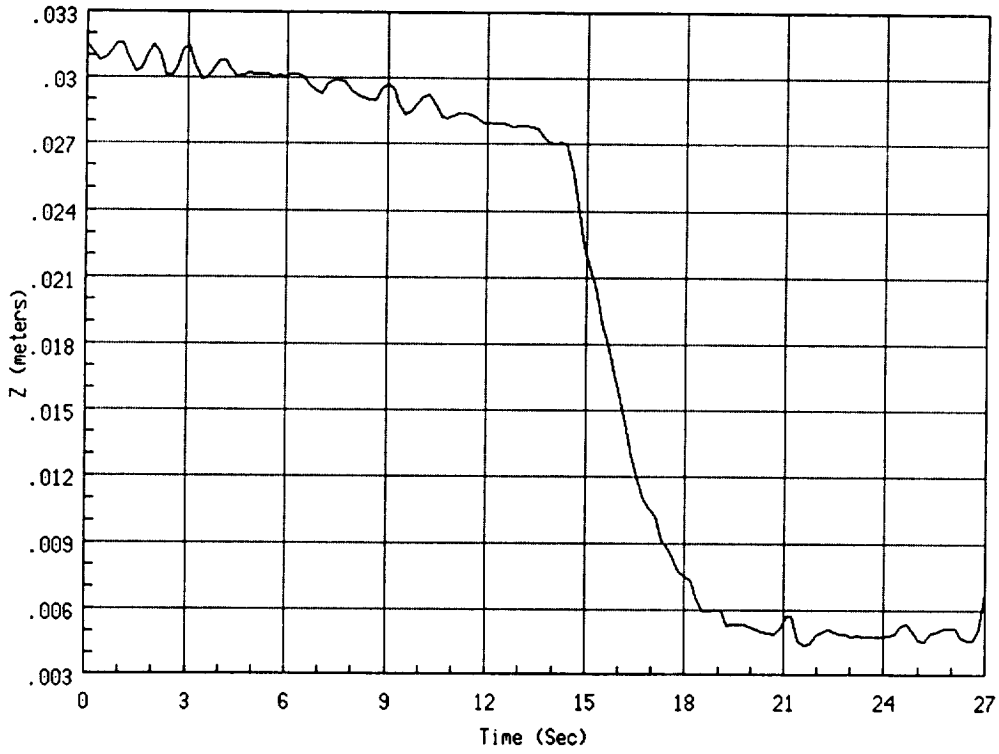

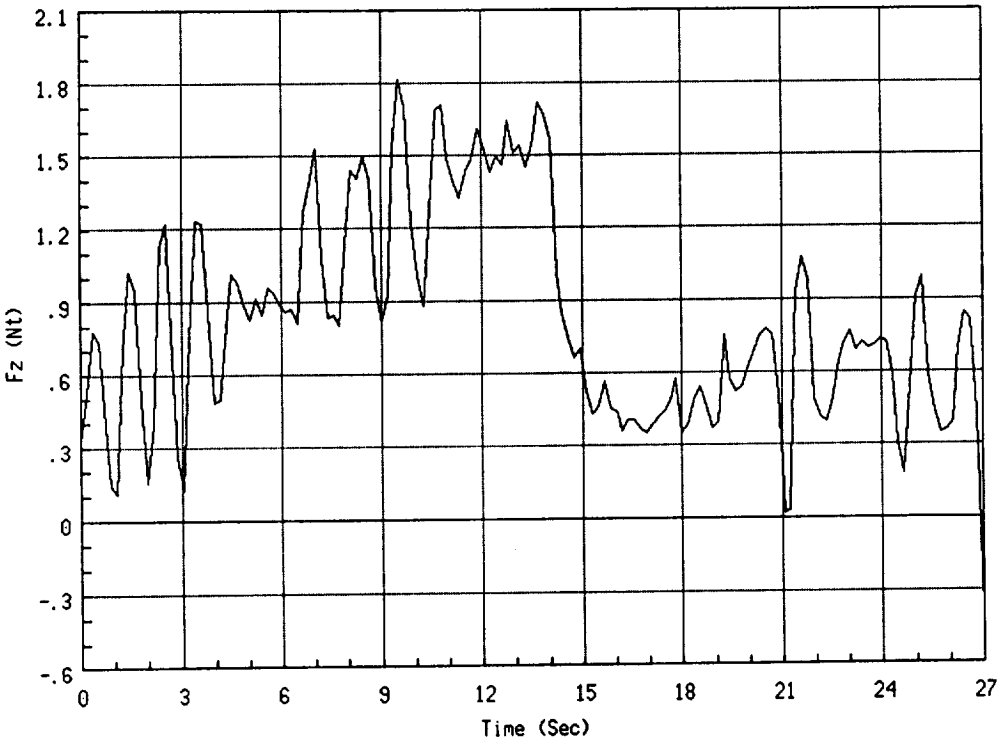

Figure 4-35: Z Axis position and force time histories for experiment 6

Chapter 5

SYSTEM DESIGN ISSUES

Once a preliminary set of static and dynamic performance requirements has been generated, the system design process will use them and evaluate the various design options to find the set of design options which satisfy the requirements for the minimum cost.

The manipulator design process is primarily concentrated in 3 disciplines:

- Mechanical design and analysis,
- Controller hardware/software design and analysis,
- Control algorithm design and analysis.

Within each of these diciplines there is a wide range of options which must be explored and evaluated against one another. In addition to these trade-offs it is vital to consider interdisciplinary trade-offs! For instance the controller hardware configuration will significantly impact the control algorithm complexity and controlled system performance. The control algorithm choice will affect the type and location of sensors which must be incorporated into the mechanical design.

A third level of trade-offs must also be evaluated. This involves modifications to the performance requirements. For instance the functional requirement to assemble two parts without exceeding a given force level during the assembly can lead to a wide range of possible performance requirements – one could specify a very high level of positioning accuracy at the end-effector, and therefore be able to specify higher levels of stiffness for the end-effector impedance; or one could specify a lower end-effector positioning accuracy and use a low end-effector impedance specification to ensure that the forces due to potential misalignments remain acceptably low.

In order to achieve this level of insight and optimization in the design of manipulation systems it is neccessary to develop the tools which will allow designers to see the effects of changes quickly and easily. We are developing the techniques and have previously developed crude prototype tools which have confirmed both their usefulness and more, their neccessity in developing a formalized approach to the manipulator design process.

Our investigation has concentrated on developing simple models which capture the key features of the system stability vs. system performance trade-off. For feedback control systems this is typically the critical issue – the system performance is limited by the system stability. We will describe our efforts to understand the fundamental properties which affect the stability of manipulator systems. Parameterizing and quantifying these relationships provides invaluable insight into the relative benefits of the various design options.

We first describe analytical efforts to predict the stability of a single manipulator during force interaction tasks. Then we compare the results of these analytical efforts

with experimental results, using one of the manipulators from the Dual Arm Testbed. We then examine the stability of a coordinated pair of manipulators, and compare the predicted and experimental results. For these investigations we have again choosen very simple tasks, examining only one Cartesian degree of freedom. Finally we look at a more realistic task, the assembly of a NASA Space Station truss connector, and show that the results from the simple tasks carry over into more complex 'real-world' tasks.

5.1 System Stability In Contact with Environment

It has been widely reported and our experience confirms that using active feedback of end-effector forces during force interaction tasks can have stability problems. The instability typically occurs when the end-effector comes in contact with the environment against which it is operating, ie. if the task is to assemble two parts the instability occurs when the two parts come in contact.

We have been actively investigating this phenomenon for the past two years, attempting to understand the causes for the instability, and be able to predict its occurance. We have developed very simple dynamic model structures which preserve the fidelity of the manipulator/environment interaction, yet provide considerable insight into the causes of instability. The stability characteristics of the system result from a complex interaction between:

- the environment dynamics,
- the closed-loop joint dynamics,
- the Cartesian impedance controller and associated Computational time delay.

We will use an "Operational-Space" approach to developing the model of the manipulator closed-loop dynamics [DEP88]. This approach involves mapping the closed-loop joint dynamics from joint space into Cartesian space. In essence the dynamic structure of the joint dynamics is locally preserved during this transformation. That is if the joint-space inner-loop dynamics were second order for all the joints, then in Cartesian space, for small disturbances, the inner-loop dynamics will be second order.

5.1.1 Stability of a Single Manipulator

We will first examine the case where the computational time delay is zero. The resulting model of the system will be linear, time-invariant. This allows us to analytically derive a closed form expression for the stability characteristics of the system.

We are interested in examining how the environmental dynamics will affect the stability of a manipulator in contact with the environment. By using an *operational space* approach we can obtain considerable insight by looking at a single Cartesian degree

of freedom. The closed loop position transfer function, $G(s)$ along a single Cartesian direction, in free-space, is approximated by

$$G(s) = \frac{X}{X_c} = \frac{K_m}{J_m s^2 + B_m s + K_m}, \qquad (5-1)$$

where J_m is the effective inertia, B_m is the effective damping, and K_m is the effective stiffness of the position dynamics. J_m, B_m, K_m are all ≥ 0. No assumptions are made as to the control structure which results in this closed loop transfer function. Notice also that this is a fairly general reperesentation of the position dynamics, since depending on the relative magnitudes of J_m, B_m, K_m, the system behavior may range from a pure positioning device to a pure inertia.

For this investigation the environment is modelled as an inertia connected to a parallel spring and damper system which is connected to inertial ground. The impedance of the environment Z_e is described by

$$Z_e = \frac{F}{X} = J_e s^2 + B_e s + K_e, \qquad (5-2)$$

where F is the force applied to the environment, X is the displacement of the environment, J_e is the inertia of the environment, B_e is the damping of the environment, and K_e is the spring stiffness of the environment. $J_e, B_e, \& K_e$ are all greater or equal to zero.

The environment dynamics will clearly impact the closed loop position dynamics of the system. The transfer function of the closed loop position dynamics, in contact with the environment can be written as

$$\frac{X}{X_c} = \frac{K_m}{J_{eq} s^2 + B_{eq} s + K_{eq}}, \qquad (5-3)$$

where:

$J_{eq} = J_m + J_e,$
$B_{eq} = B_m + B_e,$
$K_{eq} = K_m + K_e.$

Figure 1 shows the block diagram of the system in contact with the environment, and under impedance control. The position output X is multiplied by the environment impedance Z_e, to obtain the force seen by the force sensor at the manipulator/environment interface.

The force output from the force sensor F is filtered through a first order impedance filter H(s). The B and K in H(s) correspond to the desired damping and stiffness characteristics of the manipulator. Notice that if G(s) is a perfect positioning device, then the manipulator impedance would be exactly

$$Z_m = Bs + K.$$

The output of the impedance filter H(s) is a position update X_i, which is summed with the reference position X_r, to form the commanded position X_c.

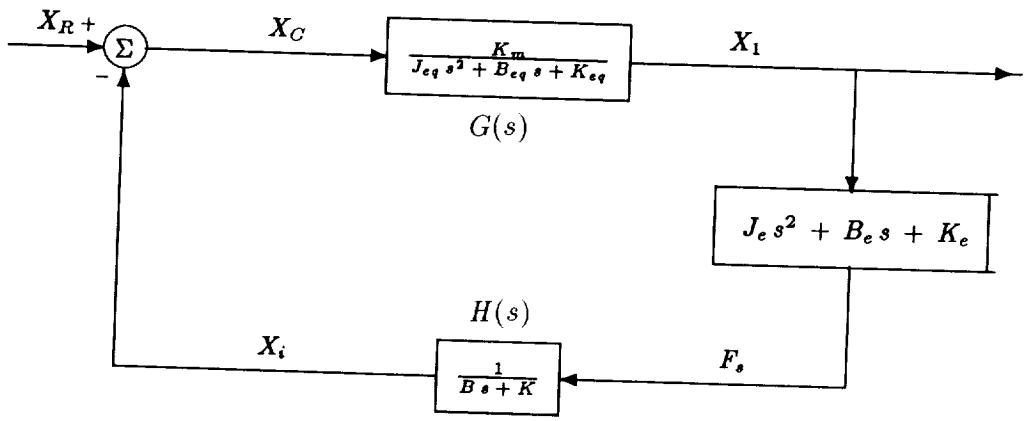

Figure 5-1: Block diagram of system in contact with environment.

The open-loop transfer function, from X_c to X_i, is given by

$$P_{ol}(s) = \frac{X_i}{X_c} = \frac{K_m(J_e s^2 + B_e s + K_e)}{(J_{eq}s^2 + B_{eq}s + K_{eq})(Bs + K)}. \qquad (5-4)$$

Notice that if $K_e = 0$ then the maximum phase loss of the open loop transfer function will be $-180°$. Therefore the system will be stable for any value of $K\&B > 0$. Thus if the environment may be modelled as a combination of inertia and damping, then the system will be stable for any $K\&B > 0$. If K_e is not zero then the stability conditions are not as clear, and it is neccessary to examine the roots of the closed loop transfer function.

The closed loop transfer function, from X_r to X, will be

$$P_{cl}(s) = \frac{X}{X_r} = \frac{N(s)}{D(s)} = \frac{K_m(Bs + K)}{(J_{eq}s^2 + b_{eq}s + K_{eq})(Bs + K) + K_m(J_e s^2 + B_e s + K_e)}. \qquad (5-5)$$

The closed loop system will be stable IFF the roots of $D(s)$ all have negative real parts. $D(s)$ may be expanded to

$$\begin{aligned} D(s) &= J_{eq}Bs^3 + (J_{eq}K + B_{eq}B + K_m J_e)s^2 \\ &+ (B_{eq}K + K_{eq}B + K_m B_e)s + (K_{eq}K + K_m K_e). \end{aligned} \qquad (5\text{-}6)$$

Using the appropriate substitutions, this may be rewritten as

$$D(s) = a_0 s^3 + a_1 s^2 + a_2 s + a_3. \qquad (5-7)$$

The Routh criteria may be applied to (7) to determine whether the system is stable. The Routh Array for (7) is given by

$$\begin{matrix} a_0 & a_2 \\ a_1 & a_3 \\ r_1 & 0 \\ r_2 & 0 \end{matrix} \qquad (5\text{-}8)$$

where:

$$r_1 = \frac{a_1 a_2 - a_0 a_3}{a_1}$$
$$r_2 = \frac{r_1 a_3}{r_1} = a_3.$$

The Routh criteria states that for a system to be stable, all of the elements of the first column of the Routh Array must have the same sign.

One may satisfy a_0, a_1, r_2 all ≥ 0 by requiring $J_m, B \& K > 0$. All other parameters in a_0, a_1 & r_2 are then required to be ≥ 0. For the system to be stable it is additionally required that $r_1 > 0$. In examining r_1 notice that $a_1 > 0$ has already been required . Therefore it is sufficient to find conditions for

$$a_1 a_2 - a_0 a_3 > 0. \qquad (5-9)$$

Refering back to (6), equation 9 may be expanded as

$$\begin{aligned} &(J_{eq} B_{eq}) K^2 \\ &+(J_{eq} B_e K_m + B_{eq}^2 B + B_{eq} J_e K_m) K \\ &+(B_{eq} B + J_e K_m)(K_{eq} B + B_e K_m) - J_{eq} B K_m K_e \;>\; 0. \end{aligned} \qquad (5\text{-}10)$$

Equation 10 is quadratic in both K and B. It may be easily solved to find the values of K which satisfy this inequality. The minimum values of K which satisfy (10) are given by

$$\begin{aligned} K \;>\; &-\frac{J_{eq} B_e K_m + B_{eq}^2 B + B_{eq} J_e K_m}{2 J_{eq} B_{eq}} \\ &+\left[\frac{(J_{eq} B_e K_m + B_{eq}^2 B + B_{eq} J_e K_m)^2 + 4 J_{eq} B_{eq} (J_{eq} B K_m K_e - (B_{eq} B + J_e K_m)(K_{eq} B + B_e K_m))}{(2 J_{eq} B_{eq})^2}\right]^{\frac{1}{2}} \end{aligned} \qquad (5\text{-}11)$$

The complexity of the expression for K notwithstanding, it is possible to glean useful information from (11). For instance if we look at the expression within the square root we see that if

$$J_{eq} B K_m K_e \qquad < \qquad (B_{eq} B + J_e K_m)(K_{eq} B + B_e K_m) \qquad (5-12)$$

then the real part of the square root expression will be less than the negative part of (11). Therefore the allowable K from (11) will be less than zero. Since we have previously restricted $K > 0$, satisfying (12) ensures that for any $B > 0$, any $K > 0$ will result in a stable system.

Figure 2 shows the stability boundaries of K vs. B for a pure stiffness environment. The region below each of the curves is the region of unstable impedance specifications, for that environmental stiffness. Notice that as the environment stiffness increases, the region of unstable impedance specifications increases dramatically.

Figure 3 shows the stabilizing effect of adding inertia to the environment. The environment is modelled as a stiffness and inertia. Again the region below each curve

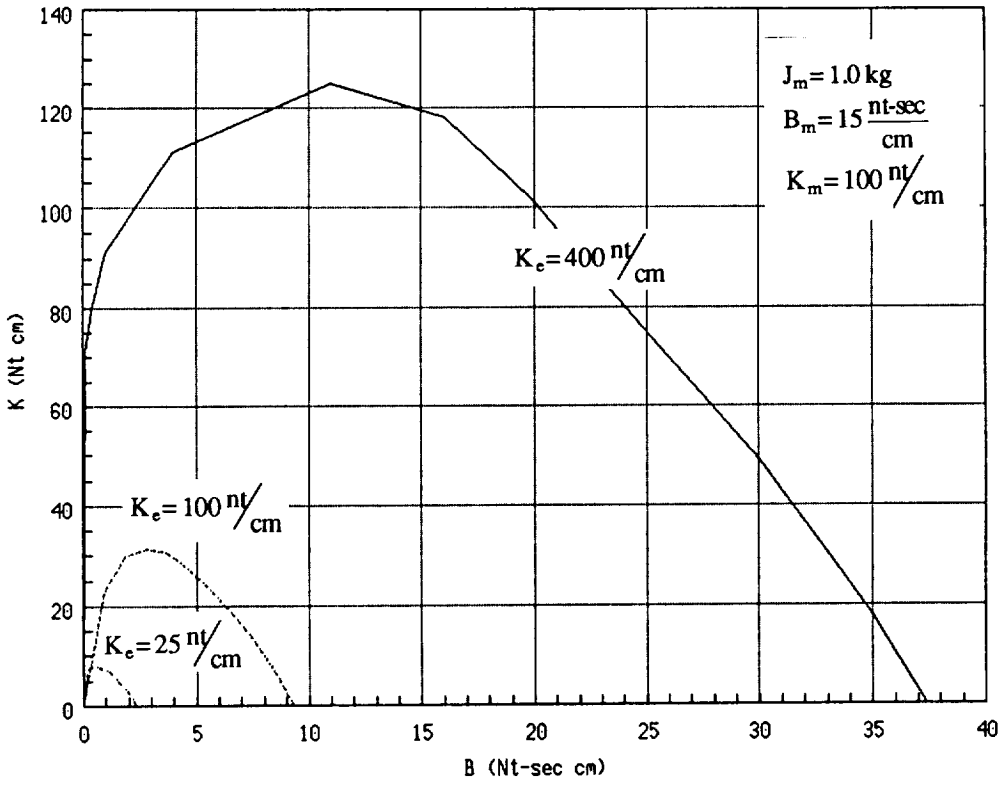

Figure 5-2: Stability boundaries for a pure stiffness environment.

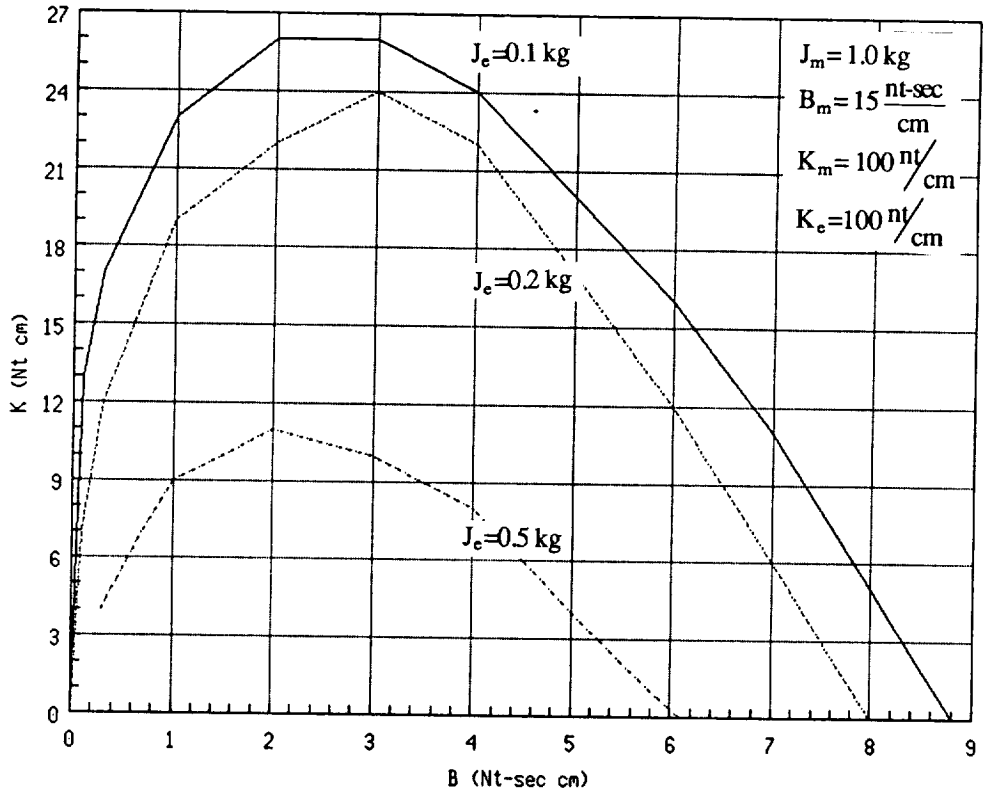

Figure 5-3: Stabilizing Effect of Environment Inertia.

corresponds to the region of unstable impedance specifications, for the particular environment dynamics. As the environment inertia increases, the region of unstable impedance specifications decreases. Relatively small amounts of inertia can have a dramatic impact on the system stability characteristics.

Adding damping to the environment will likewise tend to stabilize the system. We have limited our discussion to stiffness and inertial environments since we feel that these are the predominant dynamic characteristics in the majority of force interaction tasks. The extension of these results to other environments is straightforward.

It is critical to recognize that this analysis shows that **even for a manipulator with zero computational time delay, the combination of manipulator and environment can cause the manipulator to go unstable!** For the case shown here, two possible solutions to reduce the unstable region are:

1 to add inertia to the end-effector. This may not be practical since adding inertia at the end-effector greatly increases the torque requirements at all the joints back to the base – thus increasing system weight and power requirements.

2 to add compliance to the end-effector. For instance, if the environment stiffness was 1000 Nt/cm, it would be impossible to achieve an impedance of $K = 10 Nt/cm$ and $B = 1 \frac{Nt-sec}{cm}$. However if the end-effector was designed to have a stiffness of 50

Nt/cm, between the force sensor and the environment, the effective environment stiffness would be the series combination of the end-effector stiffness and the environment stiffness – therefore allowing us to achieve the desired impedance specification.

Effect of Computational Time Delay on System Stability

When a computational delay is included in the analysis it has a dramatic impact on the stability characteristics of the system. The computational delay has the effect of adding phase loss to the open-loop transfer function (4). The phase loss from the computational time delay will be function of frequency and is described by

$$\phi_{dly} = \omega T_{dly} \frac{180}{\pi}, \qquad (5-13)$$

where:

ϕ_{dly} is the phase loss in degrees,
ω is the frequency in rad/sec,
T_{dly} is the computational delay in seconds.

The computational delay thus lowers the frequency at which the phase crosses the 180° line. This then requires that the open-loop magnitude must cross the 0 dB line at a lower frequency to maintain closed-loop system stability.

Figure 4 shows the modelled system including the computational delay. The stability boundary for this system, in terms of the impedance specification B and K, occurs at the combination of B and K values which cause the open-loop transfer function to have zero gain and phase margin. Finding a closed form solution for this point is all but impossible, since it involves solving a set of coupled, trancendental equations (the expressions for the gain and phase of the open-loop system including time delay). However numerical optimization techniques can be employed to solve these equations, and find the stability boundary.

We are developing techniques and a prototype stability analysis package which will automate the determination of allowable impedance specifications, based on system stability. Figures 2 and 3, presented earlier, and 5 were generated using these techniques. Figure 5 shows the severely destabilizing effect of time delay. As the time delay is increased to 0.1 seconds, the minimum allowable impedance specification increases by a factor of 2, from the zero time delay case (Figure 3).

Experimental Verification of Analysis

The results using the simplified models discussed here have been verified against hardware results from our Dual Arm Testbed. Using one of the manipulators, a spring was attached between its end-effector force/torque sensor and ground. This spring served as the environment dynamics. The stiffness and damping specification of the impedance filter was adjusted to find the stability boundary.

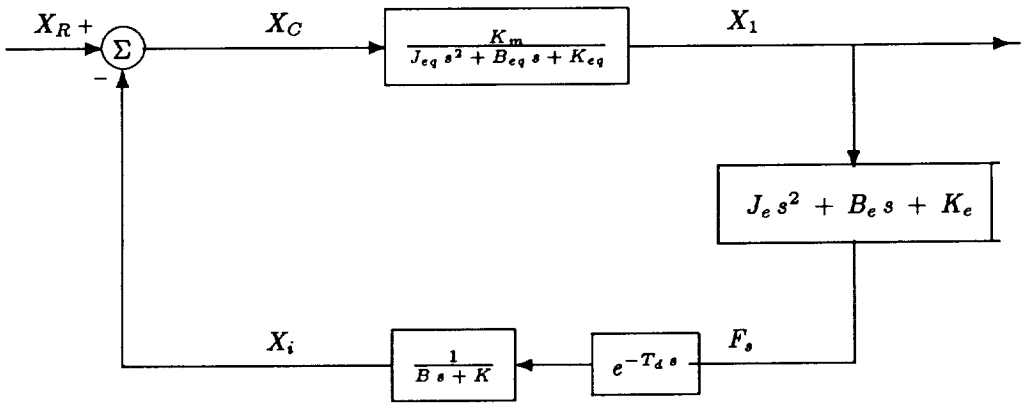

Figure 5-4: Model of system dynamics including computational time delay.

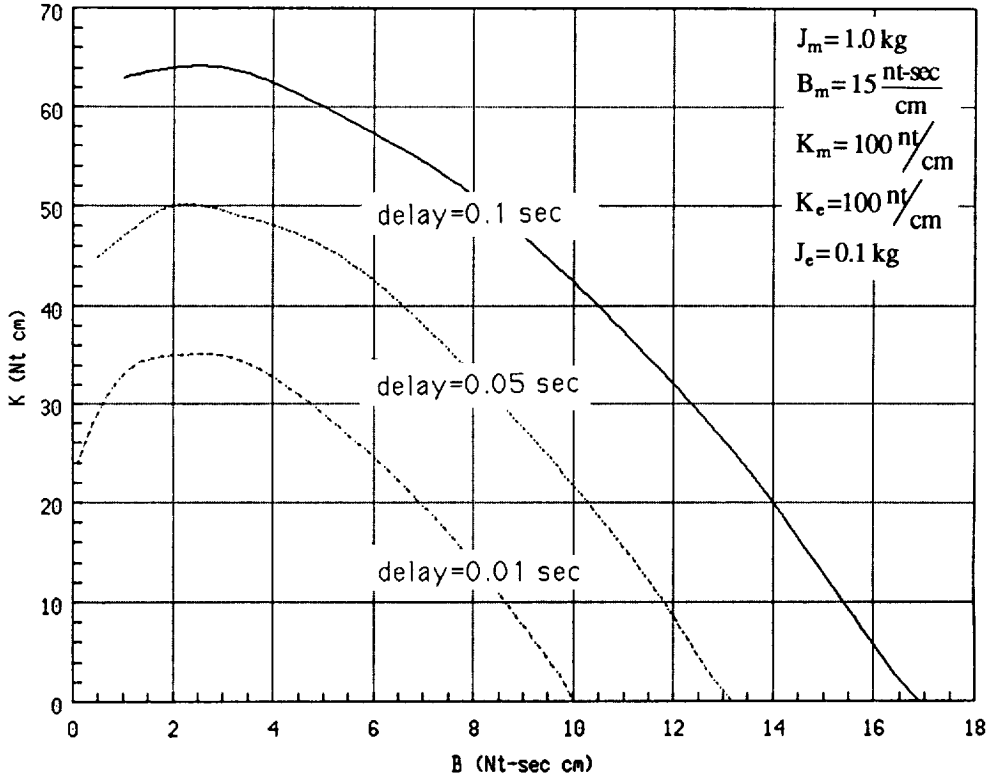

Figure 5-5: Effect of computational time delay on system stability.

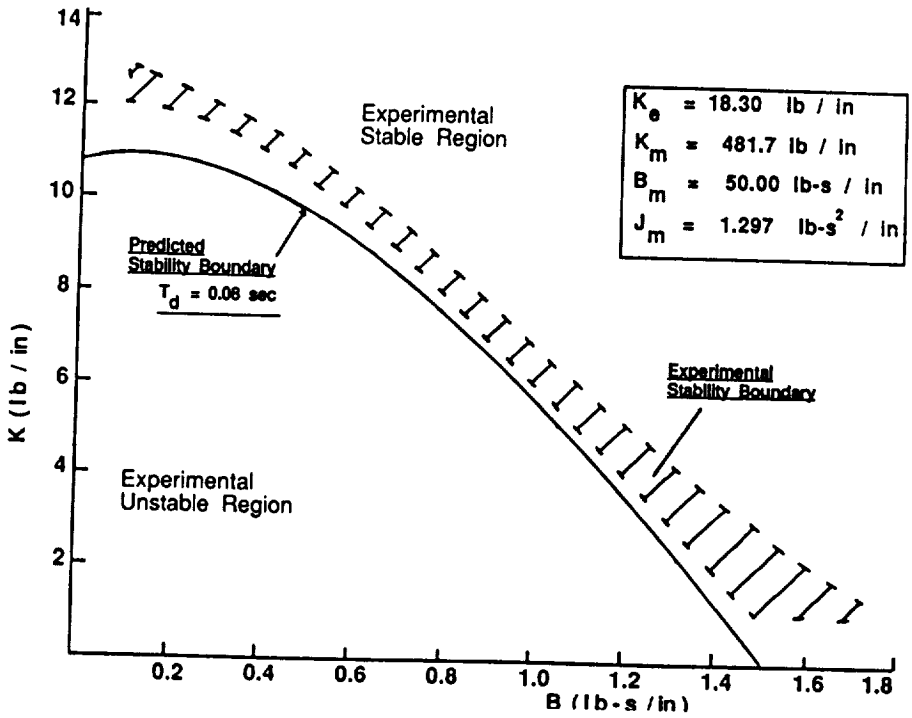

Figure 5-6: Comparison of predicted and actual stability boundary.

The time delay in the Cartesian impedance loop was then measured, and the closed loop joint dynamics identified. Using these results we computed the predicted stability boundary and compared it to the actual stability boundary. This comparison is shown in figure 6. The two show excellent agreement.

5.1.2 Stability for Coordinated Dual Arm Tasks

For coordinated dual arm tasks the stability question is much more complicated. One must still consider the effect of the external environment dynamics on the stability of each manipulator. In addition one must examine the effect of one manipulator on the stability of the other, taking into account the dynamics of any connecting structure between them.

We have investigated the validity of extending our analysis, using the simplified models of the system dynamics described earlier, to the coordinated dual arm case. Currently we have only considered the effect of one manipulator on the stability of the other, where the connecting structure is modelled as a pure spring. For this case the effective environment impedance, as seen by each of the manipulators, is simply the series combination of the connecting spring stiffness, and the end-effector impedance of the other manipulator.

Consider first the case with zero computational time delay. It is possible to derive the closed form analytic solutions for the system stability characteristics, following the same procedure used for the single arm case. It is only neccessary to supplement the expression for the environment dynamics with the closed-loop dynamics of the connected manipulator. Keep in mind that the resulting expression for system stability would be extremely complicated and it is not at all obvious that it would yield any useful insight

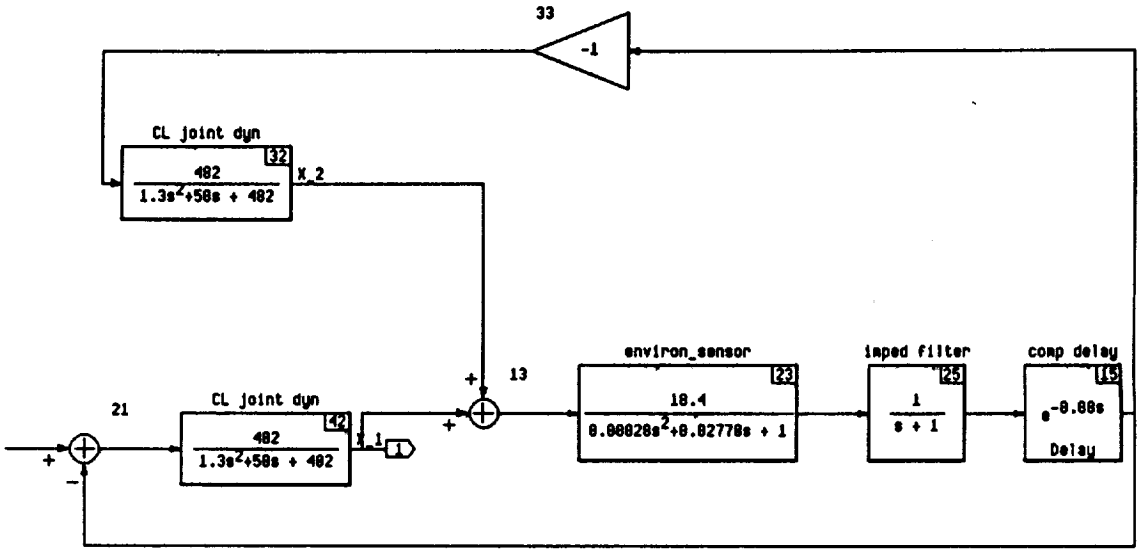

Figure 5-7: Block diagram of dynamic model for coordinated dual arm system.

into the problem. For that reason we have not attempted the algebra here.

When time delay is considered, numerical methods must again be employed to solve for the stability characteristics. These numerical techniques may then be tailored to allow parametric studies into how various system parameters (such as amount of time delay, dynamics of connecting structure, manipulator position dynamics) affect system stability. These studies can then be used to initiate further analytical investigations.

Using the simple models developed for the single arm stability analysis, we have simulated the response of the dual arm system and attempted to predict the stability boundary. Figure 7 is the block diagram of the dynamic model of the two manipulators interconnected by a spring of stiffness 18.4 lb/in. The manipulator dynamics are those of our Dual Arm Testbed, and both manipultors are considered to have identical dynamics. In addition the time delays in the two systems are identical, and the same impedance specifications were used in both manipulators.

Figure 8 compares the predicted stability boundary to the experimentally measured boundary. Again there is good agreement between the two. Notice that for this case the manipulators definitely have a destabilizing effect on one another. The region of unstable impedance specifcations has been pushed out by about a factor of two from the single arm case (Figure 6).

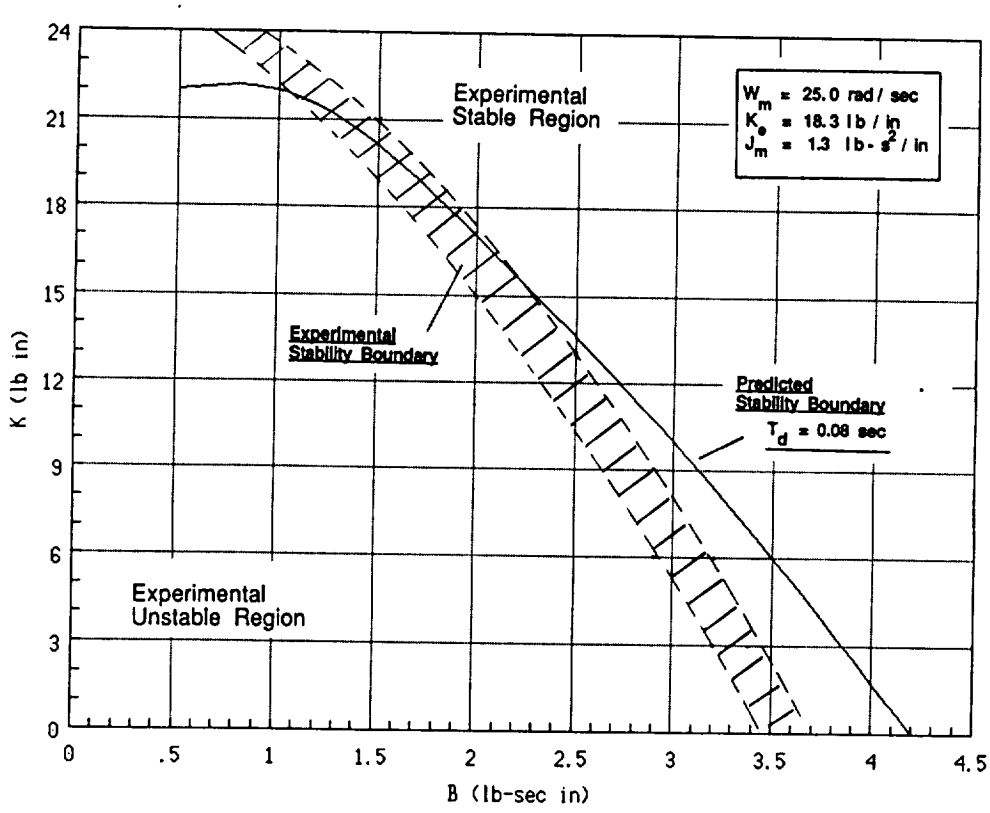

Figure 5-8: Comparison of predicted and actual stability boundary for dual arm case.

5.2 System Stability For Truss Connector Assembly Task

We have developed and verified techniques for predicting system stability characteristics using very simple environment dynamics. We now wish to examine how useful these simple models are in understanding the stability and performance characteristics for more complex 'real-world' tasks. To examine this issue we used the truss connector task, described in section 4.3 of this report. Using the same test setup as for the X axis misalignment experiments (see section 4.3.2), we reduced the Cartesian translational impedance specifications on Robot 1 until we approached the stability boundary, and Robot 1 was marginally unstable. We then first increased the stiffness specification to see its effect on stabilizing the system. Following this we increased the damping specification to examine its impact on system stability.

For the first experiment the damping of the Cartesian translational axes was set at $B_{x,y,z} = 0.54\frac{Nt-sec}{cm}$. The stiffness specifications for the X and Z axes were $K_x = 0.81Nt/cm$ and $K_z = 0.27Nt/cm$. Figure 9 shows the position and force time histories along the X axis. Notice that after the connector halves are mated a strong limit cycle develops, resulting in peak forces of 6 Nt. This force level was high enough to cause movement of the connector in the end-effector jaws.

The stiffness of both the X and Z axes were doubled for experiment 2, to $K_x = 1.62Nt/cm$ and $K_z = 0.54Nt/cm$. Figure 10 shows the X axis time histories for this experiment. The results are virtually the same as experiment 1, with the peak force remaining at 6 Nt.

For experiment 3 the stiffness specifications for the X and Z axes were doubled from experiment 2, to $K_x = 3.24Nt/cm$ and $K_z = 1.08Nt/cm$. Figure 11 shows the X axis position and force time histories. After quadrupling the stiffness specifications, from their original values, we finally see some improvement in system stability. The limit cycles are slightly reduced, and the peak force has been reduced to 4 Nt.

The next experiments examined the effect of the damping specification on system stability. Experiments 4 – 6 used X and Z axis stiffness specifications of $K_x = 1.62Nt/cm$ and $K_z = 0.54Nt/cm$.

In experiment 4 the translational axes damping specification was increased to $B_{x,y,z} = 0.63\frac{Nt-sec}{cm}$. Figure 12 shows the X axis response. The limit cycles have been dramatically reduced from those of experiment 2 (Figure 10), which used the same stiffness specification and a damping specification of $B_{x,y,z} = 0.54\frac{Nt-sec}{cm}$. The peak forces for experiment 4 have been reduced to 2.5 Nt, which is less than half of those recorded for experiment 2.

Experiment 5 used a damping specification of $B_{x,y,z} = 0.72\frac{Nt-sec}{cm}$. Figure 13 shows the X axis time histories. The peak force has been further reduced to below 1.5 Nt.

The damping specification for experiment 6 was increased to $B_{x,y,z} = 0.81\frac{Nt-sec}{cm}$. Figure 14 shows the X axis time histories. The limit cycles have been reduced to slightly over 1 mm and the peak force is only 0.8 Nt. Thus increasing the damping specification

by 50% has led to a reduction in peak forces by a factor of 7.5.

From these experiments it is clear that the system stability characteristics are much more sensitive to the damping specification than to the stiffness specification. A 400% increase in stiffness specification caused a 33% reduction in peak force, while a 15% increase in damping specification caused a 50% reduction in peak force.

These results are very consistent with those seen using the very simple environment. Looking again at Figure 6 we see that the slope of the stability boundary near the $K = 0$ crossover is fairly steep. Therefore the system stability will be much more sensitive to changes in damping specification, B, than to changes in stiffness specification, K, in this region.

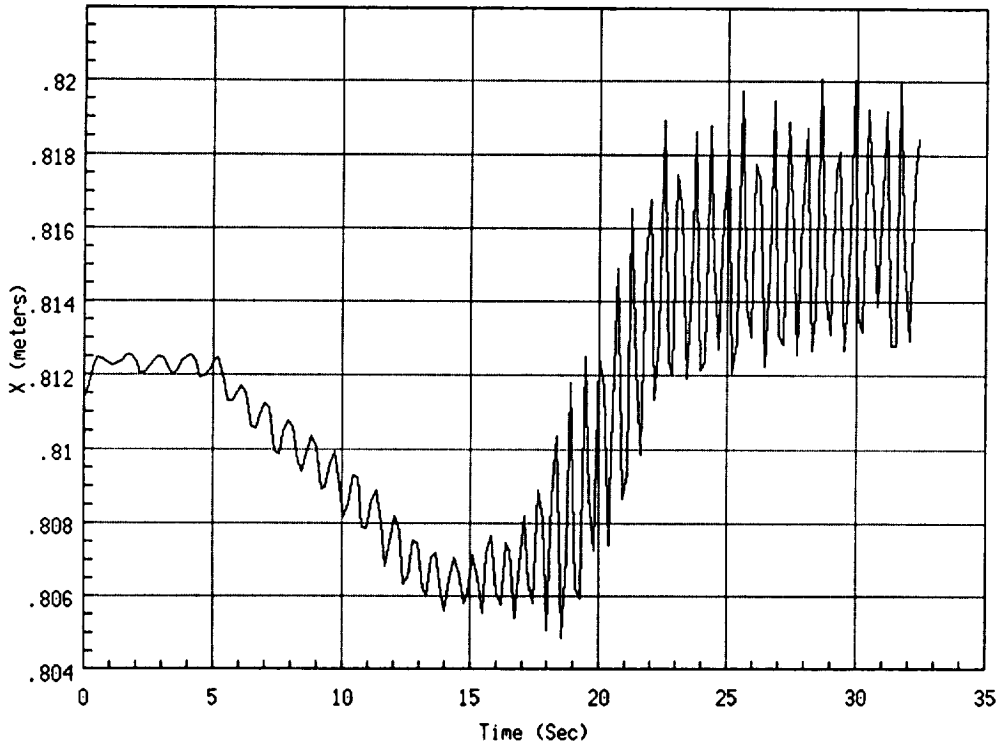

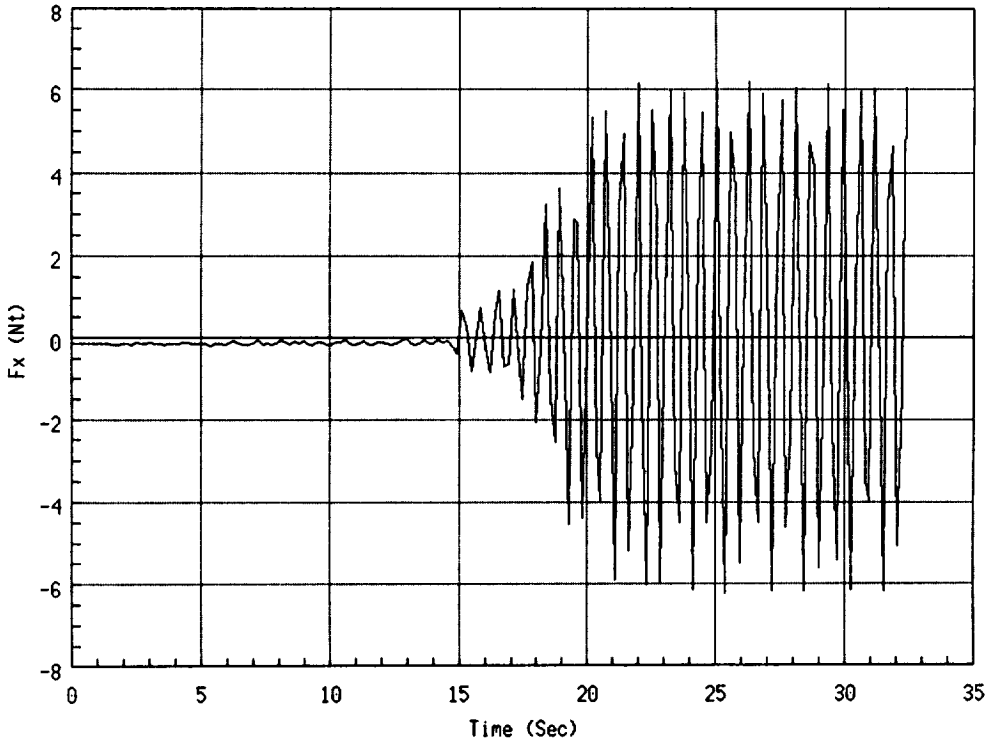

Figure 5-9: X Axis position and force time histories for experiment 1, $B_{x,y,z} = 0.54\frac{Nt-sec}{cm}$, $K_x = 0.81\frac{Nt}{cm}$, $K_y = 0.27\frac{Nt}{cm}$.

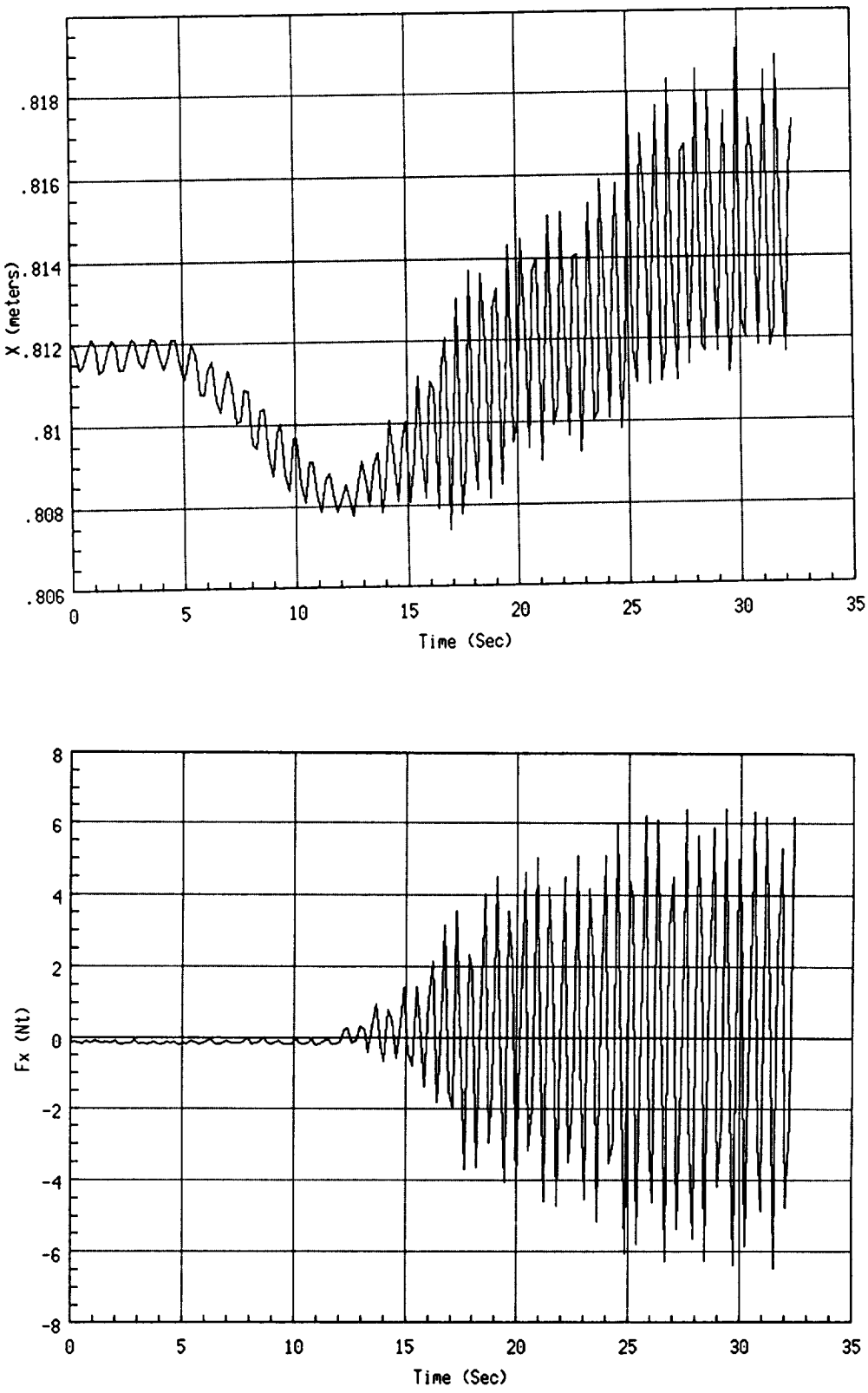

Figure 5-10: X Axis position and force time histories for experiment 2, $B_{x,y,z} = 0.54\frac{Nt-sec}{cm}$, $K_x = 1.62\frac{Nt}{cm}$, $K_y = 0.54\frac{Nt}{cm}$.

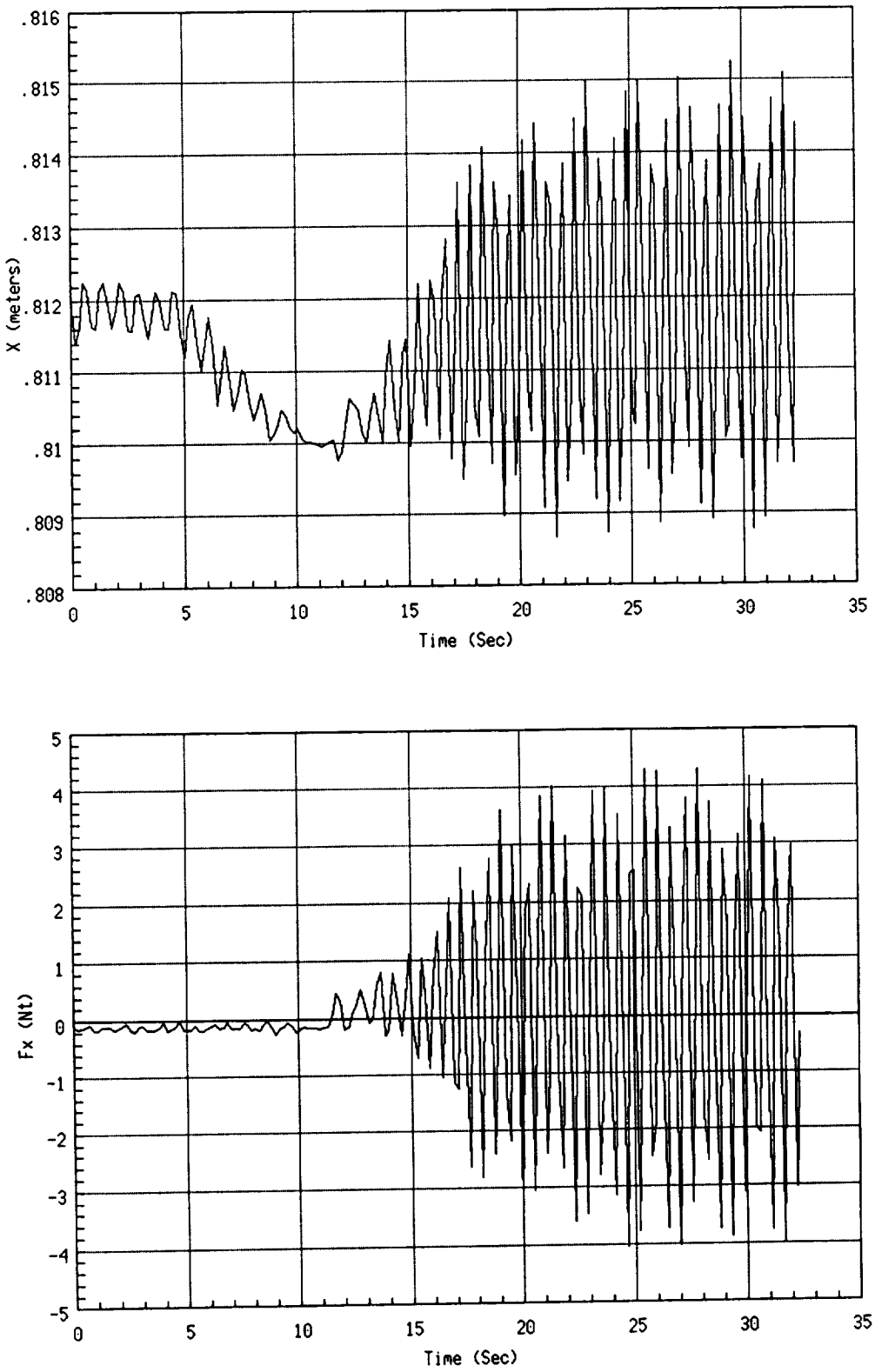

Figure 5-11: X Axis position and force time histories for experiment 3, $B_{x,y,z} = 0.54\frac{Nt-sec}{cm}$, $K_x = 3.24\frac{Nt}{cm}$, $K_y = 1.08\frac{Nt}{cm}$.

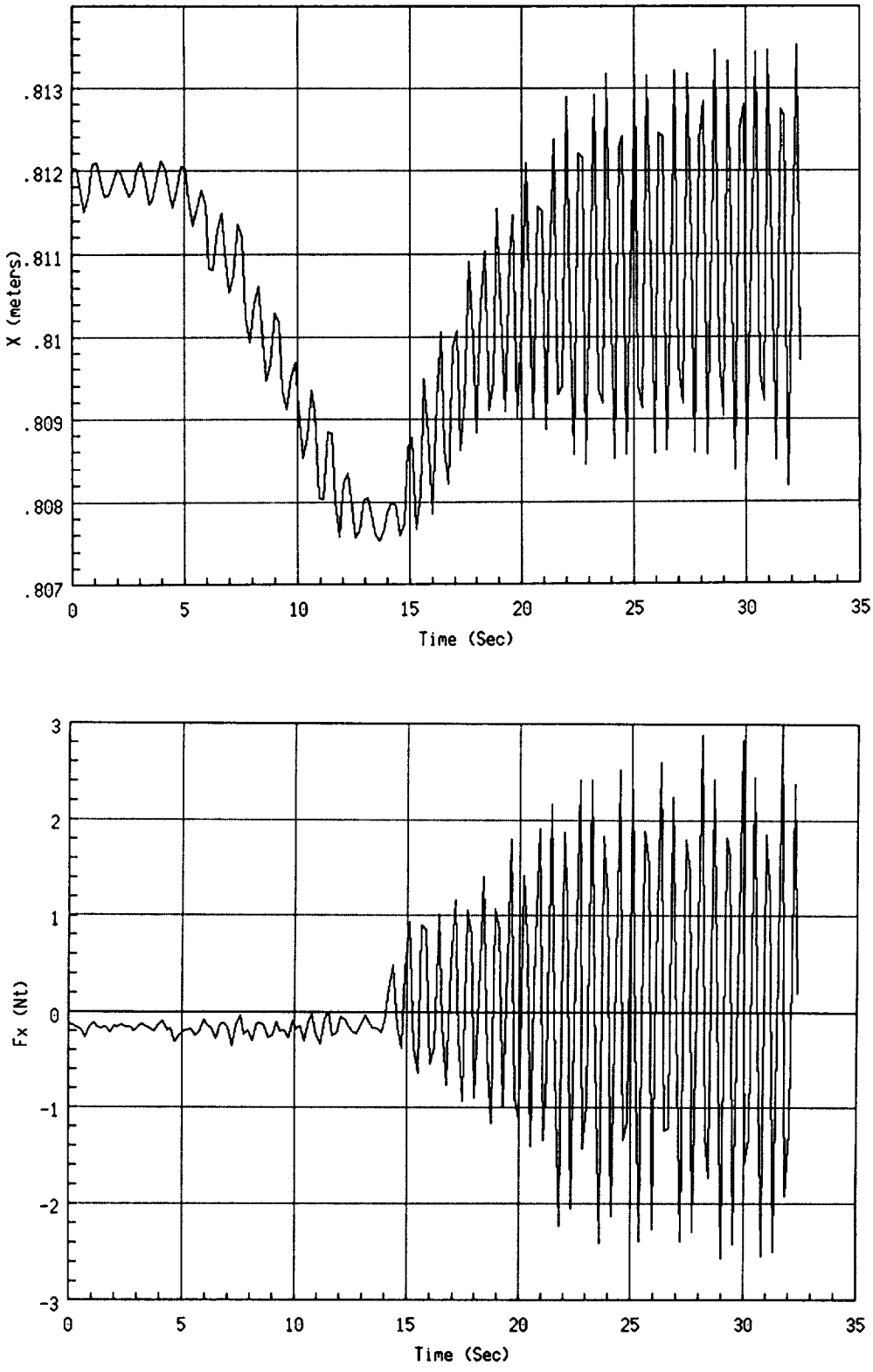

Figure 5-12: X Axis position and force time histories for experiment 4, $B_{x,y,z} = 0.63\frac{Nt-sec}{cm}$, $K_x = 1.62\frac{Nt}{cm}$, $K_y = 0.54\frac{Nt}{cm}$.

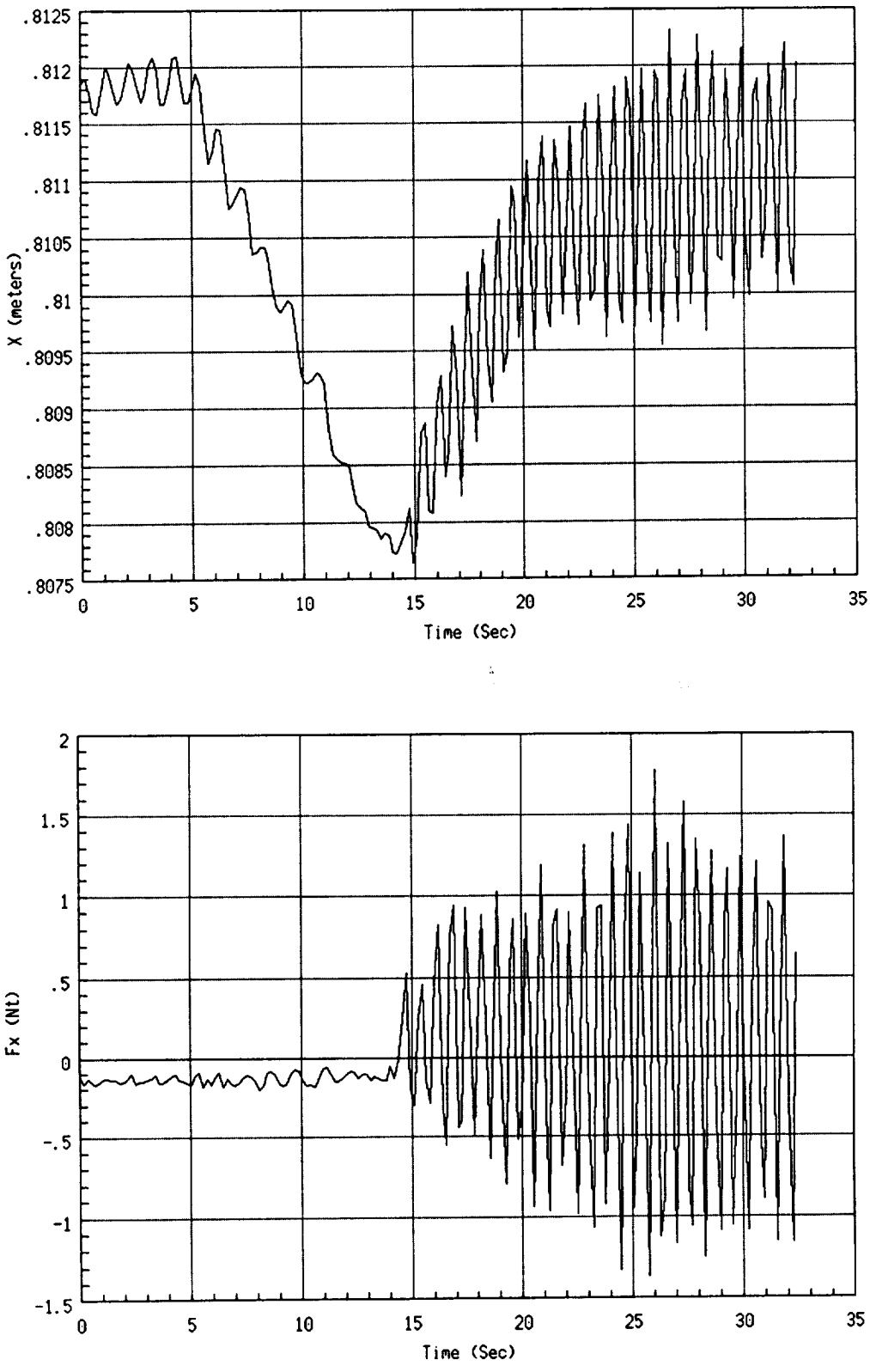

Figure 5-13: X Axis position and force time histories for experiment 5, $B_{x,y,z} = 0.72\frac{Nt-sec}{cm}$, $K_x = 1.62\frac{Nt}{cm}$, $K_y = 0.54\frac{Nt}{cm}$.

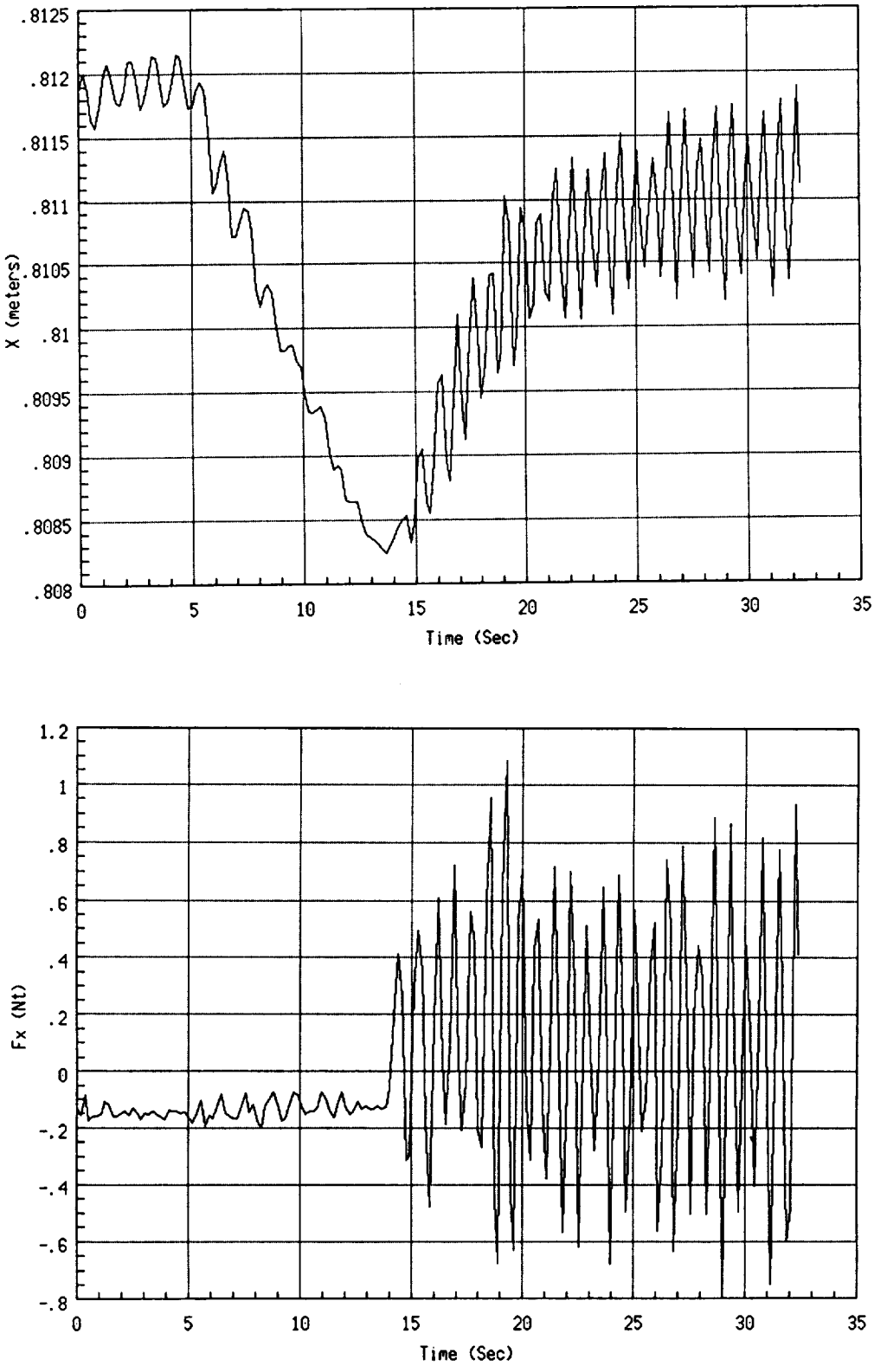

Figure 5-14: X Axis position and force time histories for experiment 6, $B_{x,y,z} = 0.81\frac{Nt-sec}{cm}$, $K_x = 1.62\frac{Nt}{cm}$, $K_y = 0.54\frac{Nt}{cm}$.

Chapter 6

VERIFICATION OF MANIPULATOR IMPEDANCE

This chapter describes an approach to determining achieved manipulator mechanical impedances which result from various control implementations. Identifying these impedances is important when impedance control is implemented, so that the actual system behavior can be compared with design goals. Such comparison provides the detailed, quantitive data necessary to determine when certain impedance objectives can be achieved, and what system components cause performance limitations. Even when impedance control is not used, that is, when the performance specification is not explicitly in terms of impedances, an identification of the achieved impedances can help in understanding the performance capabilities of the manipulator. This is especially true when the task involves environmental contact, and the environment is not highly structured or accurately known.

6.1 Mechanical Impedance Terminology and Notation

For any particular manipulator and associated controller, limitations exist in the ability to achieve various levels of stiffness, or more generally, various mechanical impedances. A proper understanding of these limitations depends on the ability to measure and quantify actual manipulator impedances. This report describes a general identification technique for achieved impedances which can be used on any robot system, controlled by any controller.

Mechanical impedance is defined as the relation between positions and forces at some point on a system. In general, it is a non-linear dynamic relation which may be quite complicated [HOG85]. When this relation exists as a single valued function in some region, an impedance and/or admittance function exists. When these functions are smooth enough so that derivatives exist, and the first derivatives are non zero, then impedance and admittance functions both exist and are inverses of one another (inverse function theorem). As a practical matter, most impedance relations satisfy these smoothness conditions, or can be closely approximated by sufficiently smooth impedance or admittance functions. Moreover, an impedance specification is likely to be as simple as possible (ie. as simple as necessary to complete a manipulation task). Thus, linear impedances will be considered exclusively in this report. This of course is a good local approximation if the desired impedance is slowly varying as a function of manipulator position.

We will consider an impedance specification which captures the dominant effects of stiffness, damping, and inertia. This is a necessary level of complexity, and additional

detail in this specification could be considered as needed in later studies. When this impedance relation is linear, it takes the form

$$F = KX + B\frac{dX}{dt} + J\frac{d^2X}{dt^2}$$

where K, B, and J are the stiffness, damping, and inertia matricies, respectively. F is the vector of cartesian forces and torques acting at the point in question, and X is the vector of cartesian positions and orientations, also measured at the point in question. (We will assume throughout that orientations are represented in the euler axis-angle form. Although this is not the most convenient representation for actual control implementation, straightforward transformantions exist from this form to quaternion and direction cosine matricies.) A mechanical system has certain restrictions on the impedance parameters. For example, the parameters must be "non-negative", and they have a special structure (they are symmetric). With feedback control, however, "unnatural" impedances can be constructed, even "negative" ones. However, until a need for more complex structure in these matrices is demonstrated by experience on real tasks, we will assume that they are all diagonal. This implies that the impedance specifications in each cartesian degree of freedom are independent from any other. This causes the impedance description above to simplify to the scalar equation

$$f = kx + b\frac{dx}{dt} + j\frac{d^2x}{dt^2}$$

along each cartesian direction.

The above linear, decoupled impedance is only a specification or a goal. For any particular manipulator under a specific control scheme, the probability is great that this desired impedance is not achieved precisely. In fact the controlled system may be unstable in the presence of certain properties of the environment, manipulator, or control parameters. See [LAW87,LAW88] for studies of impedance control stability properties. Assuming that the controlled system is stable, the performance of the closed loop system must be measured to determine the success of a particular control scheme. Here, performance is measured as the degree to which the desired impedance goal is achieved. That is, measured manipulator impedances resulting from feedback control will be directly compared to the impedance specifications used in control design.

Some portions of the manipulator impedance can be directly measured. For example, the stiffness k in a particular direction is relatively easy to measure using a force gauge and ruler. However, the damping and inertial terms are difficult to measure, since constant velocity or acceleration sources would be required for direct measurement. Another approach is taken here. Since the impedance is a dynamic function which is supposed to be linear, frequency domain techniques will be used. Measurements of position and orientation, together with forces and torques in each Cartesian direction of interest are recorded as time series. Offline computations of the Fourier transforms of these signals are computed and "divided" to form the transfer functions relating positions (inputs) to

forces (outputs), which is the frequency domain representation of impedance. These transfer functions are typically represented separately as magnitude and phase functions of frequency, although pole and zero representations are sometimes useful.

Consider the following impedance specification along a particular degree of freedom

$$f(s) = (k + bs + js^2)x(s) \qquad (6-1)$$

in the frequency domain. The transfer function $f(s)/x(s)$ is the impedance along this axis, which has the general frequency response characteristics shown in Figure 1-1. Note

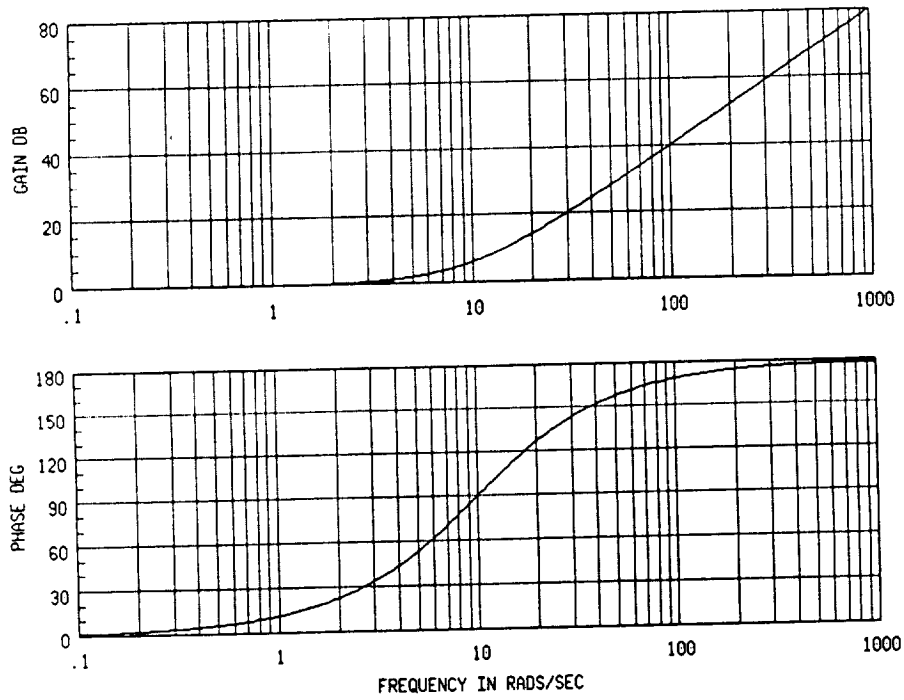

Figure 6-1: Magnitude and phase of the impedance specification $k + bs + js^2$.

that the DC value of the magnitude of the impedance is the stiffness k. As the frequency increases, damping terms dominate, followed by domination by the inertial term. At high frequencies, the slope of the magnitude function approaches 40 dB/decade. The phase function begins at zero and increases to $+\pi$ radians, or +180 degrees.

The measurement of actual impedance should closely correspond to the curves of Figure 1, when the corresponding desired and programmed impedance parameters k, b, and j are used. This can be checked along each Cartesian degree of freedom individually. Even if these curves are similar, the actual performance may not be similar to the desired performance. What are missing are the "cross impedances", those relations between one Cartesian direction's force and another's position. Since the impedance objectives are decoupled between these axes (in this report at least), the measured cross impedances

should be zero. Practically, they will not be precisely zero, particularly as frequencies increase. At high frequencies, the control designed to implement the desired objective typically is less effective due to actuator torque/speed limits. Thus, the measured cross impedance can be expected to be small for low frequencies (small magnitude *and* phase), and magnitudes and/or phases may increase at higher frequencies. The "bandwidth" of the region where the cross impedance is small, as well as the "size" of the cross impedance can be used as a measure of the degree of decoupling actually achieved.

For a characterization of all six Cartesian degrees of freedom, then, a complete measurement of the manipulator's achieved impedance would consist of a set of 36 transfer functions. For a real mechanical system, the impedance is always symmetric, i.e. the impedance from an axis **x** to another axis **y** is always the same as the impedance from the **y** axis to the **x**. In this case, the impedance matrix is symmetric, and only 21 unique impedances are possible. However mechanically non-realizeable impedances are possible using feedback control, so all 36 impedances are necessary in general.

The above impedance measurements are assumed to take place in the neighborhood of zero environmental interaction. When large forces occur as a result of deflecting the manipulator well away from this "impedance center", nonlinear effects due to torque saturation and manipulator kinematics may cause significant deviations from the linear impedance objectives. Although for some tasks this behavior is also of interest, it cannot be expected to match the simple linear impedance specification. In other words, the impedance measurements above are derived from "small signal" motion responses.

Having described the necessary quantities to measure, we now turn to a discussion of ways to obtain these measurements. What we have is essentially a multivariable system identification problem. All 36 elements in the impedance matrix must be identified using only 12 Cartesion signal measurements (six positions/orientations and six forces/torques). In principle, the easist way would be to allow motion in only one axis at a time, but measure the resulting forces along all axes. This would fill out one column of the impedance matrix at a time. A dual approach would be to allow forces only in one direction, while measuring resulting positions in all axes. This would fill out one row of the impedance matrix at a time. Both these simple approaches require a special fixture at the point where impedance is to be measured. The first is very rigid, except for one Cartesian position or orientation at a time. The second has "zero rigidity", i.e. can support no forces (both static and dynamic) in all axes but one, at any one time. Even though this is a conceptually simple approach, it may be quite difficult to carry out in practice.

A conceptually more difficult approach would be to excite motion in all axes at once, and measure all resulting forces at once, then combine all these measurements to obtain the full impedance matrix in one step. This would certainly be easier to achieve mechanically, since no special fixtures would be required. However, the impedance matrix may not be adequately "filled", since there are fewer measurements than there are variables to determine.

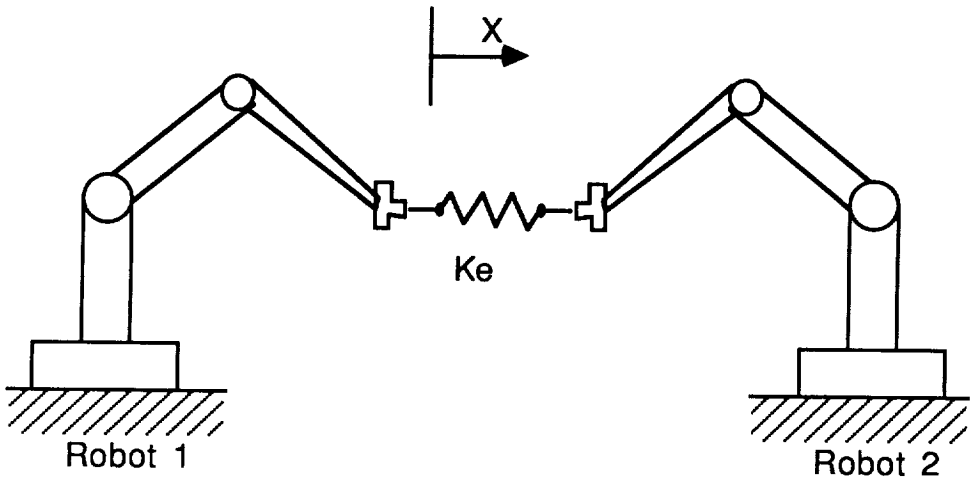

Figure 6-2: Experimental setup for impedance measurement tests.

6.2 Experimental Test and Test Objectives

To confirm our ability to measure impedances a simple test was developed using the T_3-726 Dual Arm Test-Bed. The test objectives were to individually identify both the end-effector impedance of robot arm 1 and the environment impedance (along a single Cartesian direction).

The test setup is shown in Figure 2. A fixture with a known stiffness in the X direction, and virtually zero stiffness in all other Cartesian axes, was connected between the force sensors of the two robots.

Robot arm 1 had low impedances programmed in at least the X direction for all the tests (low impedances were specified in all axes for some tests). Robot arm 2 had large impedances programmmed in all axes, thus robot arm 2 behaved very similarly to a pure position source.

Figure 3 shows a simplified block diagram of the robot arm 1 dynamics along the X axis. Notice that there are two possible sources of input signal, either X_r or X_2. X_r is the standard reference position input to robot 1, X_2 is a disturbance input from robot 2. The effect of the X_2 input is to cause a force disturbance on the end-effector force sensor equal to $f_s = (X_1 - X_2)K_e$.

If X_r is zero and the system excitation is from X_2, then the transfer function from f_s to X_1 will be the inverse of the impedance of robot arm 1. That is

$$Z_{1_x} = \frac{1}{H(s)G(s)}. \qquad (6-2)$$

If $G(s)$ has a much higher bandwidth than $H(s)$, and if $K_m \gg K_e$, then at frequencies below the bandwidth of $G(s)$ the manipulator impedance Z_{1_x} should closely approximate that specified in $H(s)$.

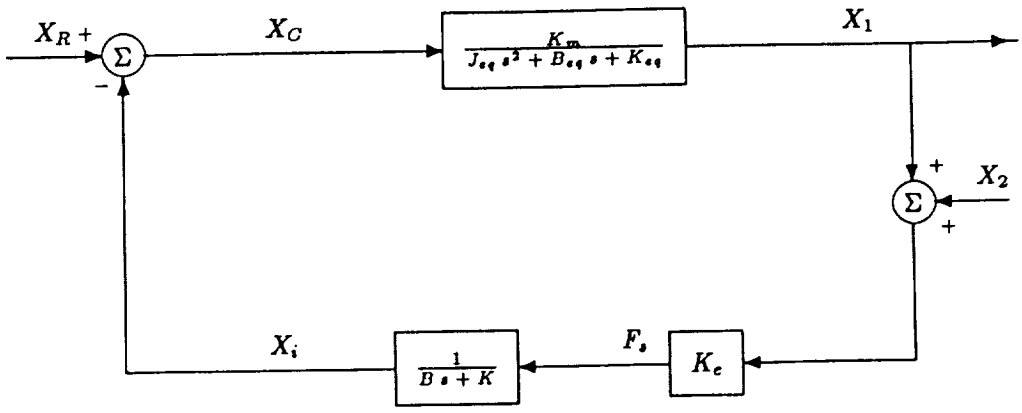

Figure 6-3: Block diagram of Robot 1 in contact with Robot 2 through spring environment of stiffness K_e.

If X_2 is constant and the system excitation is from X_r, then examining the transfer function from X to f_s will identify the environment impedance,

$$Z_{e_x} = K_e. \tag{6-3}$$

Notice that to identify different impedances we are using identical measurements, but different excitation sources. To measure the end-effector impedance we would ideally use a force source at the end-effector force sensor. To measure the environment impedance we would ideally use a reference position source.

6.3 Experimental Test Results

The results from the experimental tests are presented as a series of frequency response plots from an HP 3562A Dynamic Signal Analyzer. The 'swept-sine' input source from the signal analyzer was used for the excitation signal in all the tests. The measurement signals from which the various frequency response plots were calculated were taken off the D/A ports on the digital robot controllers. The effect of the digital controllers can be seen in the higher frequency part of the frequency response plots. At the upper frequencies the curves become very choppy. The position control loop is running at 33 Hz. Thus the maximum frequency at which the measured data will closely approximate a continuous signal is between 3 and 5 Hz.

Figure 4 shows the closed loop transfer function from X_r to X when the environmental contact is zero. This corresponds to $G(s)$ from Figure 3. The bandwidth of $G(s)$ is approx. 4.5 Hz.

The environment impedance was identified by inputting a swept sine signal at X_r and looking at the transfer function from X_r to f_s. Figure 5 shows the frequency response of this tranfer function. While the magnitude is not very smooth, its average value over the frequency range 0.1 - 5.0 Hz is approximately 33.8 dB which corresponds to an environmental stiffness of 48.9 lb/in. This stiffness compares well with the measured stiffness of the spring fixture of 50 lb/in ($^+/_-$ 5 $\frac{lb}{in}$).

The maniulator impedance was identified by inputting a swept sine signal at X_2 (using robot 2), and looking at the transfer function from X to f_s. For the first test, the stiffness and damping of the first robot were set to 3 lb/in and 3 lb-sec/in, respectively, in the X direction, and to 20 lb/in and 20 lb-sec/in, respectively, in all other axes. Figure 6 shows the frequency response of this transfer function. The dashed line below the magnitude curve is the predicted magnitude based only on the impedance specification. The marker at approximately 1.3 Hz indicates the frequency beyond which the data coherence is poor. Up to this 1.3 Hz marker there is good agreeement between the actual impedance and the specified impedance. The magnitude shows a definite first order characteristic, and the gain is shifted by only 2 dB from the predicted value. The 35° phase shift over 1 Hz corresponds to a time delay of 0.097 seconds, which is very close to the measured time delay in the force data of 0.08-0.09 seconds.

For the second case the manipulator impedance specification was set at 3 lb/in and 3 lb-sec/in in all Cartesian axes. The manipulator impedance was identified in the same manner as above. Figure 7 shows the frequency response for this case. The results are virtually identical to those shown in Figure 6.

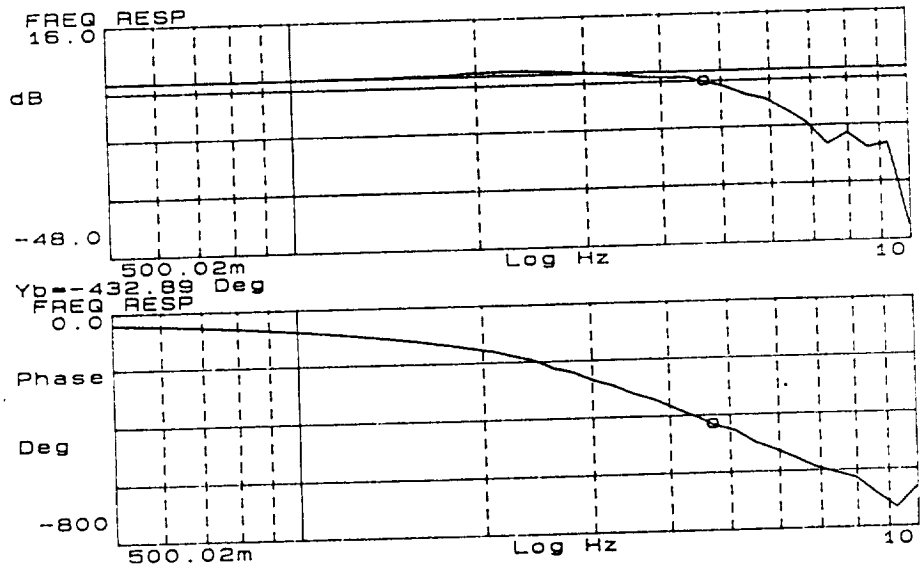

Figure 6-4: Transfer function of Cartesian position response in free-space, X/X_R.

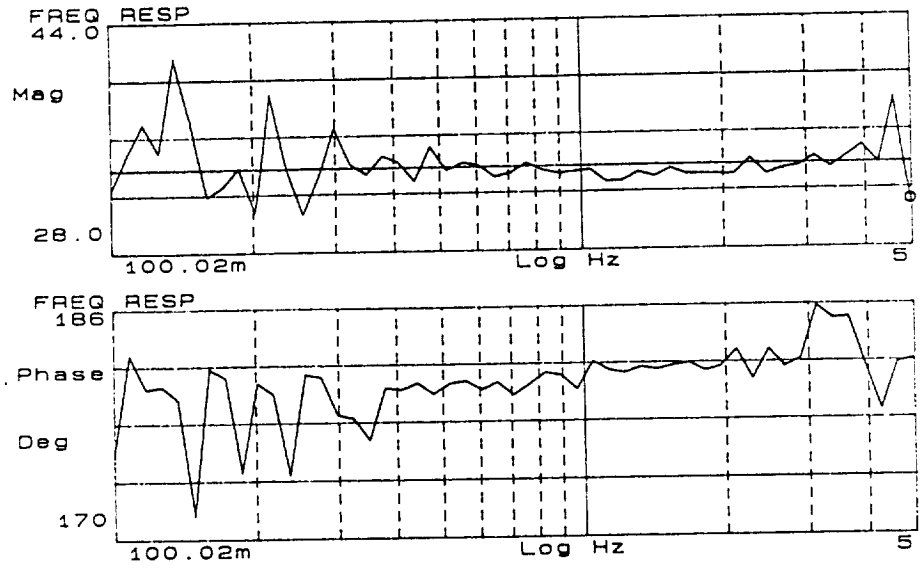

Figure 6-5: Identification of environment impedance, F/X_R.

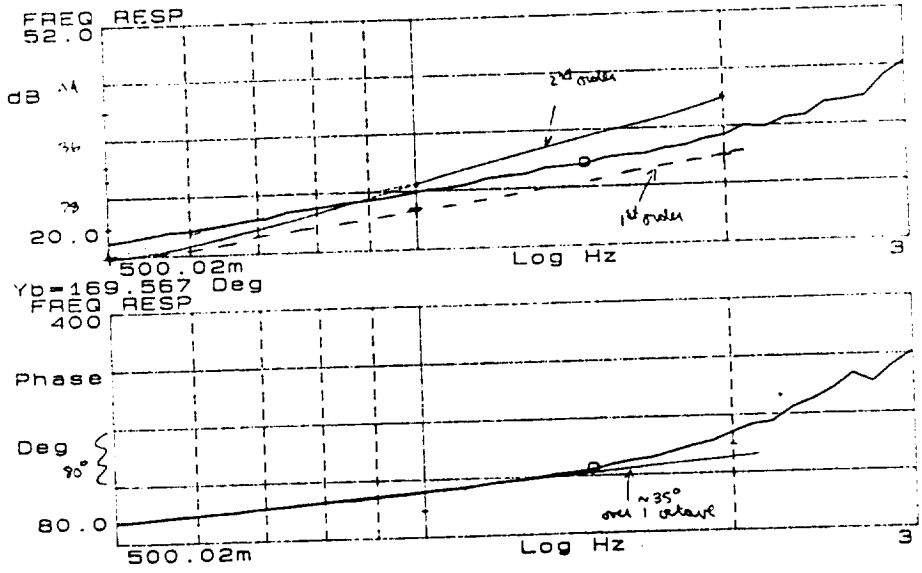

Figure 6-6: Identification of manipulator impedance, F/X, (source = X_2)

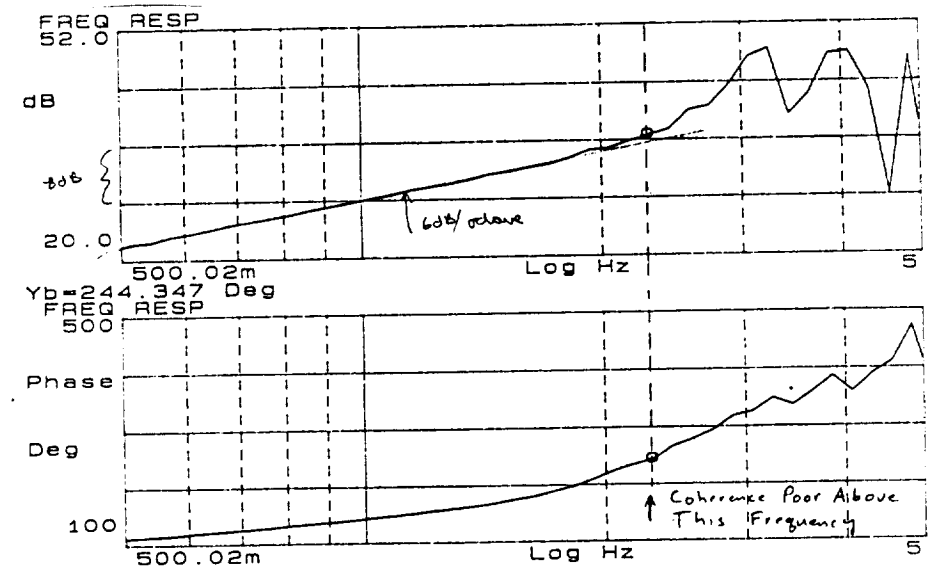

Figure 6-7: Identification of manipulator impedance, F/X, (source = X_2)

The experiments described above show that is indeed possible to measure the dynamic characteristics of both the manipulator and the environment. Both the environment stiffness and the manipulator impedance were accurately measured at low frequencies.

The experiments also demonstrated the need for much more sophisticated test facilities than were used here. The 80-90 ms. delay in the force data made it difficult to interpret the force data at frequencies above 2-3 Hz.

To measure the impedance of the manipulator, the ideal measurement technique would use a pure force source to excite the manipulator at the end-effector, and the measurements would be taken from a combination force/torque sensor and inertial position sensor, where the measurement data is either analog, or sampled at a frequency above 1000 Hz. The sensor would be attached at the point through which the manipulator is being excited.

To measure the impedance of the environment, the ideal measurement technique would use a pure position source to excite the environment, and measurements would be taken from the same sensor used above, with the sensor now attached to the environment.

The ability to measure the Cartesian impedance of the manipulator, even in the rudimentary fashion shown here, demonstrates a key technology in the thrust to develop manipulator systems which are designed to meet predefined dynamic requirements.

Chapter 7
CONCLUSION

This report has described a methodology which, if implemented, would advance manipulator design and development from a poorly understood black art to a well structured, scientifically sound and reliable technology. The key aspects of this methodology have been discussed and shown to be within current technical capabilities.

From a system design and analysis viewpoint some of the extensions required for multiple arm systems have been explored.

Significant efforts will be required in three primary areas before this methodology is fully matured. These are:

- **definition of performance requirements**
  For the near term, performance requirements will be primarily derived from experimental testing. As a large database of requirements for difficult tasks is developed work can begin on analytical methods to generalize the results in the database. This may be a fruitful application for an expert system.

- **new control structures**
  examination of the effects of different control structures and the use of more complex impedance specifications,

- **identification of impedances**
  Application of state-of-the-art recursive system identification techniques to the identification of both manipulator and environmental impedances. This approach would obviate the need for expensive laboratory test fixturing to measure impedances, and would allow for a compact, portable testing system suitable for use in the operating environment.

The application of this, or a similar methodology for manipulator design, development and testing is vital for the development of reliable manipulator systems at an affordable cost.

REFERENCES

[DEP88] T.M. Depkovich, "Experimental Verification of Dual Arm Controller Performance", *Proc. American Control Conference*, June 1988, pp 483-488.

[HOG85] N. Hogan, "Impedance Control: An Approach to Manipulation", *ASME Journal Dynamic Systems Measurement and Control*, March 1985.

[KHAT87] O. Khatib, "A unified approach for motion and force control of robot manipulators: the operational space formulation", *IEEE Journal of Robotics and Automation* February 1987, pp.43-53.

[LAW87] D.A. Lawrence and R.M. Stoughton, "Position based impedance control: achieving stability in practice", *Proc. AIAA Conference on Guidance, Navigation and Control*, August 1987.

[LAW88] D.A. Lawrence, *Proc. IEEE International Conference on Robotics and Automation*, April 1988.

[MAS81] M.T. Mason, "Compliance and Force Control for Computer Controlled Manipulators", *IEEE Transactions Systems, Man and Cybernetics*, SMC11(6), 1981.

[RAIB81] M.H. Raibert, J.J. Craig, "Hybrid Position/Force Control of Manipulators", *ASME Journal Dynamic Systems Measurement and Control*, vol 102, 1981.

[SAL80] K.J. Salisbury, "Active stiffness control of a manipulator in Cartesian coordinates", *Proc. IEEE Conference on Decision and Control* Dec 1980.

[SER87] H. Seraji, "Design of Force/Position Controllers for Manipulators", *Proc. AIAA Guidance, Navigation, and Control Conference*, August 1987.

NASA
National Aeronautics and Space Administration

Report Documentation Page

1. Report No.	2. Government Accession No.	3. Recipient's Catalog No.
NASA CR–182043		

4. Title and Subtitle
Space station Definition, Design and Development — Task 5: Multiple Arm Telerobot Coordination and Control.

5. Report Date
July 1990

6. Performing Organization Code

7. Author(s)
R. M. Stoughton

8. Performing Organization Report No.
MCR–88–612

10. Work Unit No.
590–11–41–01

9. Performing Organization Name and Address
Martin Marietta Astronautics Group
P.O. Box 179
Denver, CO 80201

11. Contract or Grant No.
NAS1–18230

13. Type of Report and Period Covered
Contractor Report

12. Sponsoring Agency Name and Address
National Aeronautics and Astronautics Administration
Langley Research Center
Hampton, VA 23665-5225

14. Sponsoring Agency Code

15. Supplementary Notes
Langley Technical Monitor: Donald Soloway
Final Report — Task 5

16. Abstract

This report describes a proposed methodology applicable to the design of manipulator systems. The current design process is especially weak in the preliminary design phase, since there is no accepted measure to be used in trading off different options available for the various subsystems. The design process described here uses Cartesian End-Effector Impedance as a measure of performance for the system. Having this measure of performance it is shown how it may be used to determine the trade-offs neccessary to the preliminary design phase.

The design process involves three main parts: (1) determination of desired system performance in terms of End-Effector Impedance, (2) trade-off of design options to achieve this desired performance, (3) verification of system performance through laboratory testing.

The design process is developed using numerous examples and experiments to demonstrate the feasability of this approach to manipulator design.

17. Key Words (Suggested by Author(s))	18. Distribution Statement
impedance, manipulator design, performance requirements, stability	Unclassified — Unlimited Subject Category 63

19. Security Classif. (of this report)	20. Security Classif. (of this page)	21. No. of pages	22. Price
Unclassified	Unclassified	108	

NASA FORM 1626 OCT 86